EXTENSION OF THE RANGE OF PRIMARY VACUUM CALIBRATION METHODS WITH THE USE OF NONEVAPORABLE GETTERS

Sefer Avdiaj

Doctoral Dissertation
Jožef Stefan International Postgraduate School
Ljubljana, Slovenia, January 2012

Evaluation Board:

Prof. Dr Monika Jenko, Chair, Institute of Metals and Technology, Lepi pot 11, Ljubljana, Slovenia

Dr. Bojan Erjavec, Member, Institute of Metals and Technology, Lepi pot 11, Ljubljana, Slovenia

Prof. Dr. Lars Westerberg, Member, Uppsala University, Department of Physics and Astronomy, SE-751 20 Uppsala, Sweden

Asst. Prof. Dr. Igor Belič, Member, Institute of Metals and Technology, Lepi pot 11, Ljubljana, Slovenia

MEDNARODNA PODIPLOMSKA ŠOLA JOŽEFA STEFANA
JOŽEF STEFAN INTERNATIONAL POSTGRADUATE SCHOOL

Sefer Avdiaj

EXTENSION OF THE RANGE OF PRIMARY VACUUM CALIBRATION METHODS WITH THE USE OF NONEVAPORABLE GETTERS

Doctoral Dissertation

RAZŠIRITEV MERILNEGA OBMOČJA PRIMARNIH VAKUUMSKIH KALIBRACIJSKIH METOD Z UPORABO NENAPARLJIVIH GETROV

Doktorska disertacija

Supervisor: Dr. Janez Šetina

Ljubljana, Slovenia, January 2012

Index

Abstract

Measurement of ultrahigh vacuum (UHV) and extremely high vacuum (XHV) is important in many advanced research and technology fields such as: equipment for surface analysis, particle accelerators, simulation of interstellar space, processing of advanced semiconductors, electron tubes, FE displays, etc. For traceable calibrations of UHV and XHV gauges we need adequate primary standards which deduce the pressure unit to corresponding base SI units. Primary standards for high and ultrahigh vacuum are normally pressure generators, which are realized and maintained at national metrological laboratories of the highest level. Basically two methods are used: static expansion and dynamic (continuous) expansion.

The aim of this work was to explore the use of nonevaporable getter pumps (NEG pumps) for extending the low range of vacuum primary standards. Since the main residual gas in UHV and XHV systems (after a suitable bake-out to remove adsorbed water) is hydrogen, the ultimate pressure and lowest limit of pressures which can be generated with high precision in primary static and dynamic expansion systems is determined by the hydrogen outgassing of vacuum calibration chambers. We used NEG pumps because they have zero pumping speed for noble gases and large pumping speed for active gases, especially for hydrogen. NEG pump can be used to mitigate hydrogen outgassing and achieve lower ultimate pressure.

Besides using pumps with large pumping speed for hydrogen in XHV systems it is also important to reduce outgassing rate of chamber walls. A study of reduction of hydrogen outgassing rate from stainless steel was performed. The outgassing rate of $q = 2.86\times10^{-13}$ mbar l s^{-1} cm^{-2} was achieved in stainless steel 304L vacuum chamber (wall thickness of 2.62 mm) at room temperature after baking the system at 250 °C for 380 h, while this outgassing rate was reduced even further to $q = 5.7\times10^{-14}$ mbar l s^{-1} cm^{-2} using $T = 350$ °C for 140 h.

NEG pump must be activated by heating to appropriate temperature (depending on getter material) to remove passivating surface oxide layer. The diffusion of oxygen in St 707 NEG material during heat treatment was investigated. NEG characterization has been carried out by techniques such as EDS and AES for determination of bulk and surface chemical composition, respectively, and by XRD for determination of morphology and crystallinity.

We have demonstrated that the use of NEG pump in static expansion calibration system can diminish the influence of outgassing and offers the possibility to reliably generate lower calibration pressures. Contamination of the inert calibration gas by outgassing was found to be the main reason for the pressure dependence of the calculated volume ratio when the gas expansion was done at lower pressures.

We have constructed a model XHV dynamic expansion calibration system with a built-in NEG pump. The ultimate pressure in the calibration chamber of the order of 2×10^{-12} mbar was achieved. System is equipped with a gas flow meter for very low flows of inert gases. Flow is measured by pressure rise method. The use of another NEG pump in the flow meter practically diminishes the effect of hydrogen outgassing on measured flow. Lower limit of pressure rise method is 5×10^{-10} mbar l s^{-1} and can be extended by constant conductance method down to $3\text{x}10^{-12}$ mbar l s^{-1}.

With this flow meter we can generate calibration pressures of argon in the range from $8\text{x}10^{-13}$ mbar up to 2×10^{-7} mbar. Based on our knowledge, this is the lowest calibration pressure reached in any National Laboratory so far. Operation of XHV calibration system has been demonstrated by calibration of two extractor ionization gauges having low pressure limit 1×10^{-12} mbar.

Povzetek

Točno merjenje ultravisokega vakuuma (UHV) in ekstremno visokega vakuuma (XHV) je pomembno v mnogih naprednih raziskovalnih in tehnoloških področjih, kot so: spektrometri za analizo površin, pospeševalniki delcev, simulatorji medzvezdnega prostora, industrija polprevodnikov, vakuumske elektronske cevi itd. Za sledljive kalibracije UHV in XHV merilnikov potrebujemo ustrezne primarne standarde. To so običajno generatorji tlaka, ki so realizirani in jih vzdržujejo v nacionalnih meroslovnih laboratorijih na najvišji ravni. V osnovi se uporabljata dve metodi: statična in dinamična ekspanzija plinov.

V tej disertaciji sem pokazal, kako je mogoče razširiti spodnjo merilno mejo vakuumskih primarnih standardov z uporabo nenaparljivih geterskih (nonevaporable getter - NEG) črpalk. Ker je glavni preostali plin v UHV in XHV sistemih vodik, je končni tlak in spodnja meja kalibracijskega tlaka določena z razplinjevanjem vodika iz sten sistema. NEG črpalke imajo velike črpalne hitrosti za aktivne pline, zlasti za H_2, žlahtnih plinov pa sploh ne črpajo. Tako lahko v primarnih kalibracijskih sistemih uporabimo NEG črpalke za ublažitev vpliva razplinjevanja H_2 ter za kalibracijski plin izberemo žlahtni plin, kot sta Ar ali He.

Poleg uporabe črpalk z velikimi črpalnimi hitrostmi za H_2 je v XHV sistemih zelo pomembno tudi da zmanjšamo stopnjo razplinjevanja s sten vakuumske posode. Zato sem opravil študijo znižanja stopnje razplinjevanja H_2 iz nerjavečega jekla pri postopku toplotnega procesiranja vakuumske komore. Po toplotnem procesiranju stene z debelino 2.62 mm iz nerjavečega jekla 304L, ki je trajalo 380 h pri temperaturi 250 °C sem izmeril stopnjo razplinjevanja $q = 2.86\times10^{-13}$ mbar l s^{-1} cm^{-2}. Po dodatnem toplotnem procesiranju, ki je trajalo 140 h pri temperaturi 350 °C se je stopnja razplinjevanja zmanjšala na $q = 5.7\times10^{-14}$ mbar l $s^{-1}cm^{-2}$.

NEG črpalke moramo aktivirati s segrevanjem do ustrezne temperature (odvisno od NEG materiala), da odstranimo površinsko pasivacijsko plast oksida. Za boljše razumevanje procesa aktivacije sem opravil raziskavo difuzije kisika v NEG materialu St707 pri toplotni obdelavi. Karakterizacija NEG materiala je bila izvedena s tehnikami kot so EDS za določitev kemične sestave v materialu in AES za določitev kemične sestave površine. Metoda XRD je bila uporabljena za ugotavljanje morfologije in kristalne strukture materiala.

Uporabo NEG črpalke sem preskusil v modelnem sistemu po metodi statične ekspanzije plina. Pokazal sem, da je kontaminacija kalibracijskega plina z vodikom, ki se sprošča s stene kalibracijske posode, glavni razlog da izračunano razmerje prostornin vakuumskih posod ni konstantno, temveč se spreminja s tlakom plina. Z NEG črpalkama v mali in veliki posodi je razmerje prostornin ostalo konstantno tudi pri zelo nizkih tlakih.

Nadalje sem skonstruiral in izdelal modelni kalibracijski sistem po metodi dinamične ekspanzije. Z vgrajeno NEG črpalko je bil v kalibracijski posodi dosežen končni tlak reda 2×10^{-12} mbar. Sistem ima merilnik pretoka plina po metodi naraščanja tlaka v zaprti posodi z znano prostornino. Z uporabo NEG črpalke lahko praktično izničimo vpliv razplinjevanja H_2 na merjeni pretok žlahtnega plina. Spodnjo mejo merjenja pretoka, ki je 5×10^{-10} mbar l s^{-1}, lahko z metodo "konstantne prevodnosti" znižamo še za dva velikostna razreda.

V sistemu lahko generiramo kalibracijske tlake plina Ar v območju od 8×10^{-13} mbar do 2×10^{-7} mbar. Po nam dostopnih podatkih je to najnižji kalibracijski tlak, ki je bil dosežen v nacionalnih meroslovnih laboratorijih. Delovanje sistema sem preskusil s kalibracijo dveh ekstraktorskih ionizacijskih merilnikov, ki imata spodnjo merilno mejo pri 1×10^{-12} mbar.

Abbreviations (Format: List of)

AES	=	Auger electron spectroscopy
SAM	=	Scanning Auger Maps
EDS	=	Energy dispersive X-ray spectroscopy
SEM	=	Scanning Electron Microscopy
SEI	=	Secondary Electron Image
XPS	=	X-ray photoelectron spectroscopy
NEG	=	Non-evaporable getter
UHV	=	Ultra high vacuum
XHV	=	Extremely high vacuum
ESD	=	Electron stimulated desorption
LHC	=	Large Hadron Collider
LEP	=	Large Electron Positron Collider
CERN	=	European Laboratory for Nuclear Research (Centre Européen pour la Recherche Nucléaire)
FWHM	=	Full width at half-maximum
WDS	=	Wavelength dispersive X-ray spectroscopy
SIMS	=	Secondary ion mass spectroscopy
ML	=	Monolayer
SEM	=	Scanning electron microscopy
NEGP	=	Nonevaporable getter pump
RT	=	Room temperature
SRG	=	Spinning Rotor Gauge
CDG	=	Capacitance Diaphragm Gauges
SS	=	Stainless Steel
SI	=	International System of Units
at%	=	Atomic percent
GR	=	Gas reservoir
CH	=	Vacuum chamber
EBSD	=	Electron backscattered diffraction
FCC	=	Face centered cubic
BCC	=	Body centered cubic
PTB	=	Physikalisch-Technische Bundesanstalt
LIP	=	Lanzhou Institute of Physics
RGA	=	Residual Gas Analyzer
IMT	=	Institute of Metals and Technology
TMP	=	Turbomolecular pump
QMS	=	Quadruple masspectrometer
EXTR	=	Ionization Extractor Gauge
CFG	=	Cross Field Gauges
ECG	=	Emitting Cathode Ionization Gauges

RoR = Rate of Rise of Pressure
RLM = Recombination Limited Model
DLM = Diffusion Limited model
AIP = American Institute of Physics

1 Introduction

> "I often say that when you can measure what you are speaking about, and express it in numbers, you know something about it; but when you cannot measure it, when you cannot express it in numbers, your knowledge is of a meager and unsatisfactory kind"
>
> Lord Kelvin [58]

Calibration determines the relation of the reading of a measuring instrument and the corresponding value of the measurand, as established by a standard under well-defined conditions. Calibrations are necessary when the output quantity of an instrument cannot be described by known input quantities via physical formula. The purpose of a calibration is to assure correct measurements by making the indicated quantity directly or indirectly traceable to SI units. This is important not only for physical but also for economical reasons. If for example a manufacturer of high vacuum pumps measures pumping speed with an ionization gauge indicating values too high, he will quote values of pumping speed which are too low, and may be disadvantaged compared to a competitor who measures correctly.

Primary method is a method of the highest metrological quality which when implemented can be described and understood completely, and for which a complete uncertainty budget can be provided in SI units. The results of the primary method can therefore be accepted without reference to another standard for the quantity being measured.

Vacuum environment at pressure below 10^{-10} mbar (ultrahigh vacuum - UHV) is currently used, not only in research, but also in the industry on a more or less routine basis. Demanding technologies require even pressures below 10^{-12} mbar (extreme high vacuum - XHV) and there is a gradual but clear increase in demand for vacuum gauge calibration gauges in this range.

1.1 Overview of primary vacuum standard

Calibration of measuring instruments has a great importance in science and technology. Also this applies to the filed of calibration of pressure measuring equipment, where absolute pressures from around atmospheric pressure down to about 0.1 mbar can be measured directly as force per unit area. In cases of pressures below 0.1 mbar, for practical areas of a few square centimeters the force becomes very small and practically impossible to measure. Below 0.1 mbar, the idea of all vacuum primary standards used today is the following: the gas is measured precisely at a pressure as high as possible, and then the gas is expanded to the desired pressure in a manner well treatable by calculation.

Commonly used high vacuum gauges rely on measurements of variables that cannot be reliably theoretically related to the quantities generally desired – pressure or gas density. As an example, the operation of an ion gauge is so complicated that it is virtually impossible to theoretically relate the measured ion current to a pressure or density with any meaningful accuracy. To relate the indicated gauge reading to accepted physical units, the vacuum gauge must be calibrated against a standard that is able to generate a suitable range of gas pressures with known uncertainty.

There are two types of vacuum calibration methods (Table 1): calibration with primary vacuum standard and comparison calibration with secondary vacuum standard. As mentioned above, primary vacuum method is designed for precise and accurate generation of pressure in a specific vacuum range, while secondary vacuum standards are employed for traceability dissemination from primary standards to other instruments to be calibrated down the traceability chain.

Table 1: Primary and secondary standards in use for pressures in the vacuum regime [12, chapter 12]

Pressure	Primary standards	Secondary standards
10^{3} mbar	Mercury column manometer	Quartz-Bourdon manometer
↓	Rotary piston gauge	Resonance silicon gauge
	Pressure balance	Capacitance diaphragm gauge
	Static expansion system	Spinning rotor gauge
	Dynamic expansion system	Ionization gauge
10^{-12} mbar		Extractor gauge
		Mass spectrometer

Primary standards are designed and developed to generate pressure with highest precision. A single type of primary standard is not capable of covering the entire technical regime of vacuum pressures spanning about 15 orders of magnitude (10^{-12} mbar to 10^{3} mbar, Table 1). In this sense, the initial step of this ladder and starting point for all vacuum primary standards are the instruments which directly measure the pressure as force per unit area at a specific temperature. These are the liquid manometers and piston gauges (pressure balances). In this thesis we will not discuss these specific types of vacuum gauges, because our goal is the extension of lower range of indirect methods: the static expansion method and the continuous expansion method.

1.1.1 Static expansion method

The principle of static expansion is shown in Figure 1. It is used as a primary standard for generating pressures mainly in the high and medium vacuum range from 10^{-6} mbar to 10 mbar [1]. The static expansion method was reported to generate calculable pressures as low as 10^{-8} mbar [2, 9].

The static expansion method or Knudsen method in its simplest form requires a vacuum system consisting of two vessels separated by a valve and a means of measuring the pressure in the first of the two vessels. Gas isolated in the first vessel is then shared between the two vessels (the second vessel is always evacuated in advance) by opening the connecting valve, thereby reducing the pressure in proportion to the change in the volume of the gas. Variations in the Knudsen gas expansion technique were described by a number of authors [1-12,16].

In the case of isothermal gas expansion the Boyle's (Mariotte's) law can be used:

$$PV = \text{constant} \tag{1}$$

The initial pressure prior to the expansion should not exceed values significantly violating ideal gas behavior. For the rare gases and nitrogen, this limit is at a pressure of 3×10^{3} mbar.

Generally it is impossible to provide precisely equal temperatures for both volumes including their connections pipes [13]. This is why calculations shall be based on the ideal gas law instead of Boyle's (Mariotte's) law.

$$\frac{PV}{T} = \text{constant} \tag{2}$$

If p_0, V_0, and T_0 denote pressure, volume and temperature, respectively, prior to expansion, whereas p_1, (V_0+V_1) and T_1 after expansion, from Eq. (2) we can obtain:

$$\frac{p_0 V_0}{T_0} = \frac{p_1 (V_0 + V_1)}{T_1} \tag{3}$$

From Eq. (3) we can calculate the pressure after expansion:

$$p_1 = p_0 \frac{V_0}{V_0 + V_1} \frac{T_1}{T_0} \tag{4}$$

The ratio $V_0/(V_0+V_1)$ is called the expansion ratio, and is a characteristic value for each expansion system. The inverse value of this is named volume ratio. The main task in static expansion method is to determine volume ratio as accurately as possible.

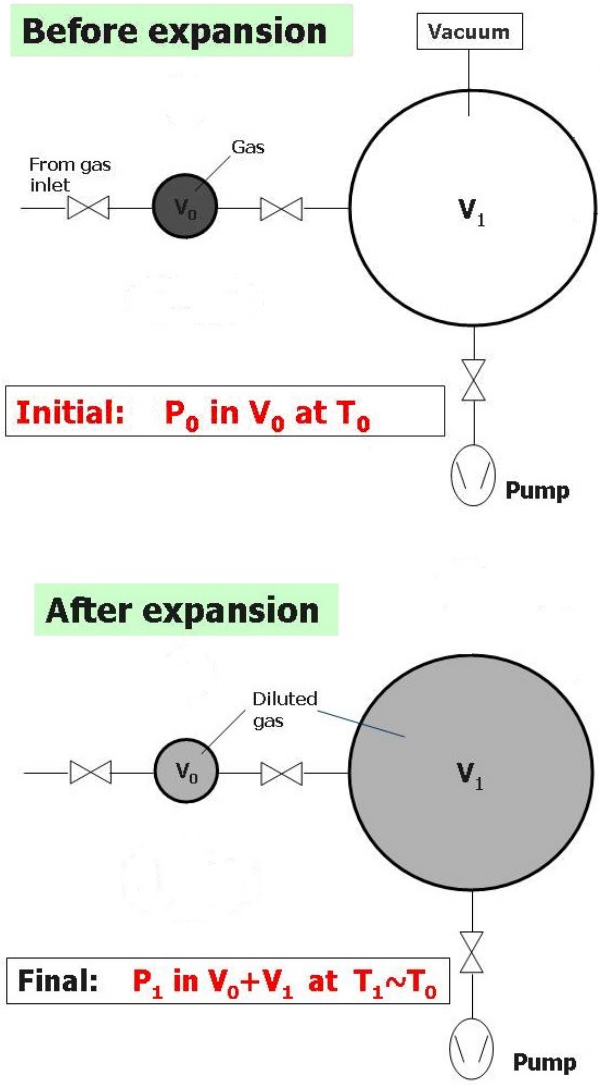

Figure 1: Scheme of the static expansion system used for generating low pressure in the vacuum regime. By expanding a fixed amount of gas from a small volume into a large evacuated volume, the initial pressure drops according to the volume ratio.

Eq. (4) is valid for ideal gas only, but in practical application we deal with real gases. The approximating equation for the real gas is:

$$p_1 V_{mol} = R_g T\left(1 + B'' p\right) \tag{5}$$

where B'' denotes the second virial coefficient. Since the pressure after expansion is much smaller than before, the term $B''{\cdot}P$ is small, and thus, it is sufficient to correct solely the term for the gas prior to expansion. Therefore,

$$p_1 = p_0 \frac{V_0}{V_0 + V_1} \cdot \frac{T_1}{T_0} \cdot \frac{1}{1 + B''{\cdot}p_0} \tag{6}$$

The gases which can be used for the static expansion method have to meet two requirements [12, 13]. Their virial coefficient should be small. A small virial coefficient means “no significant deviations from ideal gas law”. The second requirement is that this

gas should not be adsorbed on the walls of the vacuum vessel. Those gases are: rare gases, N_2, and CH_4 [20-22] which do not exhibit significant adsorption down to the pressure of 10^{-8} mbar whereas, e.g., hydrogen (H_2) can only be used down to about 10^{-4} mbar.

1.1.1.1 Examples of Static Expansions Systems in National Laboratories

After a number of improvements, this method is now being used in many laboratories of the world [19]. A few of them are: NPL (National Physical Laboratory) UK, PTB (Physikalisch Technische Bundesanstalt) Germany, UME (Ulusal Metroloji Enstitusu) Turkey, ETL (Electro Technical Laboratory) Japan, METAS (Federal Office of Metrology) Switzerland, CENAM, IMGC and KRISS.

There are two types of technique used for standard volume expansion systems: single volume expansion technique and multiple expansion technique [19]. The major disadvantage of the single expansion technique is that the wide vacuum range with the necessary accuracy cannot be achieved by this method. Multiple expansion technique can be used where a fraction of the gas expanded to pressure p_1 can be used for subsequent expansion to provide pressures down to about 10^{-6} mbar. The five-stage static expansion system that was developed in NPL in UK is shown in Figure 2 [20].

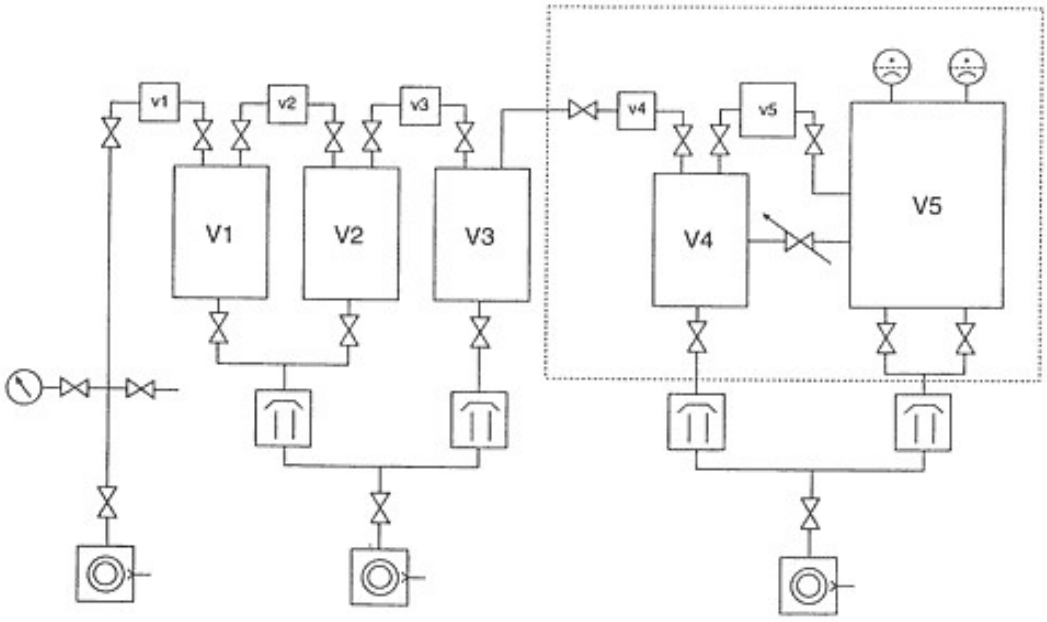

Figure 2: Schematic of five-stage static expansion standard developed at the National Physical Laboratory (NPL), United Kingdom. Reprinted from [12], with the kind permission from John Wiley and Sons.

In Figure 3 one of the two PTB static expansion standards is shown [98]. It is only a two-stage system so for the lowest pressure repeated expansions have to be applied.

Typically, the lowest calibration pressure which can be achieved in a static expansion system is 10^{-6} mbar, however there are reports in literature of using static expansion method down to 10^{-8} mbar. The lowest calibration pressure is determined by the lowest residual pressure in the chambers, outgassing rate of the inner walls of the system, and adsorption and desorption effects.

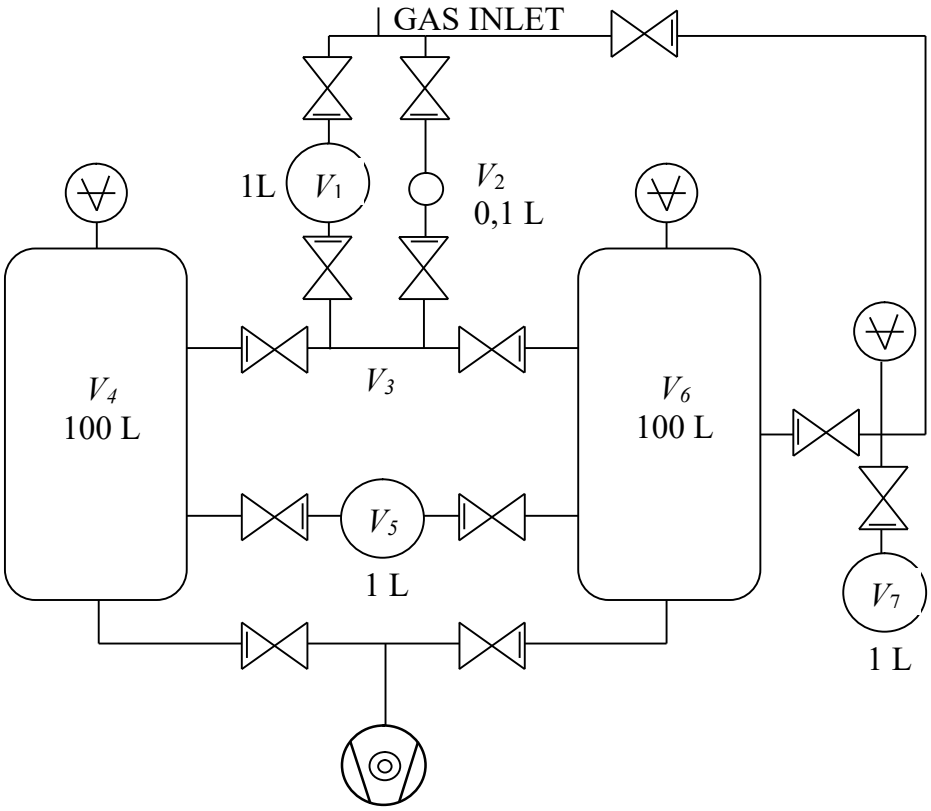

Figure 3: Example of a two-stage expansion system used at the Physikalisch-Technische Bundesanstalt (PTB), Reprinted from [12], with the kind permission from John Wiley and Sons.

1.1.1.2 Uncertainties of the static expansion method

Figure 4 shows the relative uncertainties exhibited in the pressure generation for the PTB system from Figure 3. It can be seen that the uncertainties of the generated pressures in the static expansion systems are mainly determined by the uncertainties of the expansion ratios and by the temperature measurements [13, chapter 15].

When employing the static expansion method the most challenging but essential aspect is an accurate determination of the volume ratios. Volume ratio measurement methods published up to date fall in two main groups:

- By measuring absolute volumes
  - From dimensional measurements
  - Gravimetric method
  - Constant pressure technique
- By different gas expansion methods
  - Gas accumulation methods (which was developed by NPL) [2]
  - Gas depletion methods [7]
  - Direct measurements with Spinning Rotor Gauge [1, 6]

The short description of some methods:
*Dimensional Metrology***:** This practice is accurate for volume determination of simple shapes but not suitable for precise measurement of vacuum vessels and other tubing of irregular geometry.

Gravimetric Method: This method is an established one, in which the volume to be determined is required to fill up with liquid (usually water) of exactly measured volume in a constant temperature environment. For volumes > 0.1 liter, this is the most accurate method.

Constant pressure technique: Here, a variable volume of known size is used to determine the unknown volume. After expansion into the small, evacuated volume to be measured, the variable volume is adjusted such that the gauge indicates the same reading as prior to the expansion. Volumes < 0.1 liter are best measured with this method [16].

Expansion Methods: Generally only volume ratios are determined by expansion methods. For this method, a known pressure of gas in one volume is expanded into another volume, By making use of Boyle s' law corrected for real gas behavior (Eq. (6), the volume ratio can be calculated. Many authors used different techniques for this purpose [1,4,6,7,9,10]

The main point of expansion methods is that the pressure ratio (volume ratio) has to be measured with the high accuracy. For this it is possible to use two calibrated gauges or to use a single non-calibrated gauge with a strictly linear response. Elliot and Clapham [12] used a piston gauge to generate the initial pressure and a calibrated Quartz Bourdon Spiral manometer, QBS, for the pressure measurement of the expanded gas after a series of successive expansions, whereas Berman and Fremery [6] used a single expansion where both the initial pressure and the final pressure were measured with the same spinning rotor gauge.

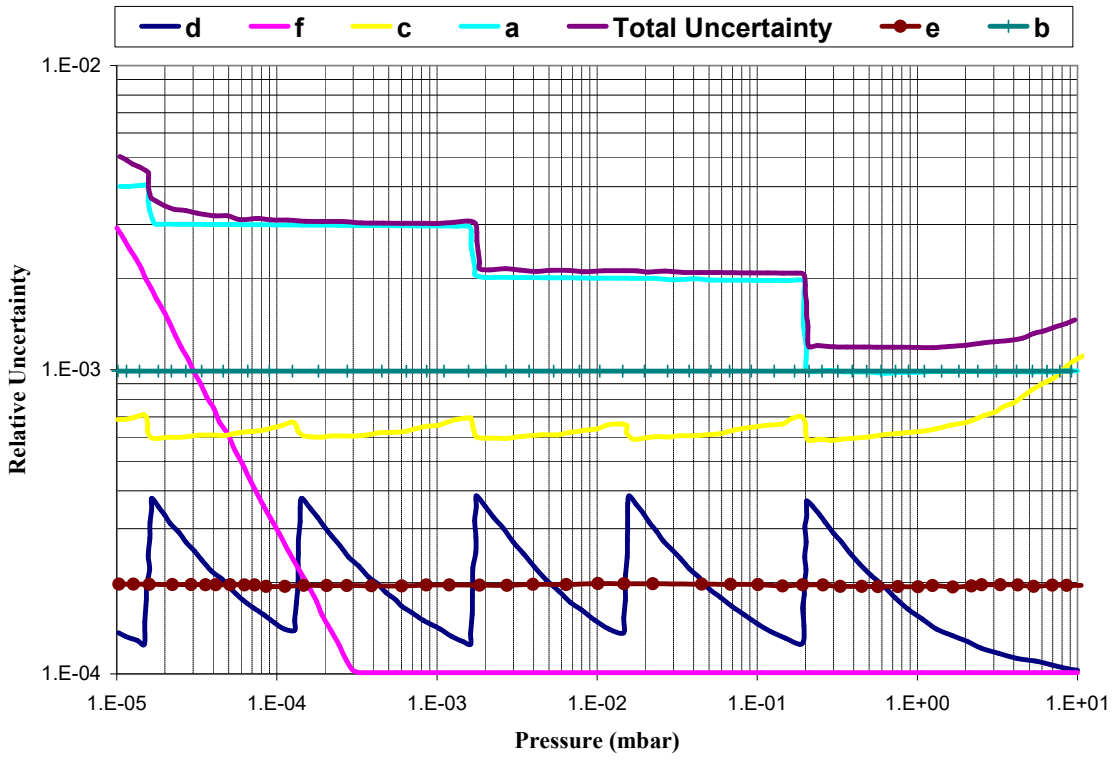

Figure 4: Uncertainties of the generated pressure in the static expansion system shown in Figure 3. The main contributions to the total uncertainty are: **a**. Uncertainty of expansion ratio, **b**. Uncertainty of temperature due to gradients, **c.** Uncertainty of gas temperature due to expansion itself, **d.** Uncertainty of initial pressure generated, **e.** Uncertainty of temperature measurement due to the drift, **f.** Uncertainty of pressure due to outgassing. We used the data from [12], by courtesy of John Wiley and Sons.

1.1.2 Dynamic expansion method

The dynamic expansion method (also called orifice flow or continuous expansion method) is an extension of static expansion method. "Dynamic method" [15, 17, 18, 25] relies on balancing the rate of flow of gas injected into a chamber against the rate at which it is being evacuated through an orifice. Under conditions of the steady molecular flow the pressure is calculated from knowledge of the gas flow-rate and the conductance of the orifice. This method is used for calibrations of ultra high vacuum (UHV) gauges and extremely high vacuum (XHV) gauges, Figure 5. While the static expansion method uses two very differently sized volumes, the orifice flow method employs two largely different conductances for the pressure reduction [13]. This method has been employed at NIST (USA), PTB (Germany), IMGC (Italy), KRISS (South Korea) etc. Poulter has reviewed various forms of this method as primary vacuum standards [8]. A variety of forms of the orifice flow method arise either from the number of orifices or flow rate measuring technique.

1.1.2.1 General principle of dynamic expansion method

The most established technique in the continuous expansion method is single orifice technique, schematic of which is shown in the Figure 5 [26]. This system consists of a thin orifice at the joint of two chambers. Most systems use a circular orifice as the control conductance since its value can be calculated fairly accurately. The first volume is the calibration chamber while the second one (pumping chamber) ensures a suitable distribution of molecular velocities on the lower pressures side of the orifice.

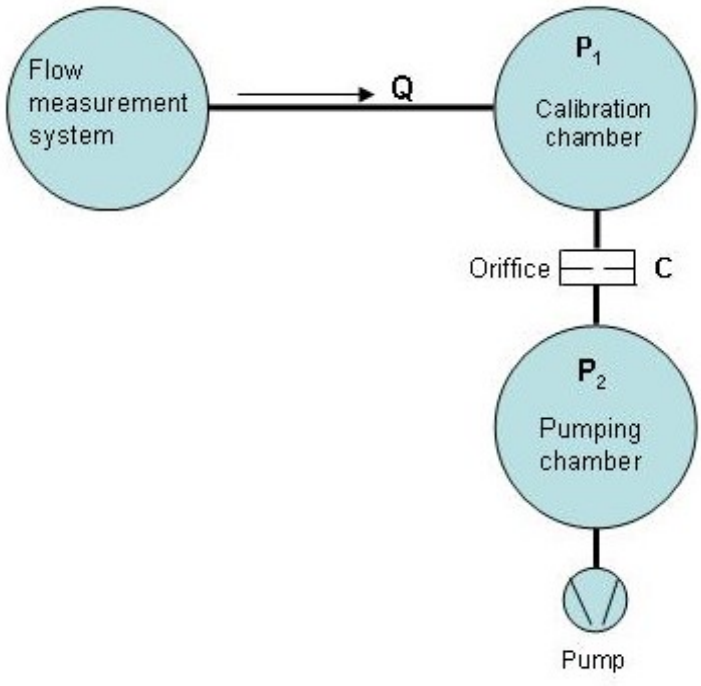

Figure 5: Continuous expansion method for generating pressures in the high and very high vacuum regime.

In the continuous expansion method clearly the gas flow rate from the flow meter must be large compared with outgassing rate of the system. Special care has to be taken when generating pressure below 10^{-8} mbar so that outgassing of vacuum vessels and the adsorption of gas molecules on the inner surfaces do not significantly falsify the calculated pressure.

Determination of generated pressure in the dynamic expansion method mainly is threefold:

- to calculate the conductance C of the orifice
- to measure the flow rate of calibration gas into the calibration chamber
- to determine the pressure ratio across the orifice

If a gas is allowed to flow in the calibration chamber from the flow meter, it will generate a pressure drop across the orifice. This pressure difference is directly proportional to gas flow rate Q and inversely proportional to the conductance C of the orifice. In this case the equation of continuity is valid (isothermal conditions):

$$\left(P_1 - P_2\right) = \frac{Q}{C} \tag{7}$$

From Eq. (7) the generated pressure is given by:

$$P_1 = \frac{Q}{C\left(1 - R\right)} \tag{8}$$

where P_1 and P_2 are the pressure above and below the orifice, respectively, and R is pressure ratio $R=P_2/P_1$.

Even though the principle procedure seems similarly simple as the static expansion method, its realization requires considerably more effort. The dynamic expansion method mainly consists of two main parts:

- UHV / XHV calibration chambers (calibration system)
- Flow measuring system

Overview about flow measuring system will be discussed in 1.1.3.

The upper pressure limit of continuous expansion method amounts to a few 10^{-4} mbar. This is determined by transition from molecular to viscous flow through the orifice. Whereas the lower limit of calibration pressure in this method is determined by the residual pressure in calibration chamber and by lowest flow rate which can be generated in the flowmeter with sufficient accuracy. The typical value of the lower limit is 10^{-9} mbar. For lower pressure, the flow division principle can be used [17,18, 27]. In more detail this technique will be discussed in chapter 8. The main benefit of the dynamic expansion method is the presence of a stationary equilibrium: the number of particles leaving the calibration chamber just balances the number entering in the chamber. Therefore, adsorption and desorption effects are relevant only until this equilibrium is reached, and a wider selection of gas species are applicable with this method than with static expansion method.

In Eqs.(7,8) the influence of temperature was not taken into account. Due to the impossibility to have exactly the same temperatures of the flowmeter and the calibration chamber the corrections for this has to be done. Standard DIN 28416 recommends referring both the temperatures of the flowmeter and the temperature of calibration chamber to a common temperature 23 °C as close as possible.

1.1.2.2 Example of a continuous expansion system at NIST [25]

Dynamic expansion method has been employed at NIST (USA); PTB (Germany); IMGC (Italy); KRISS (South Korea); NINVAST (Pakistan)[20]. Figure 6 shows the design of the system constructed at NIST [25]. The chamber is divided in the two cylindrical halves, each 27 cm in diameter and 34 cm long, separated by a central wall with the orifice in the center. A circular baffle 5 cm below the top of the upper chamber insures that gas molecules entering the top of the upper chamber from the flowmeter will experience several collisions with the chamber walls before entering a gauge or passing through the orifice at the bottom. To ensure a random distribution of molecular velocities (Maxwellian distribution) these collisions are essential. This is necessary for pressure uniformity, which is assumed in the conductance calculation.

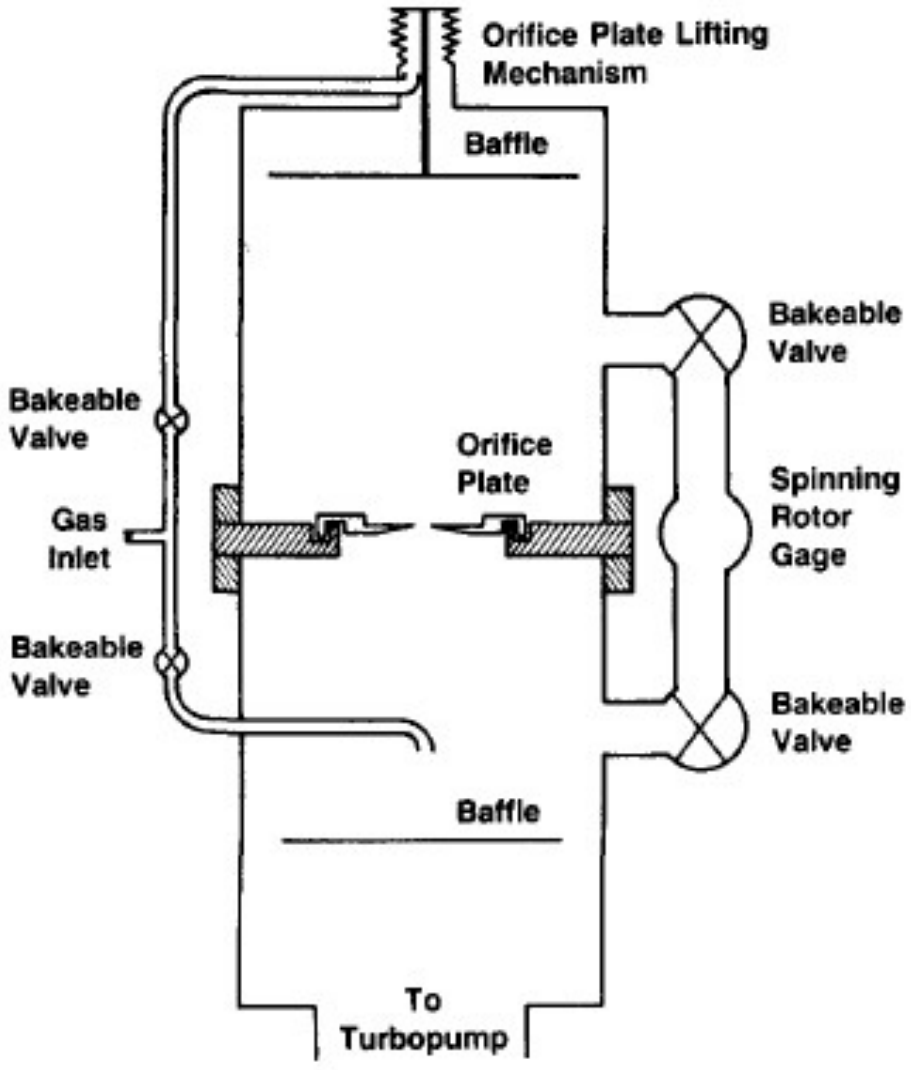

Figure 6: Schematic of the vacuum chamber showing the lifting mechanism and sealing method of the orifice plate. Also shown is the arrangement of valves and gauges permitting the measurement of the upper to lower chamber pressure and flow ratios [25].

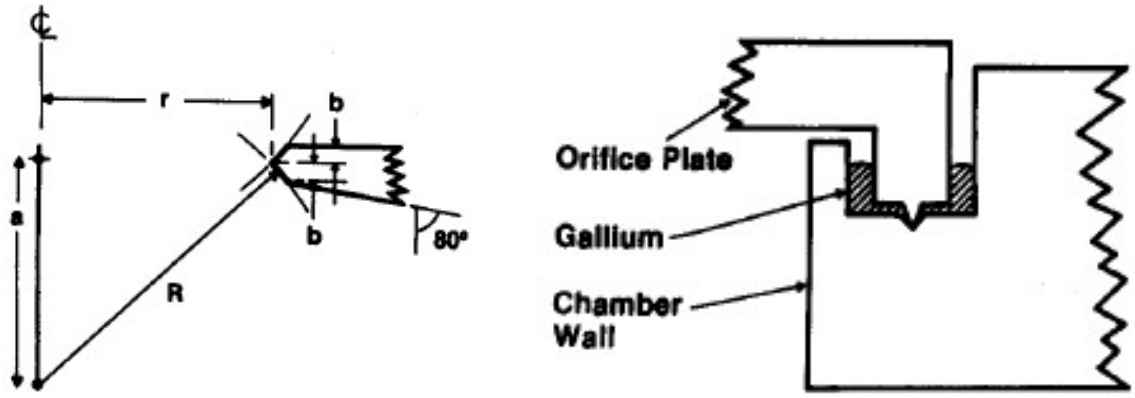

Figure 7: Detail of the orifice and the gallium-filled groove that seals the orifice plate into the wall between the two chamber halves. Reprinted from [26] with the kind permission of AIP.

The uniform distribution of the molecular flux will be perturbed by molecules entering the chamber from the inlet line and by those escaping through the orifice. These perturbations can be kept within acceptable bounds by using an orifice whose area is a small fraction of the surface area of the chamber. At the same time, the orifice conductance must be large enough to maintain a low background partial pressure and ensure a high enough flow that gauge pumping and outgassing are minor perturbations. In NIST, the compromised use was a nominal 1.1 cm diameter orifice, described in detailed in Figure 7, with a nitrogen conductance of about 12 l s^{-1} and an area of 0.03% of the chamber surface.

Some fraction of molecules passing through the orifice from the upper chamber will return back through the orifice because of the finite pumping speed available at the lower chamber. This is second order perturbation that can be readily accounted for if these returning molecules originate from a uniform flux distribution. This is achieved by making the lower chamber an almost symmetric duplicate of the upper chamber, with baffle 12 cm above the inlet of the nominal 500 l s^{-1} turbomolecular pump attached to the bottom of the chamber. The small orifice clearly would restrict the attainment of a low base pressure in the upper chamber. Therefore, the orifice is contained in a plate that seals into a liquid gallium-filled groove located in the central wall as illustrated in Figure 6. During pump-down or bake-out the orifice plate can be lifted through a bellows at the top of the chamber, opening a 12.7 cm hole between the upper chamber and the lower chamber.

The system constructed at NIST routinely attains base pressures of about 10^{-10} mbar, the residual gas in this range of vacuum being almost entirely hydrogen. The base pressure in the upper chamber increases by about a factor of two when the orifice plate is lowered and sealed in the gallium groove.

1.1.2.3 Uncertainties of continuous expansion method

In Figure 8, relative uncertainties of the generated pressure in the dynamic expansion system for three different national laboratories are shown. In most of the range, the uncertainty of the gas flow rate dominates. Only above 10^{-4} mbar does the uncertainty of conductance due to the transition to viscous flow have a significant effect [13, 29].

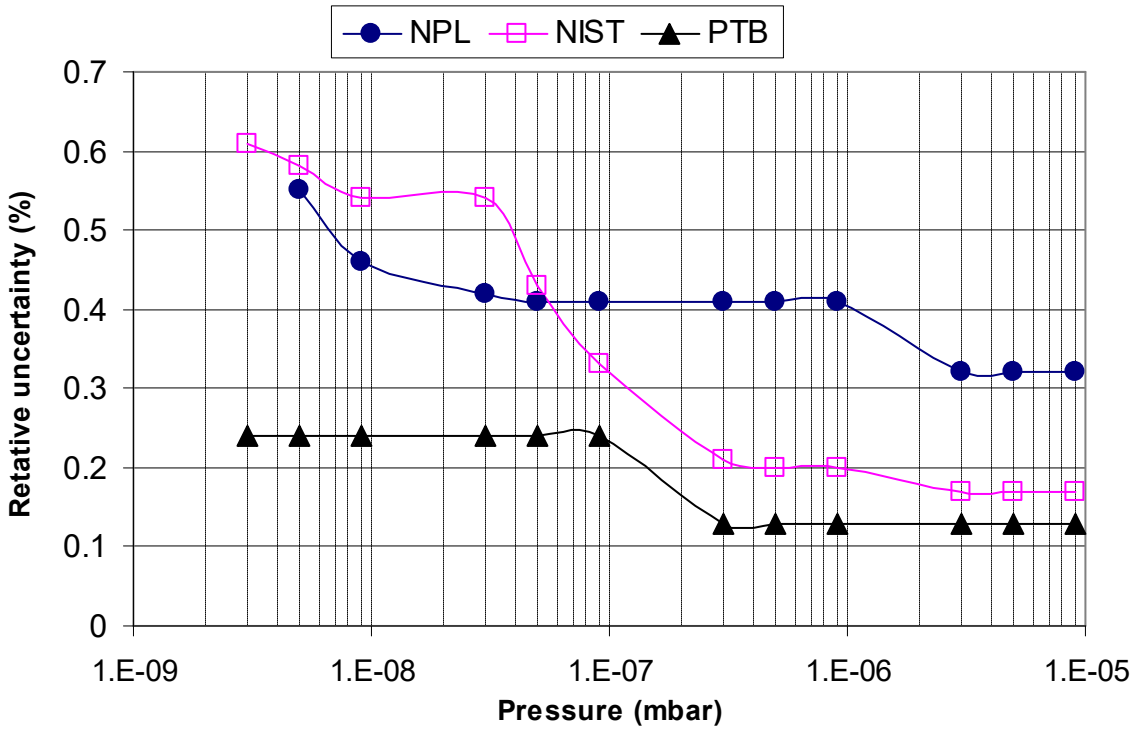

Figure 8: Relative standard uncertainties (one sigma) of the calibration pressures of the continuous expansion primary standards at NPL (UK), NIST(USA) and PTB(Germany). We used the data from [29] with the kind permission of AIP.

1.1.3 Gas flow measurements for continuous expansion method

As mentioned above, the continuous expansion systems mainly consists of two parts: flow measuring system and UHV/XHV vacuum chambers (Figure 5). Peggs has been given a review of several types of flow meters [21] suitable for continuous expansion systems.

Gas flow rate is defined as the number of molecules or moles of a particular gas species passing through a system per unit time [24]. A basic gas flow measurement must start with the equation of state (ideal gas law). For the level of accuracy required for these applications the ideal gas law suffices:

$$pV = vRT \tag{9}$$

where v is the number or moles, T is the temperature of the gas at which pressures p were measured, R is the universal gas constant, V is volume of the system. The flowmeter is temperature dependent [31]. Always it is convenient to obtain the value of the flow rate at a given temperature. This quantity, however is not incomplete if the temperature T at which the throughput was measured is not given. If the flow rate is given as molar flow rate Q_v, the value of this temperature is redundant.

As a practical matter, primary flow meters are generally realized by varying only the pressure or volume. From the differentiation of ideal gas law with respect to time t at constant temperature yields an expression that is useful in evaluating molar flow rates Q_v.

$$Q_v = \frac{dv}{dt} = \frac{\left(p\frac{dV}{dt} + V\frac{dP}{dt} \right)}{RT} \tag{10}$$

From Eq. (10) it follows that two types of flowmeters using two different techniques are possible:

a. Constant pressure with variable volume (*dP/dt=0*)
b. Constant volume with variable pressure (*dV/dt=0*)

1.1.3.1 Constant Pressure – Variable Volume Method

From Eq. (10) if the pressure is constant the flow rate will be:

$$Q_v = \frac{P}{RT}\left(\frac{dV}{dt} \right) \tag{11}$$

Basically, in constant pressure flowmeter gas flows from a small volume V through a leak valve into a vacuum system. The pressure and temperature of the gas in the volume are measured and the gas volume is decreased at a rate sufficient to maintain a constant pressure. The pressure is measured by secondary standard previously calibrated using a mercury column manometer, pressure balance, or static expansion system [13]. The volume change is generally accomplished by driving a piston of known cross section into the gas volume through sliding seals or by comprising a metal bellow. This type of flowmeter is used by most of national laboratories, for example: NIST, PTB, NBS, NPL (UK) etc.

As an example of a flowmeter the scheme of constant pressure flowmeter used at PTB is shown in the Figure 9.

Figure 9: Basic principle of a gas flowmeter: from the working volume enclosed by V2, CDG, and V3, the gas flows into the calibration system through C. The pressure in working volume can be changed by adjusting the variable volume ΔV. The pressure on the reference side of the CDG remains constant. [97]

The measuring equipment for determining the gas flow consist of a working volume (right-hand side) and a reference volume (left-hand side *p*=constant), separated by the

differential pressure gauge CDG and bypass valve V2. The working volume containing displacement bellows as a variable volume is additionally connected to valve V3 and leak valve C through which the gas is transported to the calibration system.
In the beginning of the operation, both volumes are equally pressurized with valves V1 to V3 open. After closing V2 gas will leak out of the working volume through the open valve V3 and a pressure difference across CDG will develop. In this case the pressure in the reference volume remains constant. This signal is used to drive the bellows such that the pressure remains constant inside the working volume. Two methods are available for this. The variable volume provided by a piston or bellows is reduced continuously at constant speed so that the pressure remains constant. In another way the volume can be adjusted by a fixed amount ΔV at intervals so that the pressure will vary slightly. The interval Δt between equal values of pressure is measured. The value of the gas flow in both cases is given by the volume speed of variable element $\Delta V/\Delta t$.
The main possible errors which may be made during measurements by flowmeters which should be accounted are [25]:

- Adsorption on and desorption from the walls
- Outgassing from walls of vacuum systems
- Leaks on vacuum systems
- Temperature drift
- Instability and drift of background noise
- Pumping and outgassing effects of the vacuum device

1.1.3.2 Constant Volume Method – Variable Pressure

In constant volume technique, the second term from Eq. (10) can be used to calculate the flow Q because the first term in this case is zero. If gas flows into a fixed volume V is constant, the pressure rise dP/dt is linear and the gas flow can be calculated according to:

$$Q_v = \frac{1}{RT} \times V \frac{dP}{dt} \tag{12}$$

This method of measurement of flow rate is used in some national laboratories like: NPL (India) and NINVAST (Pakistan) etc.

Flow rates down to 10^{-16} mol s^{-1} are measurable by this method when using inert vacuum gauges such as a spinning rotor gauge in a well degassed measurement volume V and the measurement interval is sufficiently long (several hours). This flow measuring technique is used also in our dynamic expansion system and it will be described in more detail in Chapter 7.

1.2 Basics of getter materials

> "They are called pumps, but they have no moving parts. They usually are not powered. Then why have them at all. The simple fact is that in many applications these "pumps" can make a difference between a process working or not working. They can significantly improve base pressure".
>
> Ferris Michael [94]

1.2.1 Definition of getter materials

A variety of sealed vacuum devices such as vacuum tubes, field emission displays, photomultipliers, cathode ray tubes, infrared detector dewars and others require a controlled ambient of vacuum or gas for their successful operation. While so called kinetic vacuum pumps transport the gas from one end to the other, the sorption pumps bind the gas to their surface in a physical way by freezing it or in a chemical way e. g. by gettering. Getters are solid materials able to fix gas molecules in the form of stable chemical compound or in other words getters are chemical pumps [32]. The action of getter materials relies on removal of molecules from gas phase by adsorption of gas molecules at the surface, absorption (dissolution of gas molecules in the solid) and chemical binding. Characteristics of a getter material are chemical affinity with gases and bulk diffusivity. The first application of getters was in the field of lamps and dates back to the end of the past century when red phosphorus was used as an element to "get" the active gases, particularly oxygen and water vapour, remaining in the glass bulb of incandescent lamps after pumping, in order to prevent a premature burning of the hot filament, whereas the term "getter" was first used by Thomas Edison's assistant Malignani in 1882 [33]. Because getters exhibit selective pumping, they are also used for inert-gas purification.

1.2.2 Quantities related to gas flow and getter vacuum performance

The performance of a given getter as a vacuum pump is mainly denoted by molecular mean free path and molecular flow regime, conductance and surface pumping, surface adsorption capacity, surface saturation time, sojourn time, ultimate pressure, etc. Atoms or molecules from the gas phase impinge on a solid surface, referred to as adsorbent. The experimental and theoretical studies of the gas surface – interaction distinguish between two types of adsorption: physical adsorption or physisorption and chemical adsorption or chemisorption [12, 35, 36]. Chemisorption can be dissociative, so that the molecules will split to individual atoms during chemisorption and can eventually diffuse into to the bulk of the getter material if enough energy is provided. Chemisorption implies chemical forces which involve interactions between valence electrons and are characterized by binding energies typically in the range of 0.8 - 8 eV per particle [13, chapter 6]. Physisorption implies van der Walls forces. They are characterized by binding energies 10 times lower than binding energies for chemisorption, so the binding energies for physisorption are of the order of 0.4 eV per particle.

1.2.2.1 Molecular mean free path

With the large number of gas particles present in a volume of gas at a given pressure, a large number of collisions can occur. Calculation of the collision frequency allows the mean free path λ of the particles to be determined. This is the average distance traveled by a particle between collisions.

$$\lambda = \frac{7.3T}{10^{20}\pi r_0^2 p} \ [\mathrm{cm}] \tag{13}$$

where T is the absolute temperature (K), p the pressure (mbar) and πr_0^2 the collision cross-section (cm^2).
At very low pressures where the mean free path is much greater than the linear dimensions of the vacuum vessel, the velocity of the molecules in the gas phase is entirely determined by collisions with the walls and the temperature of the walls. This is called molecular flow regime.

1.2.2.2 Conductance and surface pumping

The pumping speed of a pump is defined as a ratio of throughput of a given gas to partial pressure of that gas near the pump intake [34]. Usually it is expressed in l s^{-1}. The pumping speed of getter surface per unit area is defined as:

$$s = \alpha C \ \left[\mathrm{l\,s^{-1}cm^{-2}}\right] \tag{14}$$

where α is the sticking probability ($0 \le \alpha \le 1$), and C represents the conductance of an orifice per unit area [35]. In the molecular flow regime C does not depend on the pressure. It may be expressed as:

$$c = 3.64\sqrt{\frac{T}{M}} \ \left[\mathrm{l\,s^{-1}cm^{-2}}\right] \tag{15}$$

with M the molecular weight and T absolute temperature in Kelvin.
For $\alpha = 1$, C represents the pumping speed of the surface, which means every molecule impinging on a surface is captured.

1.2.2.3 Sorption capacity

This quantity represents the number of atoms or molecules which are captured by the getter before its pumping speed vanishes, i.e. before it stops sorbing gas, Figure 12, [38]. It can be expressed in the pressure-volume unit or in the number of molecules. This quantity corresponds to the amount of gas saturating the surface if there is practically no bulk diffusion, which occurs when getters work at room temperature. The monolayer capacity of an atomically flat surface is of the order of 1×10^{15} molecules/cm^2. If this monolayer of gas is released in a spherical volume of 1 liter (surface area $\approx$500 cm^2) the pressure increase would be 9.3×10^{-3} mbar.

1.2.2.4 Monolayer formation time

This term was introduced in order to estimate the period of time available for the surface analysis of a clean, pure surface at a given pressure. Monolayer time is the period in which a monolayer develops, assuming that all molecules striking the analyzed surface from the gas phase adhere to the surface permanently. The equation for monolayer time equals:

$$t_{\text{mono}} = 3.18\times10^{-25}\,\frac{n_{\text{mono}}}{p}\sqrt{MT} \tag{16}$$

For example if the residual gas is air ($M \approx 29$) at $T \approx 300\,K$, a useful approximation formula is obtained (n=10^{15} cm^{-2}):

$$t_{\text{mono}} = \frac{3.6x10^{-6}}{p}\left[\text{mbar s}\right] \tag{17}$$

If the pressure of air is p = 3.6×10^{-6} mbar, it needs just one second for one monolayer to form.

1.2.2.5 Sojourn time

When a gas molecule is adsorbed on a surface with binding energy E at a temperature T the probability of escape is:

$$\upsilon = \upsilon_0 \times e^{-\frac{\text{E}}{\text{RT}}} \tag{18}$$

where T is the surface temperature, E is binding energy, R universal gas constant. υ_0 is the attempt frequency, of the order of the vibrational energy of the adsorbed molecules ($\upsilon_0 \approx 10^{13}\,s^{-1}$).

In many cases it is more useful to use the reciprocal of this term $\tau = 1/\upsilon$, known as mean surface lifetime or mean sojourn time:

$$\tau = \tau_0 \times e^{\frac{\text{E}}{\text{RT}}} \tag{19}$$

where τ_0 is the period of vibration of the adsorbed molecule, and it is of the order of $\tau_0 = 10^{-13}$ s regardless of the gas-surface combination. When τ is much larger than the duration of the experiment, a surface provides a good pumping action.

1.2.2.6 Ultimate pressure

In the vacuum system, there are mainly three sources of gas: the gas produced or introduced by leaks, outgassing and permeation. The ultimate pressure or base pressure of a system designates the lowest total pressure that can be produced and measured reproducibly in a dynamically pumped vacuum system at room temperature, usually after bake-out or after many days of pumping at room temperature [12, 34, 37]. It is evaluated as being the ratio of the flow rate of gas entering into the system, the so-called gas load, to the effective pumping speed.

1.2.2.7 Getter pumping speed versus sorption capacity

As a result of the various possible interactions with the getter material the net removal rate of molecules from the gaseous phase is defined as sorption speed or pumping speed of the getter material. This indicates that the removal of molecules can be due to adsorption combined or not with absorption.
The gettering capacity is also called sorption capacity or pumping capacity. The maximum pumping capacity corresponds to the formation of a stoichiometric compound of gas atoms with active metal atoms of getter material. The pumping characteristics of the getter are generally represented by the sorption (pumping) speed as a function of sorbed quantity. Figure 10 shows a typical trend. From Figure 10 it is shown that Q_0 represents the total sorption capacity at zero pumping speed or Q_0 corresponds to the maximum possible amount of gas sorbed if diffusion takes place and a stoichiometric compound forms. The pumping capacity refers to the state when the surface of the getter is completely filled up. This means that in this case the pumping speed is zero.
Depending on working temperature and pressure conditions the getter pumping speed can decrease during time of sorption. It decreases more rapidly if sorption occurs at low temperatures (for example room temperature), because bulk diffusion is not promoted (expect for H_2) and in this case the capacity of getter is surface limited. If the getter is operating at high temperatures, bulk diffusion can occur, and in this case its speed is generally increased. It is found that, usually, the initial getter pumping speed is practically independent of pressure in a very wide range, from 10^{-4} mbar down to UHV conditions [38].

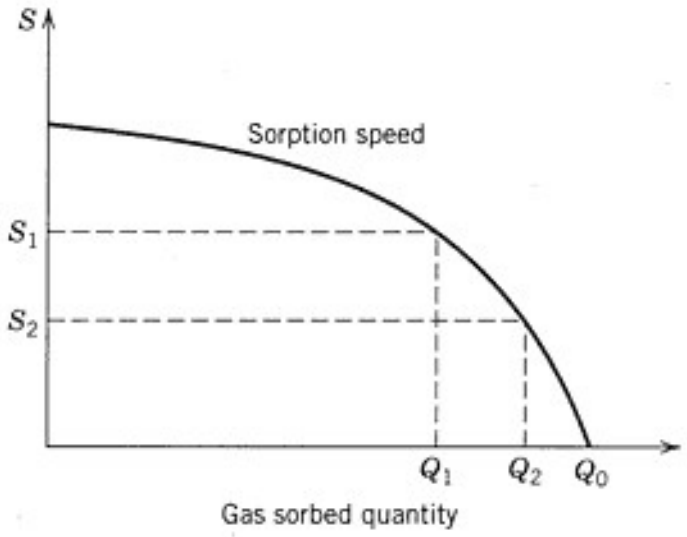

Figure 10: Typical sorption curve for a getter material. Sorption speed S versus sorbed quantity Q [12], reprinted with the permission of John Willey and Sons.

1.2.2.8 Definition of getter types

As mentioned above, getters are materials which tend to remove molecules from gaseous phase to solid phase. As a consequence a decrease of the gas pressure occurs. In order to form stable chemical compounds with impinging gas molecules the getter surface must be clean. Due to different procedures how the clean surface is achieved, getters are divided in two broad classes: evaporable and nonevaporable getters [13, 35]. Sometimes it is also common to say evaporated and nonevaporated getters.
In the case of evaporable getters, a fresh getter film is deposited *in situ* inside the chamber. This film is immediately ready to sorb gases. The geometric area and the real area of the film determine the pumping speed and sorption capacity of the getter.
In the case of nonevaporable getters, there is no evaporation or sublimation of the getter material; the gases react on the available surface of the material after this surface is activated, and if sufficient energy is supplied to diffuse the gas into the bulk.
The typical getter materials are given in the Table 1[12].

Table 2: Typical getter materials

Evaporable	Nonevaporable
Phosphorus	Zirconium
Strontium	Vanadium
Calcium	Titanium
Barium	Hafnium
Titanium	Thorium
	Rare earths
	Zr and Ti based alloys

1.2.3 The evaporable getters – thin film evaporable getters

From Table 2, the two materials most widely used as evaporable getters are barium and titanium [35]. Barium is used in large scale applications such as cathode ray tubes and some other sealed devices. Barium is usually sublimated from a $BaAl_4$ alloy by heating at $\approx 900\ ^0C$. The applications of Barium and how it works is described extensively in the literature [12, 37, 38].
On the other hand titanium is used mostly for continuous pumping of UHV and XHV vacuum systems. It can be evaporated or sublimed onto a surface to form, as in the case of Barium, a highly active film. In the case of titanium the term sublimation is used as a synonym of evaporation [12]. Titanium sublimation pumps are example evaporable getter pumps.
When evaporable getters cannot be used, e.g. because there is not enough space to produce a sufficiently large getter surface or when the evaporated getter film cannot cover delicate parts of the vacuum system or cause short circuits, non-evaporable getters can be an interesting alternative. Our attention will be focused to nonevaporable getters, because they will be used in our experiment.

1.2.4 Nonevaporable getters – porous thick film non-evaporable getters

No one adds a pump that does not give a benefit, so what benefits can a NEG pump offer that others cannot? NEG pumps are not as universally known as turbomolecular or cryo pumps, but they fill a variety of gaps in vacuum pumping technology. A good example is that they pump when the power is off. When comparing a NEG pump to a titanium

sublimation pump (TSP), the NEG does not need to evaporate a film, which can be an issue because the films can develop stresses and flake off the deposition surface. Another advantage of a NEG pump over a TSP is that the NEG can be put into a much smaller space than a TSP. The NEG also does not need a surface that can be sacrificed to titanium deposition. Another example is their affinity for hydrogen. In UHV and XHV they pump hydrogen better than other kinds of pumps. NEG pumps have other very interesting capabilities that make them attractive in many circumstances. As mentioned above, they maintain constant pumping speed over a wide pressure range. They are clean, lightweight and compact for their pumping capabilities. They can help provide better ultimate vacuum than is achievable without them. They are vibration-free. They operate unaffected by magnetic fields, and do not generate magnetic fields.

NEG pumps work by chemical reaction and phase change. There are two types of sorption by NEG pumps: reversible and non-reversible. Hydrogen is the only gas that is sorbed reversibly (this also includes the isotopes of hydrogen). Carbon, nitrogen, and oxygen form stable chemical compounds with the NEG alloy and are sorbed irreversibly. There are three parts of sorption of gases by a NEG pump: surface sorption, dissociation, and bulk diffusion. All sorption by a getter is of atoms, not molecules. All species go through the dissociation and surface sorption. So the NEG pump removes water vapor from a vacuum chamber by reacting with oxygen and hydrogen, not with the water molecule. Hydrogen molecules that land on the surface of the getter material split into two hydrogen atoms and diffuse into the bulk of the getter, forming a solid solution. This happens when the concentration of hydrogen in the getter material is at low to moderate levels. At these levels, the hydrogen does not react with the getter metal to form a new compound as the irreversibly sorbed gases do. It is distributed nearly uniformly throughout the bulk of the getter alloy. At room temperature hydrogen diffuses into the bulk of the getter, but carbon, nitrogen, and oxygen do not [40].

Figure 11: Photograph of the SAES Getters CapaciTorr pump models that use a 2 1/2” Conflat flange. The D-400 cartridge uses St 172 (Zr-V-Fe) getter alloy. CapaciTorr pumps use porous sintered getter elements in the cartridge

A commercially available NEG pump is shown in Figure 11. It consists of a flange, heater, and NEG cartridge. The heater and flange are usually combined in one unit, and

the cartridge is installed onto that unit. When the cartridge is new or when it has been exposed to atmosphere, the getter material has a passivation layer on its surface and need to be activated to be ready for use [12, 13, 36, 41]. The passivation layer allows the getter material to be handled safely in air. This layer is primarily composed of a thin, very dense layer of oxides, nitrides, carbides, . The passivation layer is a barrier to further reaction of the getter material with active gases. Familiar examples of materials that are protected from ongoing reaction with gases in the environment are stainless steel and titanium. Stainless steel and titanium are actually very reactive metals, but they form a very dense passivating oxide layer on their surfaces, which prevents further reaction. Once the getter pump is installed onto a vacuum system and the system is pumped to a suitable pressure, the pump must be heated to achieve "activation." Here, the term "suitable pressure" means at least 10^{-4} mbar, but lower pressures, such as 10^{-6} mbar or better, are preferable.
Heating of getter material promotes the bulk diffusion of oxygen and carbon of the passivating surface layer until the surface is sufficiently clean to start sorbing the active gases as it shown at Figure 12.

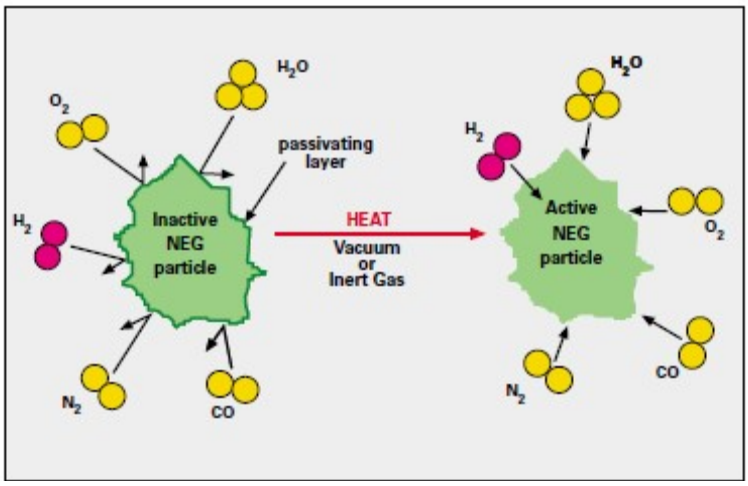

Figure 12: Representation of the activation process for a nonevaporable getter [40].

Gases which are present in vacuum devices or common residual gases in vacuum systems are: H_2, H_2O, CO, CO_2, O_2, N_2, hydrocarbons and noble gases. The first six are active gases because they can chemically interact with getter materials. Hydrocarbons are not considered active gases [12]. Hydrocarbons can be sorbed when the getter material is exposed to sufficiently high temperatures. As mentioned before, hydrogen is sorbed reversibly, while carbon remains permanently fixed. If noble gases are present in the vacuum system, they cannot be sorbed by the getter pump, because they are not active gases. In this case their removal from the vacuum system has to be achieved by other pumps. Due to the absence of chemical interaction of noble gases with getters they can be used for the purification of these gases. We will discuss more about the activation process later in Chapter 4.

During activation, the oxygen contained in the surface passivation oxide layer is dissolved into the material bulk by heating. So the selected materials should provide a reasonable solubility limit for oxygen [42, 43]. Another essential property is the high diffusivity for oxygen. In addition to the high solubility and diffusivity of oxygen, the NEG material should also have a high reactivity, i.e. large enthalpies of adsorption, for the main gases to be pumped in the UHV vacuum system, such as CO, CO_2, H_2 and a low dissociation pressure for hydrogen to provide low H_2 partial pressure in the system. In contrast to oxygen, it is not so crucial for the solubility limit for hydrogen to be high, because H_2 can

be released by heating and the NEG pump can be regenerated.

The selected getter material should also provide other essential features, namely good adhesion to the metal substrate, high mechanical resistance and high melting point [42, 43]. Among the many elements that provide good gettering properties, the transition metals of the 4B group of the periodic table (Ti, Zr, Hf) fulfill the most restrictive condition of the high solubility limit for oxygen, which exceeds 10% only for these elements. Another family of elements, the transition metals of 5B group (V, Nb, Ta) provide much higher oxygen diffusivity but a lower oxygen solubility limit. Therefore, elements of the 4B and 5B groups and some of their binary and ternary alloys have been taken as a starting point for development of different getter alloys [12, 42].

The St 707 getter material is a ternary alloy whose nominal composition by weight is: Zirconium (70%), Vanadium (24.6%) and Iron (5.4%). Activation conditions and gettering efficiency of St 707 is given in the Figure 29**.** From this figure we can see that St 707 can be partly activated already at a temperature around 200 °C. SAES Getters recommend a standard activation condition at 450 °C for 45 min.

St 172 nonevaporable getters have been developed by SAES Getters to fulfill the market needs for a sintered porous getter which is able to be activated at lower temperatures [40]. The zirconium content is about 40% by weight. The St 172 getter material is a mixture of Zirconium and St 707. The use of a high diffusivity alloy like the St 707 means that St 172 can reach an appreciable degree of activation in a temperature interval from 250 °C to 450°C. For the same reason the diffusion into the bulk of oxygenated gases and N_2 sorbed on the getter surface takes place at 150- 200°C. Recommended activation condition is 450 °C for 10 min.

St 122 is a mixture of Titanium and St 707. This non evaporable getter has low activation temperature (300 – 500 °C) and high sorption performance at room temperature. It was developed for some special applications like field emission displays (FED).

2 Aims and Hypothesis

The main purpose of this dissertation was to explore extension of the lower measure range of primary vacuum calibration methods using non-evaporable getters.

To achieve this goal, following phenomena were addressed:

1. Study of methods to reduce hydrogen outgassing of stainless steel, which is the main factor affecting lower pressure limit of static and continuous expansion vacuum standards and also all other extreme high vacuum systems .
2. Investigation of activation procedure and diffusion of oxygen in into non-evaporable getters bulk to get required pumping performance in vacuum calibration systems
3. Application of NEGs in a model primary static expansion vacuum calibration systems to demonstrate the benefit of reducing contamination of calibration gas by outgassing
4. Design of a gas flow meter for very low flows of inert gases
5. Design of a vacuum system for calibrations by orifice flow method with a base pressure in XHV range (of the order of 1×10^{-12} mbar)

In well outgassed ("baked") stainless steel vacuum systems the dominant remaining outgassing component is hydrogen, which is generated by diffusion of dissolved hydrogen atoms from the bulk toward surface, where two hydrogen atoms recombine and desorb into vacuum [44]. To reduce hydrogen outgassing from stainless steel chamber walls, the concentration of dissolved hydrogen in material has to be reduced.

NEGP has two remarkable characteristics, one is the large pumping speed for active gases, especially for H_2 at ambient temperature, and the second is a virtually zero pumping speed for inert gases [45, 46]. So the use of NEGP together with reduction of hydrogen outgassing may help to maintain the background in critical components of primary vacuum calibration systems at XHV level, without changing the gas quantity in the calibration chamber when an inert gas is used as a calibration gas.

2.1 Application of getters in model primary vacuum systems

Static expansion and continuous expansion are primary techniques used to generate calibration pressures for high vacuum gauges. Outgassing rate of hydrogen is the main problem to extend the lower measured limit of primary vacuum calibration methods. Using nonevaporable getters this problem can be diminished because of two remarkable properties of noneveporable getters: almost zero pumping speed for inert gases and high pumping speed for active gases, especially for hydrogen.

2.1.1 Application of getters in dynamic expansion systems

In a dynamically pumped vacuum system the equilibrium pressure in the system is proportional to the sum of outgassing flux and other gas sources and inversely proportional to the available pumping speed. In continuous expansion calibration systems the pumping speed is deliberately limited to few tens of l s^{-1} to retain as close as possible a Maxwellian distribution of gas molecules. It has been accepted on the basis of consensus that the area of the opening in the orifice shall be less than 1/1000 of the inner surface area of the calibration chamber [28]. If the inner surface area of the calibration chamber is A_1 and the area of the opening of orifice is A_0, the ratio A_1/A_0 >1000 assures nearly Maxwellian distribution of gas molecules in the calibration chamber [47]. The typical ratio in primary dynamic expansion systems is $A_1/A_0 = 5000$.

In such conditions it is possible to calculate the ultimate pressure in the calibration chamber. Knowing the dimensions of the dynamic expansions system at NIST which are given in the introduction, where the surface area of the orifice is A_0 =0.95 cm^2 and the area of the inner surface of the calibration chamber is A_1 = 4000 cm^2, the achievable ultimate pressure in the calibration chamber is:

$$P_u = \frac{q\left(\frac{A_1}{A_0}\right)}{C_0} \tag{20}$$

where q is outgassing rate and C_o is conductance of the orifice per unit area:

$$C_0 = 3.64\left(\frac{T}{M}\right)^{\frac{1}{2}} \tag{21}$$

where M and T are the molecular weight and temperature of the gas used respectively. From Eq. 21 we get for H_2 at T=296 K the conductance per unit area C_0 = 44 l s^{-1}. Assuming outgassing rate $q = 1\times10^{-12}$ mbar l $s^{-1}cm^{-2}$ we obtain from Eq. 20 the ultimate pressure $P_u \sim 1\times10^{-10}$ mbar.

This ultimate pressure can be reduced by baking out the chamber and using NEGP.

2.1.2 Application of getters in static expansion systems

In static expansion systems outgassing rate determines the rate of pressure rise in expansion volumes. The volume ratio of static expansion chambers can be determined from the ratio between pressures before and after expansion only when the total amount of gas remains unchanged. Because of outgassing from the chamber walls, it becomes difficult to fulfill this condition in practice when the gas pressure after expansion is

reduced below 10^{-5} mbar. From Figure 4 it can be seen that the uncertainties of the generated pressures in the static expansion systems are mainly determined by the uncertainties of the expansion ratios and by the temperature measurements. For pressures below 10^{-4} mbar the uncertainty due to outgassing increases significantly (red curve) [12]. If we extrapolate (Figure 13, red line) to lower pressure we can see that for pressure 10^{-6} mbar the uncertainty contribution due to outgassing increases to a few % and becomes the dominant contribution. Because of this fact the main task in reducing the uncertainty of generated pressure in static expansion system is to reduce influence of outgassing.

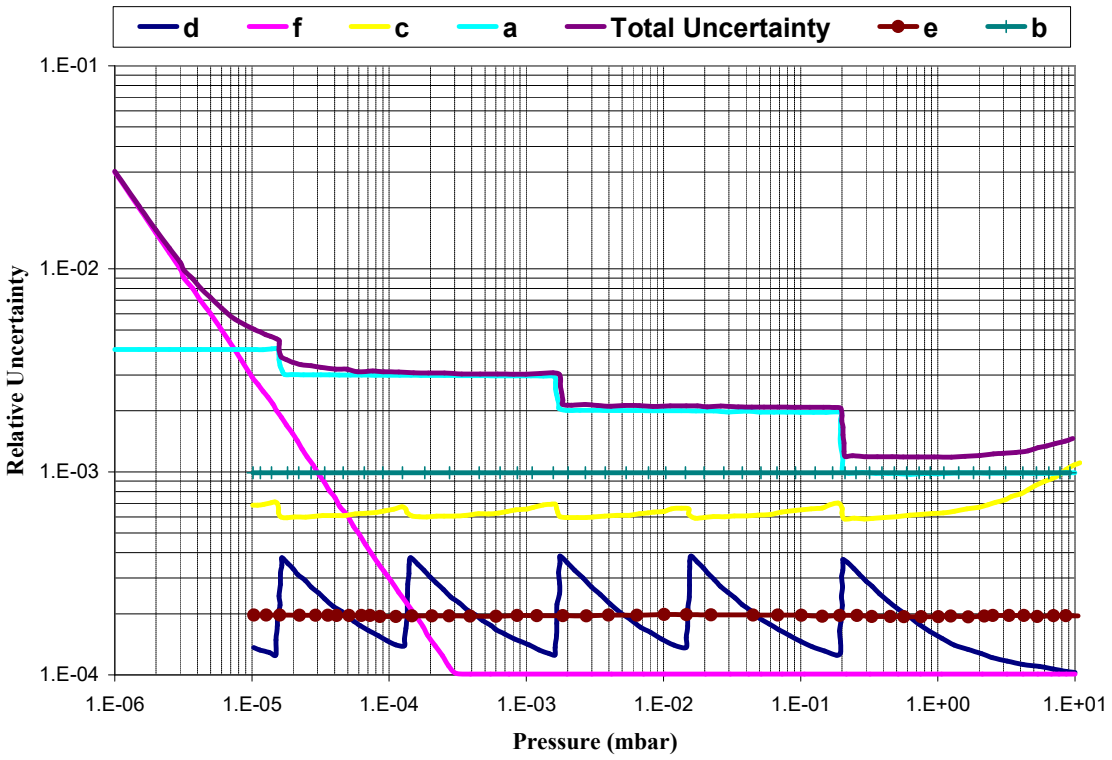

Figure 13: Extrapolated curve of uncertainty of generated pressure (from Fig. 4) due to the outgassing effect of inner surface of calibration chamber in static expansion system constructed in PTB.

2.2 Critical analysis of existing XHV orifice flow calibration systems in other laboratories

As mentioned above, under conditions of the molecular flow regime, the known gas flow is injected into the calibration chamber continuously and pumped through an orifice of known conductance. Through this method the dynamic equilibrium pressure, which can be calculated accurately, is obtained in the calibration chamber. This pressure is reference (standard) pressure for calibrating vacuum gauges. However, the lower limit of calibration pressure in continuous expansion method is only down to 10^{-9} mbar and this is limited due to residual pressure in the calibration chamber and by the lowest flow rate that can be generated with sufficient accuracy in the flowmeter. In order to extend the lower pressure limit of dynamic flow method to XHV in the calibration chamber we have to reduce the ultimate pressure in the calibration chamber and also extend gas flow rate measurement capabilities to lower values.

2.2.1 PTB system

The further reduction of calibration pressure to XHV was realized at PTB in Germany by applying a gas flow divider technique [18]. Their system is schematically shown in Figure. 14. The gas flow generated by the flowmeter is injected into a flow division chamber and then divided into XHV and UHV calibration chambers through two orifices with largely different conductances. Nominal values of conductances are C_{01}=5 l s^{-1} and C_{02}=0.05 l s^{-1}. So the system is constructed in such manner that XHV chamber through C_{01} takes up 1% of the gas flow, while the UHV calibration chamber through C_{02} takes up 99% of the gas flow. As can be seen from Figure 14 both calibration chambers are evacuated with large cryo condensation pumps during calibration. So the generated pressure in V_1 will be a factor of 100 higher than in V_2. The pumping speed of cryo pumps is 10000 l s^{-1} while effective pumping speed of calibration orifices C_1 and C_2 for N_2 is 100 l s^{-1}.

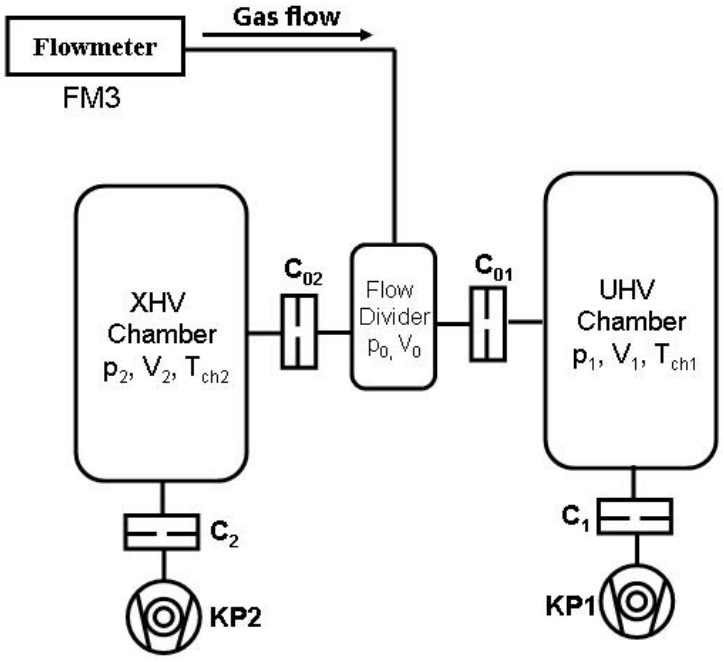

Figure 14: Scheme of the calibration system CE3 at the Physikalisch-Techniche Bundesanstalt for the continuous expansion method with flow divider technique. KP:Cryo condensation pumps [97].

To obtain the very low outgassing rates of 10^{-14} mbar l s^{-1} cm^{-2}, PTB used chambers made from austenitic stainless steel (AISI 316 LN), vacuum fired at 950 °C for 2 h. However, a residual pressure of 9×10^{-12} mbar has been obtained in the XHV calibration chamber (after in situ bake out at 120 °C for 60 h).
With the flow divider technique the primary system constructed in PTB can generate changes of calibration pressure of the order 1×10^{-12} mbar, but only as addition to the ultimate pressure of 9×10^{-12} mbar. This means that the lowest pressure during calibration can be only around 1×10^{-11} mbar.

2.2.2 LIP system

The XHV calibration system of Lanzhou Institute of Physics (LIP) in China can be seen in Figure 15. It is also using flow division technique like in PTB. LIP calibration apparatus can be roughly divided into three parts, that is, XHV system, UHV system, and

flow separation system [19, 48]. To reduce the outgassing rate the XHV chamber was made of stainless steel SS 316 L; vacuum fired at 950 °C for more than 2 hours. The conductance of the orifice 9 for Nitrogen is 100 l s^{-1}.

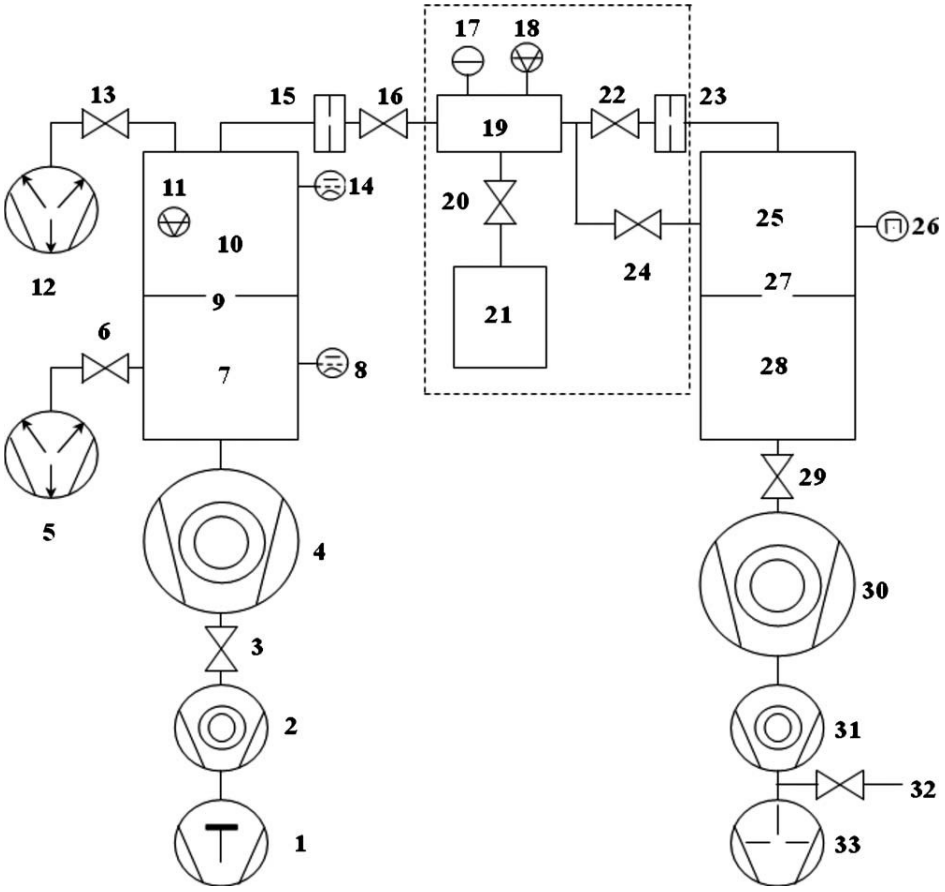

Figure 15: The scheme of the UHV/XHV calibration apparatus. 1-dry pump; 2,30,31-turbomolecular pump; 3,6,13,16,20,22,24,29 - isolation valve; 4 - MTMP; 5,12 – NEGP; 7 – XHV pumping chamber; 8,14 – hot cathode ionization gauges; 9,15,23,27 – orifice; 10 – XHV calibration chamber; 11,18 – SRG; 17 – CDG; 19 –separated flow chamber; 21 –flowmeter; 25 –UHV calibration chamber; 26 –cold cathode ionization gauge; 28 –UHV pumping chamber; 32 – venting valve; 33 –rotary pump. Reprinted from [19] with the kind permission of AIP.

The XHV pumping system is the combination of Maglew turbo (with pumping speed 2200 l s^{-1}) and two NEG pumps CapaciTorr B-1300. To increase the pumping capability for the low compression ratio gas, especially for H_2 and He, two turbomolecular pumps are used in series. The combination of MTMP and NEGP results in the large pumping speed for H_2, because H_2 is the main residual gas in this range of vacuum.
Even by using NEGP, LIP reported that the residual pressure still was 7.9×10^{-12} mbar which is quite similar to the PTB system.

The two primary calibration systems for the lowest pressure that were published up to now by PTB and LIP are limited by the ultimate pressure in XHV calibration chambers to approximately 8×10^{-12} mbar. This means that up to now there are no systems available in the world which could offer calibrations over the full measuring range of available XHV ionization gauges like extractor gauges (down to 1×10^{-12} mbar).

2.3 Proposed solution for improving volume ratio measurements in SE systems at low pressure and extension of SE range

To reduce the outgassing rate of stainless steel chambers the established procedures are [49]:

- Surface treatments in order to reduce surface roughness and create oxide layer (oxide layer acts as a barrier for diffusion of hydrogen from the bulk).
- Vacuum firing (high temperature bake-out) become an alternate method and widely accepted practice for reducing the amount of hydrogen dissolved in SS.

But these methods do not completely eliminate the outgassing effect. Therefore, the extension of lower pressure limit of the static expansion method can be done using a non-evaporable getter pump (NEGP) if an inert gas is used as a calibration gas, because NEGP pumps hydrogen and other active gases but have a negligible pumping speed for inert gases.

2.4 Proposed solution to reach XHV in a DE calibration system

- reduction of outgassing by
  - low T bake out (long time...)
  - thin wall of vacuum chamber, minimizing massive SS parts (flanges, valves...)
  - reduced surface area (smaller chamber- but also smaller orifice...)
- use of NEGP with high pumping speed for H_2
  - setting NEGP directly inside the calibration chamber

2.5 Flow meter for generating a very low flow of inert calibration gas

It is a common requirement of all the various types of gas flow calibration devices that the gas flow rate to the apparatus needs to be measured precisely. As mentioned in the introduction (paragraph 1.1.3) different methods may be uses for this purpose. In PTB and LIP they used a flowmeter based on constant pressure variable volume. Through this method it is very difficult to measure the gas flow (throughput) $< 8\times10^{-8}$ mbar l s^{-1}, because at lower fill pressures (< 0.1 mbar) the change of volume ΔV is to small to obtain sufficiently large pressure changes in the working volume compared with short and long term pressure drifts on the CDG. So the throughput (gas flow) generated by flowmeter in PTB and LIP is injected into flow separation chamber and then divided into XHV and UHV calibration chambers through two largely different orifices. Only 1% of the gas flow from the flowmeter was directed into XHV calibration chamber, which means the gas flow in XHV calibration chamber, can be reduced down to 10^{-10} mbar l s^{-1}.

The possible solution to go to lower throughput is:

- to decrease the influence of outgassing of flowmeter chamber using NEGP.
- to use variable leak valve to control gas flow. Leak valve should be operated in molecular flow regime, where the conductance is proportional to pressure. If conductance is known, the throughput can be reduced by reducing gas pressure at the high pressure side of leak valve.

3 Construction of Ultra High Vacuum (UHV) and Extreme High Vacuum (XHV) Systems

The word “vacuum” comes from the Latin “vacua”, which means “empty”. However, there does not exist a totally empty space in nature, there is no “ideal vacuum”. So vacuum is only a partially empty space. In scientific/engineering terms, a vacuum is referred to as a space in which gaseous pressure is less than standard atmospheric pressure on the Earth's surface. The pressure on earth surface is 1013.25 mbar (101325 Pa). One can also express the level of a vacuum in a space by the gaseous density, which is about 3×10^{19} atoms per cubic centimeter (cm^{-3}) at standard atmospheric pressure. If we consider that creating a vacuum is nothing more than removing gas molecules from the chamber until the number of molecules per volume is less than the number of molecules in the same volume outside the chamber, we can begin to develop a set of reasons for doing so. This lowered molecular population can be viewed as pressure, number of molecules, distance between molecules, number of molecular collisions, or number of collisions of molecules with a surface. Although all of these views are physically interconnected and mutually interdependent, any one of these possible reasons can be carried into process description with its attendant requirements and justifications

3.1 Basics of UHV/XHV system constructions

Technically, vacuum levels are broadly categorized as ranges shown in Figure 16. While Ultra high vacuum (UHV) is defined as the range of pressure between 10^{-8} to 10^{-12} mbar and extreme high vacuum (XHV) ranges below 10^{-12} mbar, in addition the vacuum range of UHV in USA is defined as the range of pressure between 10^{-9} and 10^{-12} mbar.

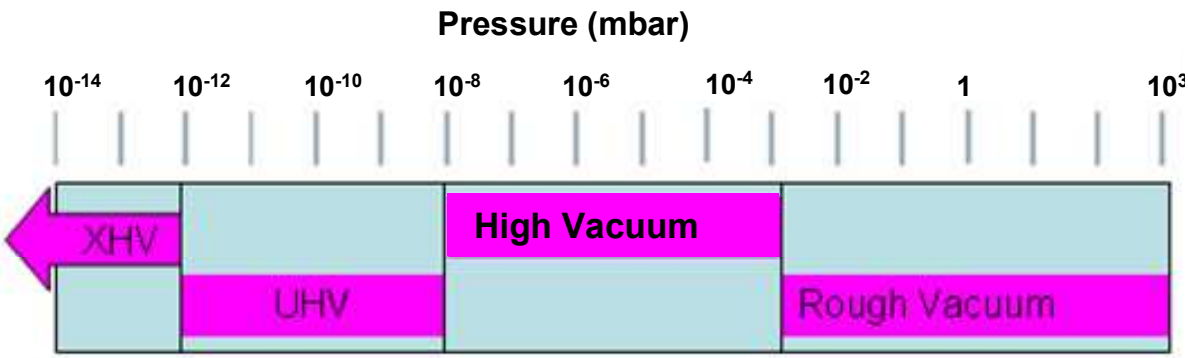

Figure 16: Overview of classification of vacuum ranges

UHV is widely used in industry in the development and manufacture of semiconductor devices to keep surfaces uncontaminated during processing and testing. UHV technology is widely used in industry and the laboratory whenever it is essential to keep surfaces free from contaminations, gases pure and charged particles unscattered. So the need for UHV is widespread, whereas XHV is achieved in only a few specialized laboratories (physics research) with difficulty although using special equipment and procedures. The need for XHV is limited at this moment to some accelerator and storage ring facilities, to simulation of interstellar space, processing of advanced semiconductor devices, and to a few other specialized applications.
It is routine to generate rough to high vacuum by using off-the-shelf equipment. To achieve UHV and XHV, however, is everything but routine. Only certain types of clean vacuum pumps are suitable to use in these pressure ranges. Not only one have to ensure that the vacuum enclosure is absolutely leak-free, but it is also vital to have everything in the interior of the vacuum enclosure clean. Any contaminants, such as machining oil, residual grease from a finger print, on an in-vacuum part will compromise its ability to reach UHV/XHV. The development of vacuum technique adequate to reach ultrahigh vacuum started with Langmuir and his associates in 1912-1913.
Table 3 indicates the variation of molecular density, mean free path and monolayer coverage time with pressure. In this table in a general way the properties of the UHV and XHV environment are presented, which make it essential for studies requiring clean surfaces, pure gases and unscattered particles.

Table 3: Gas phase parameters at UHV/XHV

Pressure [mbar]	Molecular density (298 K)	Molecular Mean Free Path (N_2 at 295 K)	Monolayer time
10^{-6}	$2.5\times10^{10}\,cm^{-3}$	34 m	0.95 s
10^{-9}	$2.5\times10^{7}\,cm^{-3}$	34 km	16 min
10^{-12}	$2.5\times10^{4}\,cm^{-3}$	3.4×10^{4} km	22 days
10^{-15}	$2.5\ cm^{-3}$	3.4×10^{7} km	60 years
10^{-19} (interstellar space)	$0.25\ m^{-3}$	0.03 light years	6×10^{5} years

Designing vacuum systems comprises a number of tasks from different engineering disciplines such as mechanical engineering, electrical and electronic design, software engineering, and vacuum engineering. The main tasks in the vacuum engineering step are the selection of appropriate types and sizes of pump sets, sizing of pipework, valves, and other components influencing pressure of flow distribution in the system according to the process requirements [50].

The pump set on a vacuum system has to perform two tasks.

- It has to evacuate the system starting from atmospheric pressure within a certain time
- It must be able to maintain a specific pressure during the vacuum process operation

The problems in achieving UHV and XHV can be seen in a general way by examining the conservation of mass equation for the vacuum system of volume V and surface area A, pumped by a pump of speed S with a leak rate L and an outgassing rate per unit area q. If L, q, and S are constant and a single gas is predominant, we obtain,

$$V\frac{dp}{dt} = L + qA - Sp \tag{22}$$

It is essential for the UHV/XHV system the leak rate to be $L=0$, and when ultimate pressure is reached, this means that $dp/dt = 0$. After that from Eq. (22) we obtain:

$$p_{\text{ult}} = \frac{qA}{S} \tag{23}$$

From equation (23) there are two main requirements to reach ultimate pressure p_{ult} in the UHV and XHV systems. To reduce ultimate pressure one needs to decrease outgassing rate q and/or to increase pumping speed S.

The maximum pumping speed that can be applied to a vacuum system of arbitrary size is approximately proportional to the surface area of vacuum system. The outgassing rate in this case is from the walls and internal parts of the system, and in particular from vacuum gauges, residual gas analyzers and other components with a hot cathode. Thus from equation (23), it is obvious that when the maximum pumping speed is applied to a system, the ultimate pressure is proportional to the outgassing rate and is independent of the system volume. The principle method to reduce outgassing is baking at elevated temperature for sufficiently long time. Achieving UHV and XHV is a very complex work. Further discussions will be about factors that influence this aim.

3.2 Outgassing of vacuum materials

Requirements for materials of vacuum technology are manifold, depending on the particular type of usage (depending what they will be used for). Choosing the materials to use in a vacuum system design is not just a case of finding the materials with the lowest gas loads (outgassing), but to also consider the various physical or chemical properties that will fulfill the process's requirements. The main requirements that a material has to fulfill his use in building vacuum systems are [51, 57]: sufficient mechanical strength, corrosion resistance, high gas tightness, low intrinsic vapour pressure, low foreign-gas content, favorable degassing properties, high melting and boiling points, clean surface, adopted thermal expansion behavior and high thermal fatigue resistance. These requirements become more specified in the case when we want to build UHV/XHV systems.

Any material which has been exposed to - or manufactured in – atmospheric air will have gas adsorbed on the surface, or either dissolved or absorbed in the bulk. During evacuation, therefore, the walls of a vacuum system and the components and material being processed inside will tend to re-emit (release) this gas. This phenomenon is generally termed outgassing. Redhead [52] gives the definition of two terms of outgassing: outgassing flux and outgassing rate. According to Redhead, outgassing flux of a solid or liquid is the quantity of gas leaving the surface per unit time. Whereas the outgassing rate of a solid or liquid is the quantity of gas leaving per unit time per unit of exposed geometric surface. This gas release is actually a result of several processes. Figure 17 shows the possible sources of gas in addition to the gas located in the volume of the chamber: They include leaks through any connections (flanges etc.), leaks from

trapped gases (such as inside screw holes), permeation through the chamber wall (including diffusion from the bulk), and desorption of water and other gases from all inside surfaces. Gases and vapors released from the surface are a result of vaporization, thermal desorption, diffusion, permeation, and stimulated desorption.

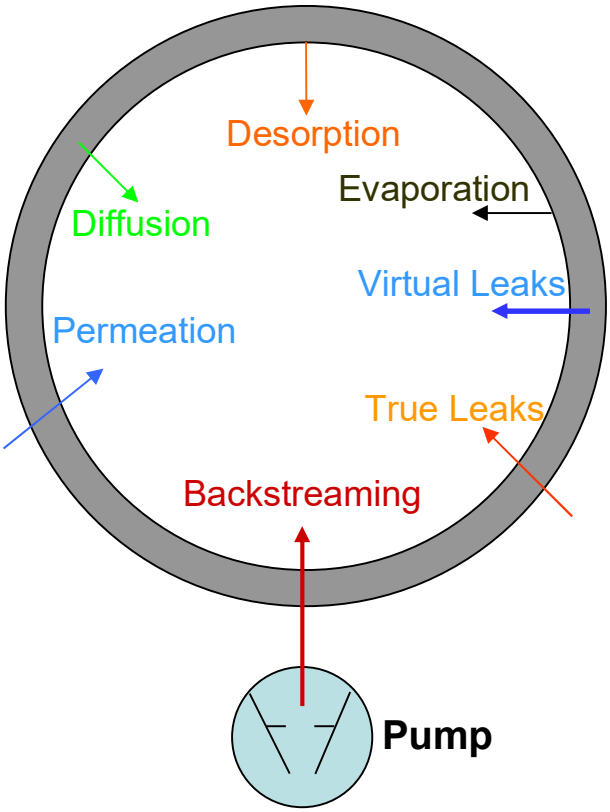

Figure 17: Potential sources of gases in a vacuum system.

The outgassing from a surface will act as a gas source and after the removal of the most of the "volume" gas, will determine the system pressure. The outgassing rate from a surface decreases gradually as a function of time under vacuum. The outgassing rate of the various materials is given in the Table 4. In general, organic materials have an outgassing rate about 4 orders of magnitude higher than inorganic materials so one should stay away from organics wherever possible, the organics should not be part of the UHV vacuum envelope because of permeation issues as well.
The development of the science and technology of ultrahigh vacuum (UHV) and extremely high vacuum (XHV) have been strongly coupled to the development of increasingly larger and more sophisticated devices for physics research, such as particle accelerators, magnetic fusion devices, gravity wave observatories and many surface analysis techniques. Associated with these technological developments are scientific advancements in the understanding of outgassing limits in UHV/XHV.
The performance of vacuum system is limited because it is impossible to eliminate all sources of gas in vacuum systems. Even in the best-designed vacuum systems for UHV/XHV outgassing is present.

Outgassing means usually two things [44]:

a. Molecules diffusing from the bulk material of a vacuum chamber, entering the surface and desorbing from it.
b. Molecules which have been adsorbed previously, usually during venting of the vacuum chamber, that desorb again, when the chamber is pumped to vacuum.

Table 4: Outgassing rate of various materials after 1 hour under vacuum [58, p.49]

Material	Outgassing rate [mbar l $s^{-1}cm^{-2}$]
Aluminum (fresh)	8.4×10^{-9}
OFHC Cooper (mech. Polished)	4.7×10^{-9}
Stainless Steel (mechanical polished)	2.3×10^{-9}
Stainless steel (vacuum baked at 250 °C for 30 h	4.0×10^{-12}
Aluminum (vacuum baked at 250 °C for 15 h	5.3×10^{-13}
Pyrex (fresh)	9.9×10^{-9}
Neoprene	4.0×10^{-5}
Polystyrene	2.7×10^{-5}
Plexiglas	4.1×10^{-6}
Viton A	1.5×10^{-6}
PVC (24 h at 95% RH)	1.1×10^{-6}
Teflon	8.7×10^{-8}
Viton A (baked)	1.1×10^{-8}

Due to vaporization or sublimation of atoms and molecules from some materials with a vapour pressure higher or comparable to the vacuum pressure, those materials will contribute to increase the effect of outgassing. For this reason not all types of materials can be used to build vacuum systems, and sometimes it is very difficult to select appropriate materials that will fulfill the requirements of the processes. Therefore, among technical alloys stainless steel exhibits several advantages compared to other alloys, so it is the most widely used as a construction material for building of vacuum chambers, instruments and components. Stainless steel (SS) is by far the most important construction material for UHV systems because of its good vacuum and mechanical properties [53]. 1. SS it is corrosion resistant and chemically inert, nonmagnetic, 2. it can be machining and welded by standard procedure, and relatively cheap, 3. SS has negligible vapor pressure at room temperature, negligible permeation of atmospheric gasses [49].

It is generally agreed that outgassing of hydrogen from stainless steel is the main gas load in UHV/XHV systems [51]. So, in stainless steel vacuum systems hydrogen outgassing is the most significant factor limiting the attainment of outgassing rate below 10^{-12} mbar l s^{-1} cm^{-2} [54]. By reducing the hydrogen content in the bulk the hydrogen outgassing can be reduced to lower values.

Techniques that may be used for the mitigation of outgassing of vacuum systems are described in many papers:

a) Surface treatments to reduce surface roughness. This includes electro-polishing and surface machining under special conditions[49]
b) Surface treatments to create oxide or other films to act as a barrier for diffusion of hydrogen from the bulk [49]
c) High temperature bake-out (vacuum firing) to reduce the amount of dissolved H (for stainless steel as high as 1000 °C) [12]
d) Baking the vacuum system to remove water vapour. It has to be done at 150-450 °C [12]
e) Degreasing and chemical cleaning [12]
f) Deposition of films as a barrier layer on internal surface [55]
g) Choose a metal with low solubility for hydrogen (e.g. copper) [12]

h) Reduce surface mobility by introducing surface trapping in order to reduce the recombination [55]
i) Decreasing surface outgassing by thin film getter coatings [56]

The published results of outgassing rates from stainless steel are often inconsistent, so there are still challenges for the future work in this field.

3.3 Factors involved in the achievement of UHV/XHV

The major steps in building vacuum systems are: designing the system, cleaning and preparing the system for the use, pumping it down, baking it etc [49]. Construction of a vacuum system is unforgiving of mistakes. A careful analysis of the materials that will be exposed to the vacuum system will help avoid those dire mistakes that can kill the design [49, 54, 55].

3.3.1 Materials for construction of UHV/XHV systems

A typical ultrahigh vacuum system consist of a stainless steel chamber with a variety of ports to accommodate pumps, gauges, instrumentation, sample manipulation, windows, and interconnection with other chambers.

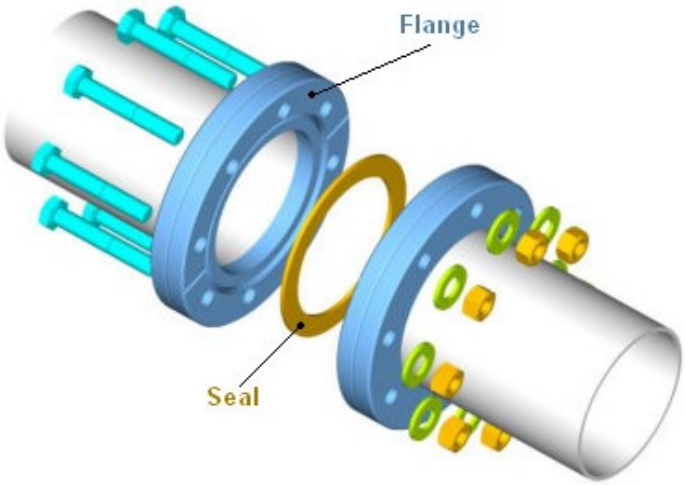

Figure 18: Schematic diagram of a conflat flange before assembly, showing the copper gasket between the two mating surfaces. Photo from Trinos Vacuum Systems Inc. Catalog [59]

All of those components have to be baked in order to decrease the outgassing rate**.** Components are most often made from 304 stainless steel. For special applications they can be also made from 316 stainless steel which is more expensive. Connections to the ports have to be made via “CF” or “Conflat” flanges, which are bolted together. Conflat flanges are sealed by means of a cooper gasket which is sandwiched between knife edges on the mating stainless steel faces (see Figure 18). A new gasket should be used each time the flanges are bolted together, and the bolts should be tightened evenly around the perimeter of the flange. It is more important to tighten the bolts evenly than to do them up extremely tightly. If the knife edge on either flange is damaged (for example by scratching or hitting), it may no longer be possible to make a UHV/XHV seal. It is therefore of great importance to avoid damaging the knife edges.
Because the vacuum is very sensitive to the desorption rate of materials inside the chamber, many common materials are unsuitable for use in UHV/XHV because of their

high vapor pressure. In particular, most organic materials including lubricants must not be used in UHV chamber. Table 5 shows a selection of suitable and unsuitable materials for UHV. Thus, the main requirements specific to materials which can be used to build UHV/XHV systems are [57].

- strength (sufficient to accommodate the structure of the system and hardness sufficient for metal to metal seals
- bake-out temperature (sufficiently high to achieve desired bulk gas depletion in a short time)
- surface finish (amenable to polishing to minimize the surface area and porosity)
- outgassing (low enough after bake-out to achieve desired UHV/XHV pressure

Table 5: A selection of suitable and unsuitable materials for use in UHV/XHV [13, 50, 57, 59]

	Acceptable	Not acceptable
Pure materials	Aluminum, copper, molybdenum, silicon, tantalum, titanium, zirconium, hafnium, tungsten, precious metals, nickel,	Zinc, cadmium, lead
Stainless Steel	316LN, AISI 316L, AISI 304L	
Alloys	Copper-beryllium, aluminum alloys, nickel alloys,	Brass, zinc alloys
Insulators	Ceramics: Al_2O_3, BeO, MgO, ZrO_2, Glasses: soda lime, borosilicate, potash soda lead Macor, Kapton, sapphire	Organic materials (with some exceptions)

3.3.2 Surface conditioning

Desorption of surface gas is a major component of outgassing load and it is therefore to be expected that the condition of internal surface layers play important role. Significant factors include: chemical compositions, structure and thickness of oxide layers since these affect adsorption and desorption from the surface as well as diffusion from underlying metal. Outgassing rate can be reduced by proper surface treatment affecting surface chemistry, surface structure and surface cleaning.

Not only do we have to be careful about what materials go into an ultrahigh vacuum chamber, we also need to be careful about how we clean and handle components that will go into UHV/XHV. In particular, all components need to be “degreased” before going into the vacuum chamber. Dusts can be removed from components and samples by blowing a stream of dry nitrogen gas across them. All tools used for assembling components and mounting samples should be also cleaned.

The simplest surface treatment is low temperature bake-out to reduce water outgassing. When an UHV chamber is first pumped down after being vented, the dominant gas inside is water, desorbing from the walls. In order to get rid of this water, UHV chambers are baked at $\geq 100^0 C$ for 12-24 hours. This speeds up desorption of water, and after cooling down the dominant gas in the chamber is usually hydrogen.

Other techniques of surface treatment are: mechanical polishing and electro polishing which reduce surface roughness and ensure creation of controlled oxide layers, respectively.

3.4 Overview of the pumps used at UHV/XHV range

The pumpdown process that spans the entire vacuum range from atmospheric pressure to ultrahigh vacuum can be divided into three discrete zones shown in Figure 19. Since there are always gas molecules entering even the best UHV/XHV chamber, continuous pumping is needed in order to achieve UHV/XHV.

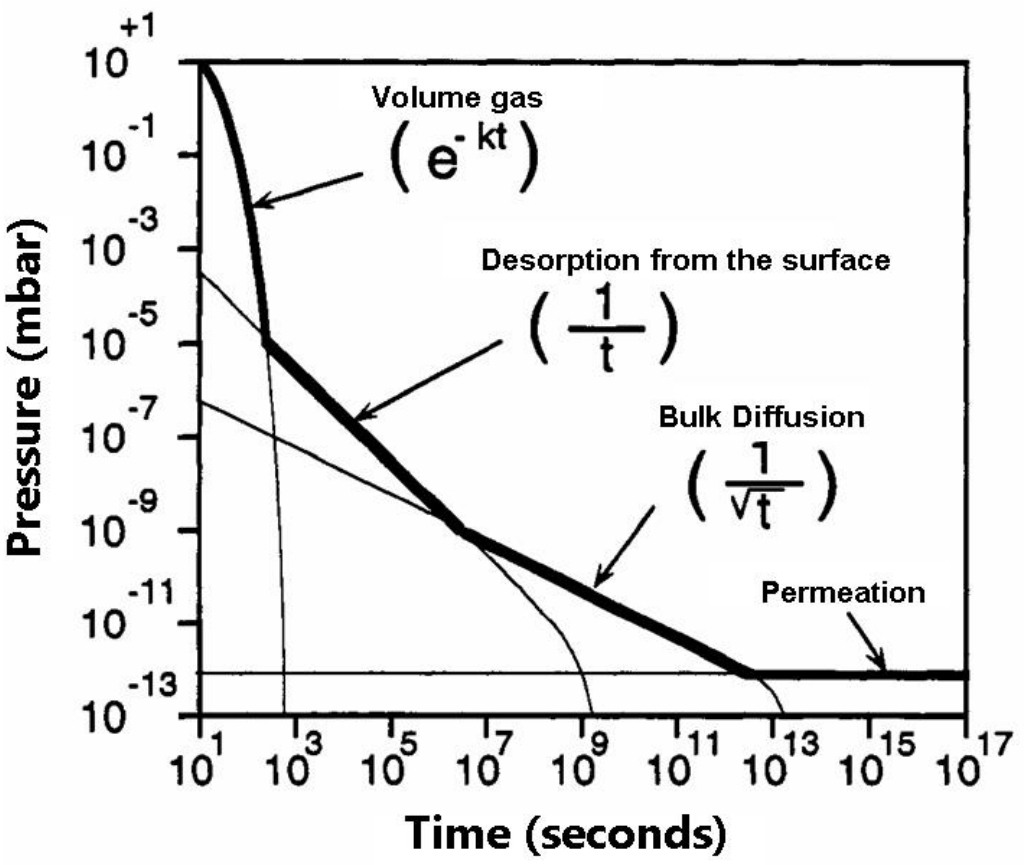

Figure 19: Pump-down curve as a function of time [61], reprinted with kindly permission of John Wiley & Sons

A particular vacuum-related process might only require pressures within a single zone, or it might require the traversing of several zones. These three distinct zones, starting at ambient or atmospheric pressure are the volume zone, surface desorption zone, and diffusion zone (so called hydrogen zone).
Vacuum pumps, either singly or, more usually, as part of a pumping system, create or maintain the conditions appropriate to a required process. As it is known pumps sets for UHV/XHV systems have to operate in the pressure range from atmospheric pressure to the system base pressure which may be 10^{-12} mbar. This range covers 15 orders of magnitude.
According to this wide range of vacuum technology, appropriate vacuum measuring and vacuum generating techniques have had to be developed, exploiting various physical properties of gases. Figure 20 shows the pressure ranges of the huge variety of vacuum pumps. An UHV/XHV pump cannot pump against atmospheric pressure but can pump against a lower pressure, so a backing pump is required to maintain a low pressure at the exhaust of the main pump. These backing pumps are also often used as a roughing pump to reduce the pressure in the vacuum chamber from atmosphere to a “rough vacuum”. For example, typical pumping speed versus pressure curves for high-vacuum and backing pump are shown in Figure 21.

Each of the types of vacuum pump available has a characteristic working range in which it is effective. Outside that range shortcomings in performance become apparent, as can be seen in Figure 21.

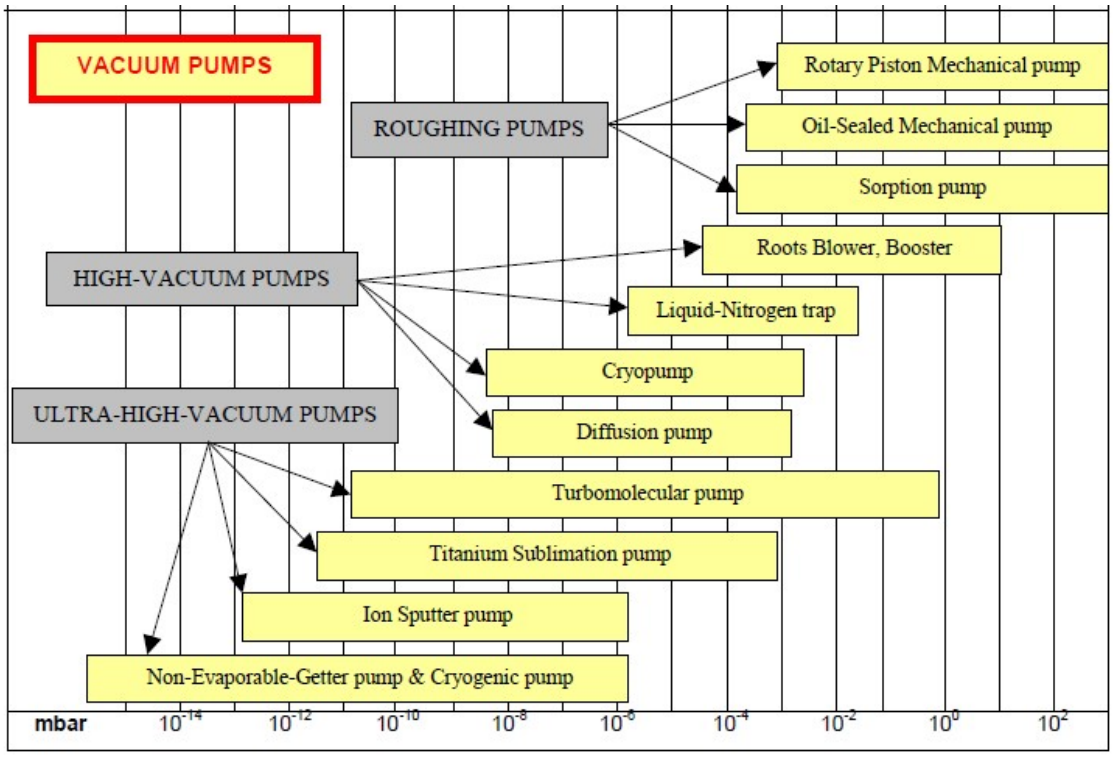

Figure 20: Pressure range of vacuum pumps [34]

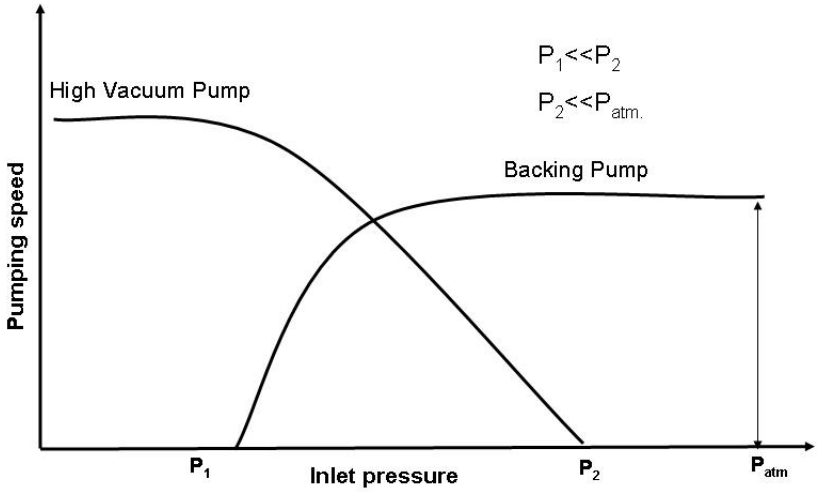

Figure 21: Backing-pressure requirements in the changeover from roughing- (backing) to high-vacuum pumps

The vacuum pumps which can reach high and ultrahigh vacuum are divided manly in two categories: kinetic pumps and capture pumps [51].
Kinetic pumps impart momentum to the gas molecules and remove them from the vacuum system. This principle is employed in diffusion pumps and turbomolecular pumps. The advantages of kinetic pumps are they can maintain a low pressure indefinitely

and remove large quantities of gas permanently from the system.
Capture pumps trap gas molecules by ionic entrapment, condensation, adsorption, or chemical reaction at a surface within the vacuum system. The disadvantage of capture pumps is that they do not permanently remove the gas from the system and they require some form of regeneration after they have pumped a specific quantity of gas [60]. Following pumps belong to this type: ion-sputter, cryo, titanium sublimation, and NEG pumps.

3.4.1 Turbomolecular pumps (TMPs)

They are compressors and are limited inherently by the low compression ratio for hydrogen which is the main residual gas in a UHV system. To achieve pressures approaching 10^{-10} mbar or less this type of pump is often combined with a titanium sublimation pump (TSP) for the above reason. TMPs can usually be baked to a maximum of about 120 °C and for some models less, hence some thought is necessary when designing connecting manifolds to avoid overheating the pump and at the same time minimizing the area of metal that is heated only to low temperature during bake out. Lower cost TMPs have hydrocarbon oil or greased bearings which is a potential source of contamination but providing the pump is operated correctly hydrocarbon molecules will not migrate into the vacuum vessel. Higher cost TMPs are available with magnetic bearings which avoid these possible problems.

3.4.2 Ion Pumps (IP)

Ion pumps will pump to 5×10^{-10} mbar or less. To go below 10^{-10} mbar they are often combined with a TSP or NEG pump. In many respects the ion pump which has no moving parts or working fluids is ideal for UHV in cases where there is no substantial process gas load. The IP does have certain characteristics which the user needs to be aware of and may cause problems in some circumstances:

(i) Selective pumping. Pumping is by gettering for chemically active gases and burial for inert gases, which occurs at a much lower pumping speed. Inert gases will therefore tend to build up as a residual gas background, the lighter noble gases (He and Ne), are particularly prone since these may diffuse out again from beneath the surface. Hydrogen readily diffuses into titanium as a solid solution, but will be released again on heating. The presence of argon in the residual gas enhances sputtering and hence the chemical removal of hydrogen as titanium hydride. Methane is normally present in the residual gas since it is generated at titanium surfaces although it is also removed by dissociation in the pump discharge.

(ii) Memory effects. These are characteristic of IPs and will affect the residual gas composition; gas ions buried in the cathodes earlier in the life-cycle are released by subsequent sputtering. The effect can be particularly bad for inert gases and leads to the phenomenon of argon instability where significant amounts of released argon lead to periodic increases of pressure. This has been designed out of some models of pump by slotted cathodes, triode structures or Ti/Ta cathodes.

(iii) No tolerance to gas load. IPs are not suitable for high gas loads and particularly inert or hydrocarbon gases; once the pressure inside the pump rises above 10^{-6} to 10^{-5} mbar, the pumping speed falls and pumping may become unstable. This can eventually lead to heating inside the pump and the additional release of hydrogen, helium and neon. Undetected leaks during

starting can be a particular problem.

(iv) IPs have magnetic fields which can interfere with processes unless screened which is not always possible. The ion pump may be operated with sorption pumps for starting, to produce a completely contamination free system. The whole system including the pump can be baked, the baking temperature depending on whether the ion-pump magnets are removed. A high vacuum valve, which increases outgassing load and reduces pumping speed, is not necessary although this can be useful for isolation for faster starting during pump-down.

3.4.3 Cryo-condensation pumps (CRP)

These pumps are limited by their capacity to cryosorb hydrogen onto cold charcoal. An ultimate system pressure somewhat below 10^{-9} mbar is typical. The capacity to adsorb hydrogen will decrease with time once the hydrogen cryosites are used up and this can result in an increase in system pressure. CRPs cannot be baked and moreover must be shielded from radiated or conducted heat caused by baking or processing schedules of the main system. The area of unbaked shields and tubulation must be minimal if UHV pressures are to be achieved. Some manufacturers have incorporated additional radiation cold shields and baffles into their pump designs to reduce the scale of this problem. Cryopumps have very high pumping speeds for water-vapour, but in a UHV system water-vapour is removed by baking so that this may not be such a great advantage. CRPs require periodic regeneration and a high vacuum isolation valve; for the lowest pressures an all metal bakeable design is necessary, but many UHV systems operate satisfactorily with a viton plate seal and copper gasket or wire seals for flanges with a bellows sealed drive. The viton seal can be baked safely to 120 °C closed and 150 °C in the open position. As stated above the area of metal not heated to the full baking temperature must be minimized.

3.4.4 Titanium Sublimation Pumps (TSP)

Those pumps are used mainly in combination with ion getter pumps and turbomolecular pumps. Evaporated titanium films at room or liquid nitrogen temperatures have been used, in combination with other pumps needed to remove the rare gases and methane, down to pressure of 10^{-11} mbar and below. These pumps need renewal of the film after about a monolayer of gas has been adsorbed.

3.4.5 Bulk getter pumps (Non-Evaporable Getter - NEG)

NEG are used mainly in combination with the pump which pumps noble gases and methane, because NEG has no pumping speed for those gases. In detail the importance of NEG in vacuum technology is described in Chapters 1 and 4. They have high pumping speed for hydrogen even in XHV below 10^{-12} mbar.

3.5 Total pressure measurements of UHV/XHV

It is a vital to understand the function and limitation of the vacuum gauges which might be used in UHV/XHV systems. The pressure range measured in vacuum technology spans across 15 powers of ten. No single gauge type covers the whole range. Figure 22 shows the range over which the various types of vacuum gauges may be used to measure pressure.

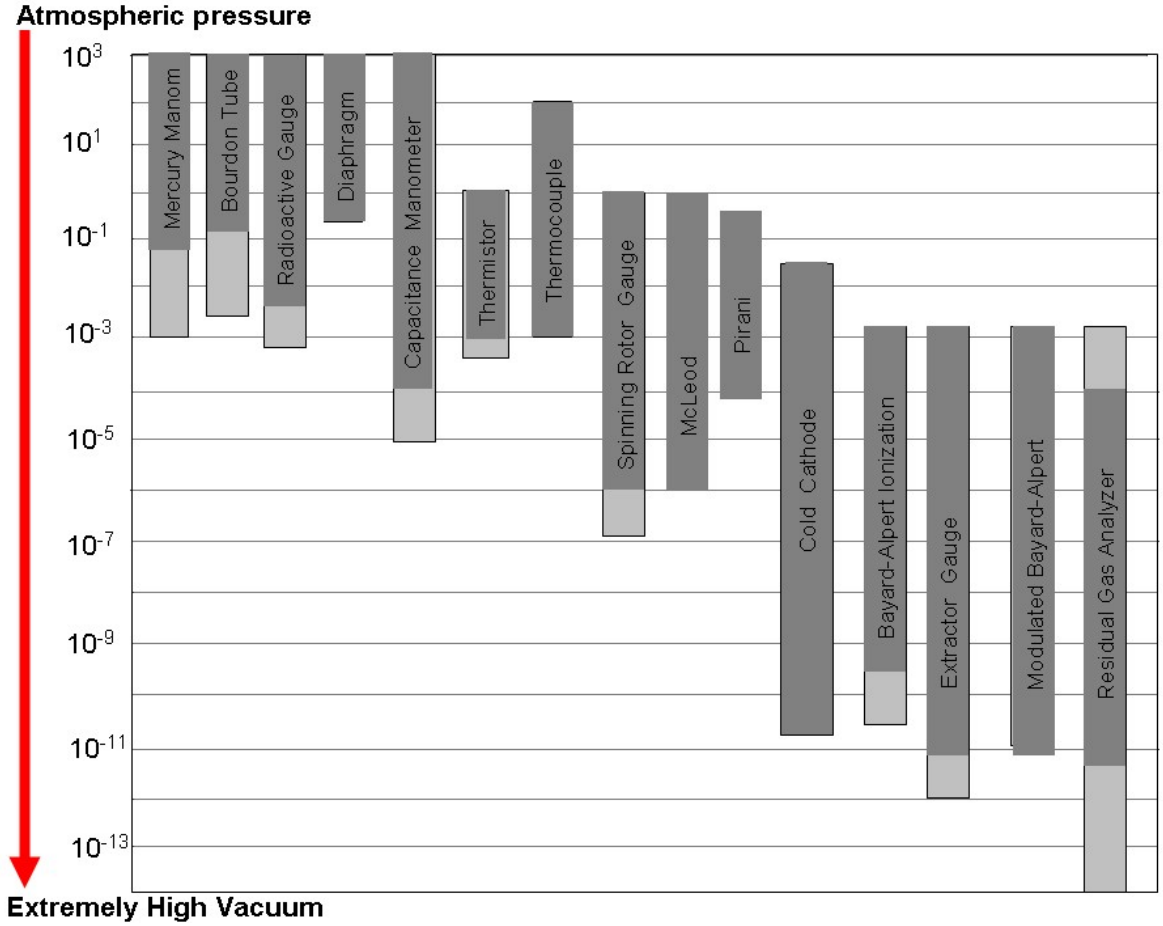

Figure 22: Pressure range of vacuum gauges [61], adopted with the permission of John Wiley & Sons

Vacuum gauges used in vacuum technology measure pressure by two general procedures: directly or indirectly. The classification of vacuum gauges according to their physical measuring principles is given in Figure 23. Direct methods are based on the fact that the force that constitutes pressure can physically shift a surface to which it is applied. Indirect methods monitor either the particle number density or property which depends on number density: thermal conductivity and viscosity of the gas. Direct methods yield pressure information that is independent of the nature of the gas whilst pressures indicated by indirect methods are dependent on gas type. The need to have the two methods arises from the fact that, at low pressure approximately 1×10^{-5} mbar, the force involved is extremely low and direct measurement become difficult if not impossible. So the quantity of interest at these low pressures is not the force exerted on the wall, but instead the gas density.

As it can be seen from Figure 22, only the various types of ionization gauge or residual gas analyzers are capable of making pressure measurements in the UHV/XHV region. In ionization gauges the indirect pressure measurements are performed through ionization of gas molecules and collection of some fraction of the ions, which means the number of ions collected, is related to the number of gas molecules present. Ionization gauges measure gas density rather than pressure.

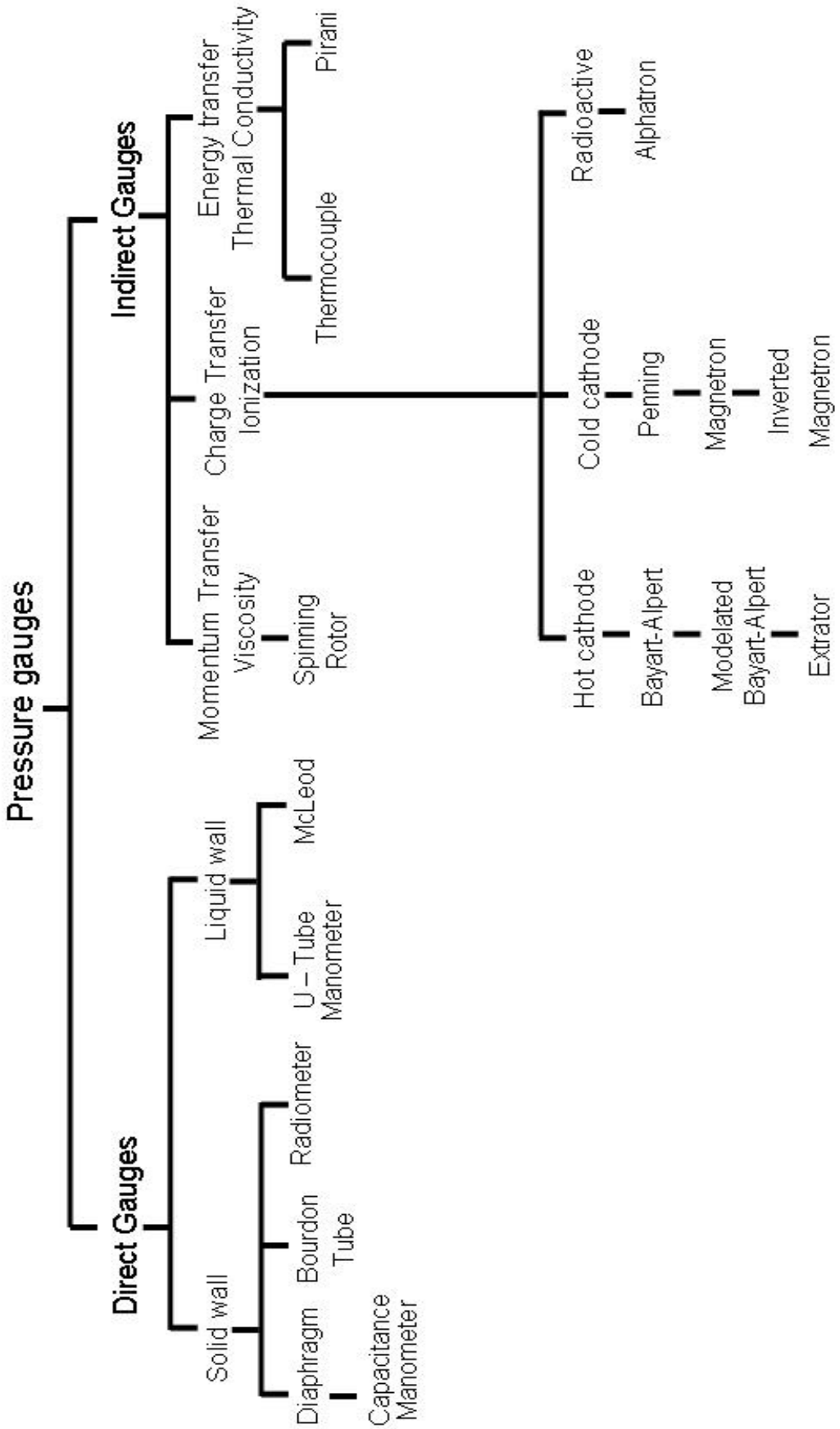

Figure 23: Classification of measuring vacuum gauges according to their principle measurement

Ionization by electron impact is used: the electrons being generated either thermionically (hot cathode gauges) or in a magnetically sustained gas discharge (cold cathode gauges). An electrical quantity proportional to the particle number density is measured. For hot cathode gauges, this is the ion current. For cold cathode gauges, the discharge current is measured.

3.5.1 Cold cathode gauges

They also named “crossed field” gauges due to the presence of electric and magnetic fields perpendicular to each other. Cold cathode ionization gauges essentially consist of only two electrodes, a cathode and an anode, between which a high voltage is applied.

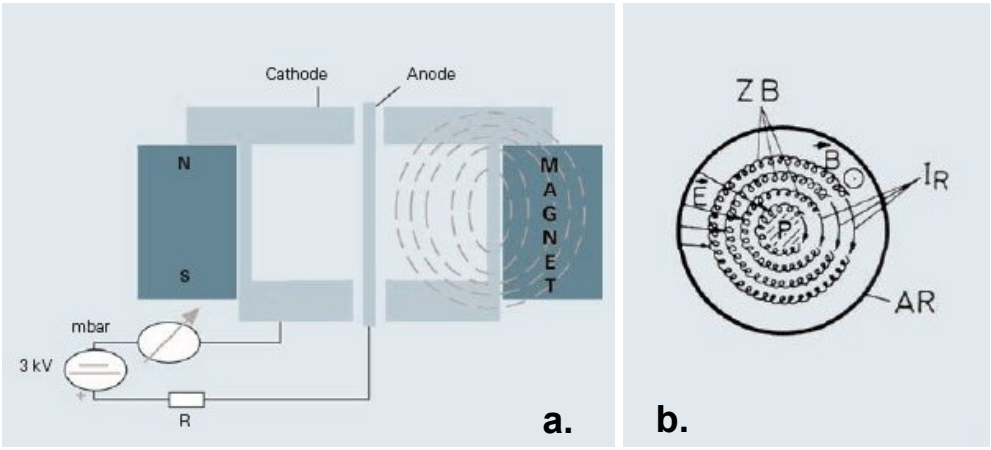

Figure 24: Cold cathode gauge a). Design, b). Operating principle [99]

Negatively charged electrons leave the cathodes because of the high voltage, moving at high velocity from the cathode toward the anode. As they travel this path, they ionize neutral gas molecules, which ignite a gas discharge. The measured gas discharge current (Figure 24a) is a parameter for pressure. However, only few molecules are ionized with straight electron trajectories. A design to avoid this disadvantage is to put an axially magnetized, cylindrical, permanent magnet ring on the exterior of the measurement chamber to generate magnetic field within chamber Figure 24b. Since the path of the electrons is increased by a magnetic field one electron may collide with several atoms with consequent production of positive ions and other electrons. The ions produced in the discharge are accelerated to the cathode where they are partly retained and partly cause sputtering of the cathode material [61, 63].

3.5.2 Hot cathode ionization gauges

As opposed to cold cathode ionization vacuum gauges, electrons are generated with the aid of heated cathode. One of those gauges is Bayard-Alpert gauge which is shown in Figure 25. It consists of three electrodes: cathode, anode and ion collector. Electrons are emitted thermionically from the heated cathode. A voltage that is applied between anode and cathode accelerates all emitted electrons toward the anode. A thin wire is arranged in the middle of the cylindrical, lattice-shaped anode. This wire serves as the ion collector. The emission current is measured in the anode circuit, which can be set by means of the heat output of the cathode. As the electrons travel toward the anode, gas molecules are ionized by electron collisions. They are attracted by the ion collector. The measured collector current is proportional to a gas density or pressure.

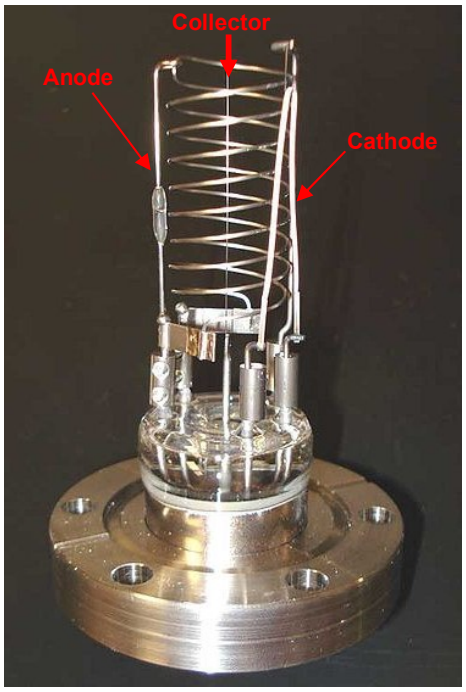

Figure 25: Bayard-Alpert gauge

Table 6: Some corrections factors for the adjustment of indicated ionization gauge pressure to gas type [13, 62]

Gas species	Correction factor
N_2	1.00
He	7.24
Ne	4.55
Ar	0.85
Kr	0.59
Xe	0.41
H_2	2.49
O_2	1.07
Air	1.02
D_2	2.5
CO_2	0.70
CO	0.97
I	0.17
CH_4	0.71
C_2H_6	0.37
C_3H_8	0.22
CF_2Cl_2	0.36
Oil vapors	0.1

Detailed discussions about those measuring instruments are given in many papers and books like [12, 13, 61].
Common characteristic for all ionization gauges is that their measurement is gas dependent. Because some gases are ionized easily, and some are more difficult, the response of an ionization gauge depends on the gas being measured. An unexplained

phenomenon has been observed which seem to indicate that the ease of ionization of a molecule is related to the number of electrons in the molecule. A molecule with fewer electrons seems to hold on to its electrons much more tightly. Table 6 shows some of the sensitivities of different gases.

Ionization gauges usually are calibrated using N_2 as the reference gas. To obtain the actual pressure for gases other than N_2, the indicated pressure must be multiplied by a correction factor for the given gas involved. Or in other words if the gauge reads for example pressure 8×10^{-10} mbar, and the gas being measured is hydrogen, there is about more than twice (2.5) this amount of gas, since hydrogen gives up its electrons only about less than half (0.4) easily.

3.5.3 Limitations of ionization gauges

The intrinsic measurement accuracy of a given instrument in a UHV/XHV system, the veracity of total or partial pressure indications is quite dependent on the magnitude of the instrument background. The several physical and chemical processes limiting the minimum measurable pressure of ionization gauges and RGAs in the UHV/XHV range include [12]:

- X ray limit
- Electron-stimulated desorption (ESD) of positive and negative ions and neutrals
- Effects at hot cathodes (increased outgassing resulting from heating of electrodes and the envelope by radiation from the hot cathode and desorption of neutrals and ions from the cathode)
- Chemical reactions of gas molecules at the hot surface resulting in changes in gas composition
- Desorbing from the gauge electrodes and walls by soft X-rays produced by ionizing electrons

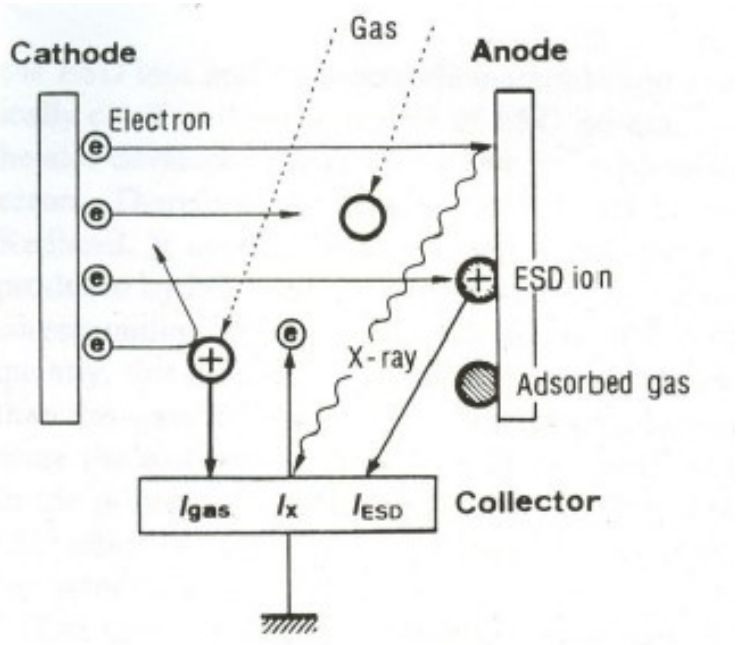

Figure 26: Physical phenomena involved in ionization gauge behavior [64]

Some of those limiting effects present in ionization gauges are more important for cross field gauges (CFG) and some of them are more important for emitting cathode ionization gauges (ECG). Perhaps the most critical issue is the choice of gauge for measuring extremely low pressure because of these limiting processes and accuracy. Table 7 summarizes advantages and disadvantages of both types of ionization gauges.

Table 7: Comparison between ionization vacuum gauges with emitting cathode (hot cathode gauges) and with crossed electromagnetic field (cold cathode gauges) [65]

Criterion	CFG	ECG
Errors due to pumping speed	High	Low
Accuracy, stability	Moderate	Good
Size, mechanically stability	Good	Moderate
Sensitivity towards external magnetic fields	Low	High
Produces outside magnetic field	Yes	No
Susceptibility to contamination	High	Moderate
Start-up problems	Occur	None
X – ray limit	None	10^{-12} – 10^{-8} mbar
Electron stimulated desorption	Negligible	Yes, gas species dependent

Methods to reduce those limiting effects are discussed in detail by Watanabe [95]. Historically, the most attention has been paid to reducing the X-ray limit; it was the most significant limiting factor; indeed it remains a concern [61]. Table 8 lists six hot cathode gauge designs with X-ray limits in the XHV range. Some of them are able to separate ESD ions from gas phase ions.

3.5.4 What is X-ray limit?

Electrons in hot cathode ionization gauges that strike the anode cage cause X-rays to be emitted, some of which strike the collector and create photo-electrons. Emitted photo-electrons flow from the ion collector toward the anode. The resulting photo-electron current is added the pressure dependent collector current and falsifies the information on gas density in the system. Consequently the collector wire should be selected as thin as possible so that it collects only little X-ray radiation [64].

3.5.5 Electron stimulated desorption (ESD)

The energy of electrons emitted from the filament is high enough to desorb neutral molecules and ions when they strike vacuum surfaces. This effect is called electron stimulated desorption (ESD).

ESD ions can directly increase the pressure proportional ion current. Desorbed neutral molecules increase local density of gas molecules in the ionizing region of the gauge which also increases reading of the gauge. ESD can be a significant, but a variable and an unpredictable source of error in vacuum measurement using hot cathode ionization gauge. In many cases ESD errors can be larger than those caused by X-rays, especially after exposure of the gauge to higher pressure. Most emitted electrons are striking the anode grid so the release of previously adsorbed gases on the grid is main source of ESD. O' Hanlon [61] is discussing that by heating the grid of an ionization gauge the ESD can be significantly reduced. He gives an example of experiment where ESD signal disappeared when Bayard-Alpert grid was resistively heated above 500 °C. Conclusion was that at this

temperature gases could not adsorb on the grids. In another experiment heating the grid to 900 °C and then to an operational temperature of 560 °C removed the bulk hydrogen and minimized the surface adsorption. By this grid-heating technique, the error in hydrogen measurement was reduced from 614 % to less than 8% [57, 58].

Similar experiment was done by Watanabe [66, 95]. An ionization gauge where the grid could be resistively heated has shown that heating the grid at about 600 °C resulted in a reduction of the ion collector current by a factor of 10 or more (Figure 27). The reduction in indicated pressure is caused by the reduction of the flux of ESD neutrals from the heated grid. Study of ESD of neutrals of several adsorbed species, including hydrogen, on the grid of a residual gas analyzer (RGA), by first cleaning the grid by heating at 900 °C and then heating the grid to 500 °C showed that the spurious ESD peak of hydrogen decreased by over three orders of magnitude and the mass spectrum consist mainly of H_2 molecules, reflecting the true hydrogen pressure.

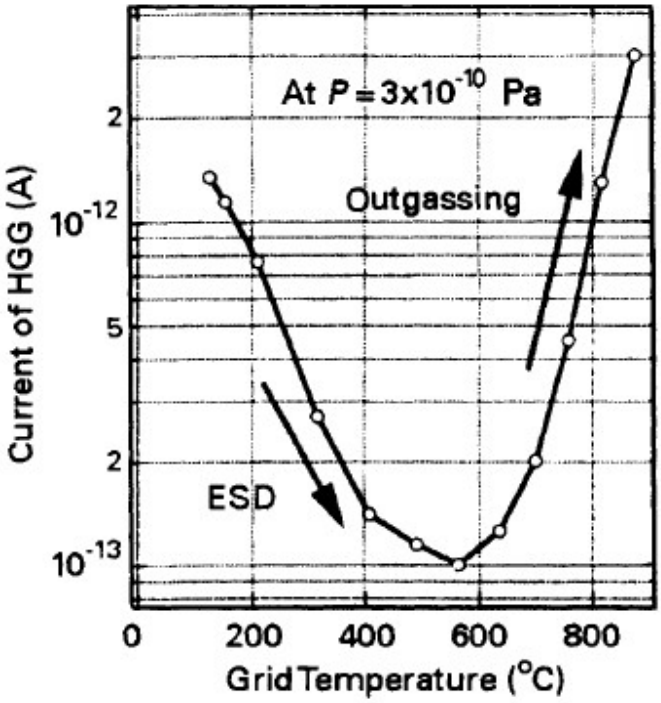

Figure 27: Ion current versus grid temperature in a hot cathode UHV ion gauge. Electron stimulated desorption of the grid decreases with temperature up to a temperature of 600 °C . The increased signal at high grid temperatures is believed to be caused by the outdifision of hydrogen from the grid wire. Reprinted from [66] with permission of John Wiley & Sons.

Commercial hot cathode ionization gauges do not have a possibility to operate with continuously heated grid. Instead they enable to degass the grid before measurements either by resistive or by electron bombardment heating. Errors due to ESD can be also reduced by operating the ion gauge at high electron emission current as this helps to keep the grid free of adsorbed ions because it is continuously cleaned by electron bombardment.

As it is know the hydrogen is the predominant residual gas in metal vacuum systems at very low pressure in the UHV/XHV ranges. The problems of measuring hydrogen pressure in this range are discussed by Redhead [67]. Special ionization gauge and RGA designs have been developed which permit the separation of ESD from gas phase ions. The separation of ESD from gas phase ions is based on the difference in initial kinetic energy of two groups of ions.

Another problem in vacuum measurements using hot cathode ionization gauge are chemical reactions in the presence of hot filaments. The atomic H which is evolved by dissociation of H_2 at hot metal surface can interact with adsorbed species on the cold surface of the vacuum system to produce a variety of gaseous contaminants such as H_2O, C_xH_y. Electrons striking the grid and ion collector release previously adsorbed gases. Prior exposures to oxygen results in desorption of CO formed by reaction of dissociated oxygen and carbon impurities in metals.

For the extractor gauge, which was also used in our work (see chapter 9) Redhead [96] pointed out that the ESD effect is significantly reduced compared to Bayard-Alpert gauge. In extractor gauge the electric field for extraction of ions from ionizing region and collection on fine collector wire is optimized for gas phase ions, but collection efficiency for ESD ions which have significantly higher kinetic energy is very small.

Table 8: Characteristics of gauges for XHV [12, 51, 61]

Gauge	Electron Emission (A)	The X ray limit [mbar] *	Approximately lowest pressure
Hot-cathode magnetron (Lafferty gauge)	1×10^{-6}	6×10^{-15}	10^{-16}
Extractor (Leybold IE511)	1.3×10^{-3}	2×10^{-12}	10^{-13}
90^0 Bent-beam (Helmer gauge)	3×10^{-3}	$< 2 \times 10^{-14}$	10^{-14}
180^0 Bent-beam (Ion spectroscopy gauge)	5×10^{-3}	$<2.5 \times 10^{-15}$	$< 10^{-14}$
256.4^0 Bent beam	1×10^{-4}	$< 6 \times 10^{-14}$	4×10^{-15}
Bessel box (A-T gauge)	3×10^{-5}	3.5×10^{-13}	10^{-14}
Bayard-Alpert gauge		9×10^{-11}	

- Pressure at which the ion current equals the residual current

3.5.6 Thermal outgassing of ionization gauges

The thermal outgassing resulting from cathode and by heating of gauge walls, which is a particular problem at XHV, can be minimized by three methods:

- Using a low work function cathode to reduce the heating power required; thoria or yttria coatings on a refractory metal have been used successfully
- Using a cold emitter such as FEA, though the issues regarding reliability and outgassing of these cathodes for use in vacuum gauges have not been fully solved yet
- The metal envelope of the gauge can be replaced with the material of low emissivity and high conductivity to reduce the power required to heat the cathode. Stainless steel is not suitable material for gauge envelope while cooper is better. If copper is used to make gauge envelope instead of stainless steel then the outgassing rate can be reduced by a factor 10 [51].

3.6 Partial pressure measurement and residual gas analysis

In some cases measurement of total pressure in not sufficient for the characterization of vacuum systems. Detailed information can only be obtained by the identification of components present in the gas phase by means of residual gas analysis. Having established gas composition, however, the determination of partial pressures is relatively straightforward.

Measurement of total pressure in a vacuum system is often not sufficient to characterize the vacuum for processing or experiments; hence the accuracy of the total pressure measurements is a direct function of knowing the gas composition in order to take into account the partial pressures and associated gauge sensitivity of each gas. Knowing the identity of the gas phase species within a UHV/XHV system is extremely important for assessing the pumping status of the vacuum system or for controlling a particular vacuum process. It was pointed out before that some of the pumps used at UHV/XHV systems are selective when pumping gas mixtures, often leaving some gases virtually unpumped. As previously mentioned the primary residual gas in UHV/XHV systems is usually hydrogen, but there can be significant fractions of other species such as CH_4, CO and CO_2. Particular operation employing process gases can substantially change that background signature. Measurement of partial pressures of the residual gases in a vacuum system is usually performed by mass spectrometers. The most common type is quadrupole mass spectrometers (QMS). Recently, optical absorption techniques to measure partial pressure of specific gas species have been introduced also [13].

The mass spectrometer provides, first of all, a build in leak detector, which is absolutely necessary to confirm the vacuum integrity of a system. Secondly, it provides the state of cleanliness of a system by indicating the magnitude and type of the residual gases. Thirdly, it is a research tool that provides several diagnostics capabilities in addition to determining gas purity, gas desorption from elements of interest and gas changes that occur during various processes.

The QMS consist of three subsystems, shown in Figure 28 [57, 58, 65]:

- the ion source (for generation of positive ions from the systems gases)
- mass filter (quadrupole separation system in which a combination of DC and high frequency AC voltages select ions with stable paths in the filter)
- ion detector (ion currents associated with ions that pass the filter are measured at the detector)

Operation of QMS is provided with:

- control and data-acquisition electronics, as well as
- a computer and software providing a user interface

3.6.1 Ion creation

An ion beam extracted from the ion source passes to the mass separation system where continuous changes in the voltages applied to the electrodes allow ions of the appropriate mass/charge *m/e)* ratio to achieve stability in the mass filter and pass to the detector. A spectrum is therefore generated giving the variation of the amplitude of the detector signal with m*/e.* The m*/e* value enables the mass fragment to be identified and the signal amplitude (as ion current *I+)* indicates the amount of the species present. Although there are various ways to ionize molecules, the only method used in QMS is electron impact, other methods such as chemical ionization, proton transfer reaction, ion attachment, and

laser ionization etc. are applied for special analysis methods. The concerns for ionization gauges are also important for ionization sources in QMS, but there are significant differences between an ion gauge (a total pressure gauge) and mass spectrometer. For an ion gauge, the ions are created and are collected and counted simultaneously, without separating the different species. In a mass spectrometer, the ions are created in a manner similar to that of an ion gauge after that different masses are separated, and measured sequentially, giving a display of a number on ions with each mass (actually the mass of charge ratio).

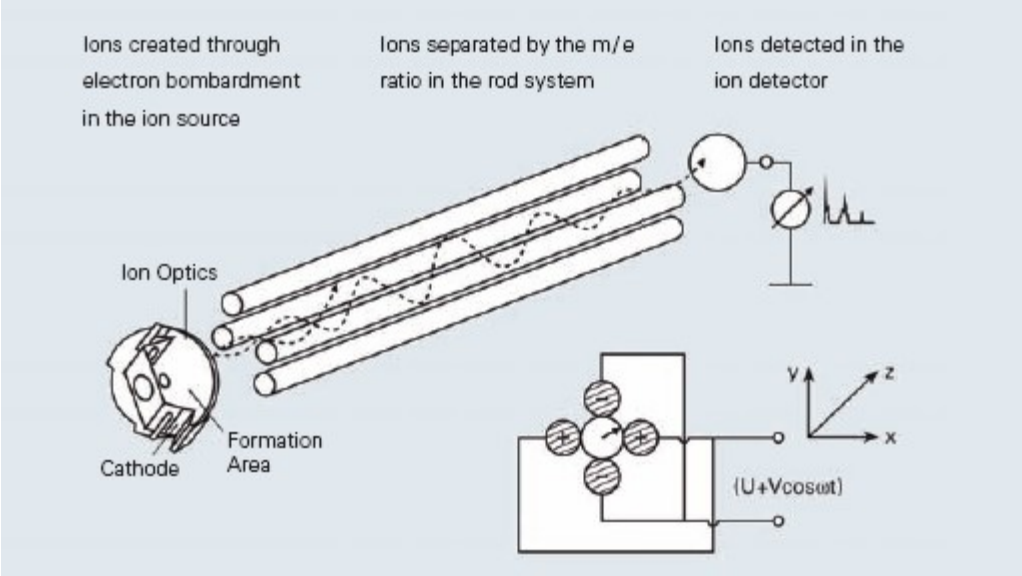

Figure 28: The functional units of mass spectrometer [99]

3.6.2 Mass separation

Ions created in the ion source are injected with energy of a few electron volts into a high-frequency electrical field established among four metal rods, as shown in Figure 28. Only ions with a well-defined ratio *m/e*, where m is their mass and *e* their charge, can travel on stable trajectories in this field. The mass resolution of the instrument is adjusted by the ratio *U/V* and a mass scan is performed by increasing the absolute value of *U* and *V* [61]. U – is DC voltage, V – is High frequency voltage amplitude.

3.6.3 Ion detection

The primary quantity to be measured at the exit of the filter is an ion current. When ions exit the mass filter, an ion current representative of the particular species being sampled is measured with a Faraday cup or with an electron multiplayer (discrete or continuous). The magnitude of this ion current is directly proportional to the magnitude of the species and knowing the instrument sensitivity allows the determination of the partial pressure. For UHV/XHV systems a lower detection limit and higher sensitivity are required, then the arriving ion current has to be amplified in the vacuum, either electronic (electrometer) or physical (electron multiplier) or both.

3.6.3.1 Faraday cup

This type of detector is used when stables signals are required and there is sufficient pressure to provide a detectable signal with electronic amplification alone. In the simplest case, the ions strike a Faraday collector (Faraday cup), where they emit their electrical

charge. The resulting current is converted to a voltage that is proportional to the ion current by means of sensitive current/voltage inverter (electrometer amplifier). Currents of about $1x10^{-14}$A are measurable with a good electrometer, but, in general, $1x10^{-13}$A is a practical limit [57]. Considering the sensitivity of the most mass spectrometers, this limit would translate to a pressure of $1x10^{-7}$ Pa or higher.

3.6.3.2 Electron multiplier

If extremely small ion currents are to be measured or if an extremely high measuring speed is required, the physical pre-amplifiers, so-called secondary electron multipliers are employed. Such an amplifier is the electron amplifier. The instrument is usually a discrete stage or a continuous stage multiplier. Particles (ions, neutrals, electrons, photons) hitting a surface with high kinetic energy release several 'secondary electrons'. The amount of the secondary electrons released depends on the surface material. The use of several dynodes in combination with the appropriate dynode material allows for an amplification up to 10^8. One single ion impinging on the first dynode will cause an avalanche of electrons. This current can be converted to a transient in voltage and thus single-ion counting is possible with such a device too, provided the current pulse is short enough (10^{-8} s).

Secondary electron multiplier offers the following advantages over a Faraday cup:

- It dramatically increases the sensitivity of the instrument, affording sensitivity increases of up to 10A/mbar
- The lower pressure can be scanned at shorter intervals of time with the downstream electrometer amplifier

However an secondary electron multiplier also has disadvantages:

- Its amplification can change due to contamination or a chemical change in the active layer
- The number of electrons (conversion factor) that generate a colliding ion (approximately 1 to 5 electrons) will be a factor of the ion energy (mass discrimination).

Extremely fast measurements are possible with the aid of secondary electron multipliers. The measuring speeds are significantly higher than with a Faraday cup.

Electron multipliers should not be used in high pressure applications because the collector and dynodes can be destroyed if the average current exceeds a few microamperes. Another significant problem of the multipliers is the gain dependence on the mass of the ion. So the gain of a specific electron multiplier needs to be accurately known, a calibration curve of gain versus mass must be experimentally measured for all gases and vapors of interest [O'Hanlon].

3.6.3.3 Microchannel plate multipliers

Instead of one long tube to increase the number of collisions, e version with an array of many short tubes in parallel can be used. This device works on the current gain sum of these continuous dynodes arrayed over disk. This is useful for space limitations where a single disk can provide gains up to $2.5x10^4$, but can be increased by stacking of the plates.

4 Investigation of Oxygen diffusion in nonevaporable getters (NEG)

An important property of NEG pumps is their activation energy, i.e. the heating temperature which is required to obtain the desired functional NEG properties in a certain time. Generally the heating is obtained by passing a suitable AC or DC current through the getter material; however, under some circumstances indirect heating may also be applied. The definition of the activation temperature is phenomenological, i.e. it depends on the NEG application. The activation temperature may be for instance defined as the temperature to which the NEG must be heated in order to provide a specified pumping speed. Full activation corresponds to the maximum sorption speed obtainable or practically to the complete removal of the passivating layer; however, partial activation can often be perfectly acceptable in some cases. The activation process is regulated by diffusion laws, which means it is not only related to temperature but also to time, even if it is more strongly dependent on temperature. The process is therefore identified by a suitable combination of two parameters depending on the requirements of the application involved. So many detailed investigations have been made on getter materials to more quantitatively determine the effects of temperature and time parameters on the degree of activation.

4.1 Getter Activation

Figure 29 shows, for example, the various activation degrees obtained with different temperature/time combinations for the nonevaporable getter St 707. The distinguishment between activation and reactivation is: activation is the first removal of the passivation layer from the surface by providing sufficient energy in the form of heat to allow the sorbed species on the surface to diffuse into the bulk of the getter material. This means

that activation is the first cleaning of the surface on a new cartridge, while reactivation is any subsequent activation process. There are two types of sorption by NEG pumps; reversible and nonreversible. Hydrogen and its isotopes are gases that are sorbed reversibly, whereas Carbon, Nitrogen, and Oxygen form stable chemical compounds with the NEG alloy and are sorbed irreversibly. These atoms are diffused into the bulk of the getter until a complete saturation occurs, whereas hydrogen atoms react differently. They diffuse into a getter material body more quickly than other atoms and distribute almost uniformly within the bulk even at low temperatures, i.e. hydrogen sorption is reversible. In addition, because of the relatively weak forces that bind these atoms to the alloy, some of the hydrogen sorbed at low temperatures can be released at higher temperatures. The difference between activation/reactivation and regeneration is that in activation/reactivation the gases that are diffused into the bulk do not go away – they build up in the getter alloy. So, regeneration is the removal of hydrogen from getter material and renewal of the getter capacity. It should be emphasized that in the case of regeneration it is necessary to have in the vacuum system a forepump to draw out the hydrogen that is released through regeneration.

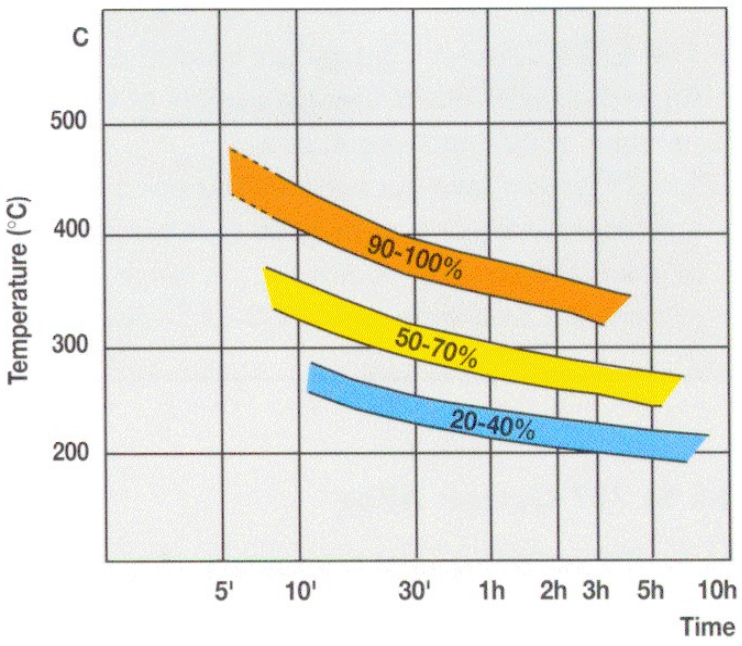

Figure 29: Activation conditions and gettering efficiency of St 707 [98]

The surface of the powder particles of any type of getter material is readily covered mainly by an oxide layer when exposed to air the first time after its manufacturing. This layer usually passivates the getter material thus preventing further pick-up of gases. The getter material, therefore, is not immediately active and ready to work when introduced in the vacuum environment. In order for the getter to be ready to chemisorb gases, the pasivation layer has to be removed. During the activation process of NEG material, the oxygen atoms contained on the surface passivation oxide layers are dissolved into the material bulk by heating, i.e. the oxygen atoms are moved from the surface oxide to the solid solution. A thermodynamic description of this process is given in literature [36]. The most important requirement for a good NEG material is a high solubility limit for oxygen in order to allow several NEG activations to be carried out. Another essential parameter property is a high diffusivity for oxygen. These requirements are best fulfilled by the transition metals of the 4B group of the periodic table (Ti, Zr, Hf). Another family of elements, the transition metals of the 5B group (V, Nb, Ta) provides a much higher

oxygen diffusivity but a lower oxygen solubility limit. Therefore, combinations of elements of the 4B and 5B group and some of their combinations can fulfill the conditions for lower activation energy [42, 43]. Since solubility and diffusivity limit of oxygen are two important parameters for the description of the activation mechanism, we investigated in our work the oxygen diffusion in St 707 during heat treatment. The diffusivity and solubility limit of N, H, and C are also important because these elements are the main impurities in nonevaporable getters after oxygen.

4.2 Specimen preparation

The specimens for our investigations are alloys with mass fractions of Zr(70)-V(24.6)-Fe(5.4) % (Figure 30). Specimens were in the form of tablets compressed from St 707 powder. The dimensions of the tablets were diameter 6.17 mm and height 2.02 mm. The mass of the tablet (specimen) was 0.275 g.

Figure 30: Shape of the specimen (getter pill) used in our experiment

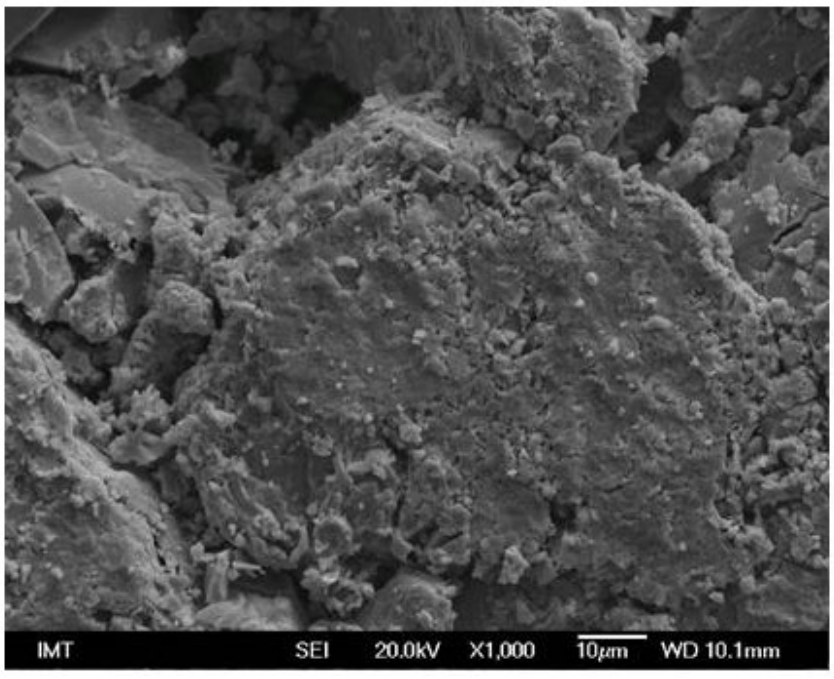

Figure 31: Secondary electron image of St 707 “as received” specimen

The as received specimen was observed by SEM, Figure 31. The surface is quite rough because of the manufacturing technique (sintering from powder). Such rough structure is not suitable for surface analysis. So the specimens were further prepared through grinding and polishing, and then immersing in an ultrasonic bath with alcohol for cleaning.

SE image of a polished surface of the “non-oxidized” specimen is shown in Figure 32. The typical particle sizes were from 50 μm to 100 μm. From Figure 32 it can be seen that the getter alloy is biphasic. Phases are pure zirconium and Laves phase Zr $(V_{0.83}Fe_{0.17})_2$.
Further in this chapter three different states of the specimen shall be defined a). As received specimen b). Non-oxidized – only polished specimen c) Oxidized specimen (the polished specimen treated at oxygen flow at high temperature).

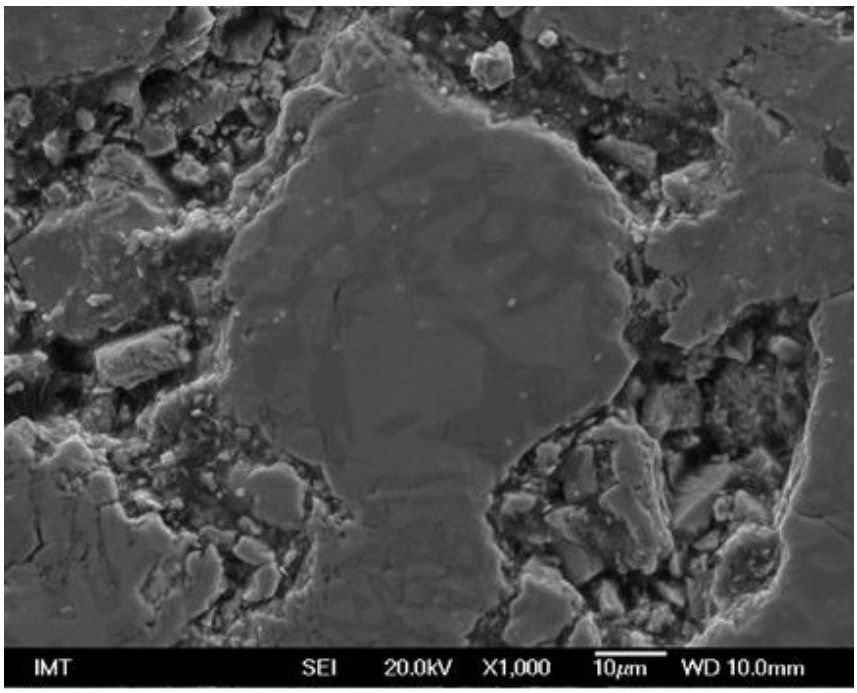

Figure 32: SEI - Secondary electron image- of a polished surface of the “non-oxidized” specimen St 707 alloy.

4.3 Experimental procedure for oxygen adsorption and diffusion

After grinding, polishing, and cleaning the specimens were inserted into the test chamber (CH2), Figure 33. The same experimental setup and procedure were used for the determination of pumping speed and sorption capacity of nonevaporable getters in the publication [71]. Then we pumped the gases out of the CH2 (through the turbo molecular pump) until the pressure in the vacuum chamber reached 10^{-7} mbar. Afterwards, the specimen was heated for activation, and simultaneously the temperature was measured by a thermocouple attached to CH2. In the experiment the specimen surface was exposed to the given partial pressure of test gas at elevated temperature. The sources of the test gases are gas cylinders. When the desired temperature was reached, the regulating valve was opened and the gas (in our case pure oxygen) was permitted to flow into the system.
Opening of the regulating valve was controlled to reach the pressure of 1.2×10^{-6} mbar in the CH2, while, the temperature was 450 °C. The specimen was treated at these conditions, for a time of one hour. During this treatment the diffusion of O_2 into the specimen started. The purity of the oxygen admitted to the getter specimen was better than 99.99 %. The investigation of the diffusion depth of oxygen was performed using SEM and AES with different accelerating voltages and different magnifications. The crystal structures of the obtained specimen were characterized by powder X-ray diffraction (XRD). The specimens were characterized in both the as-received and oxidized states.

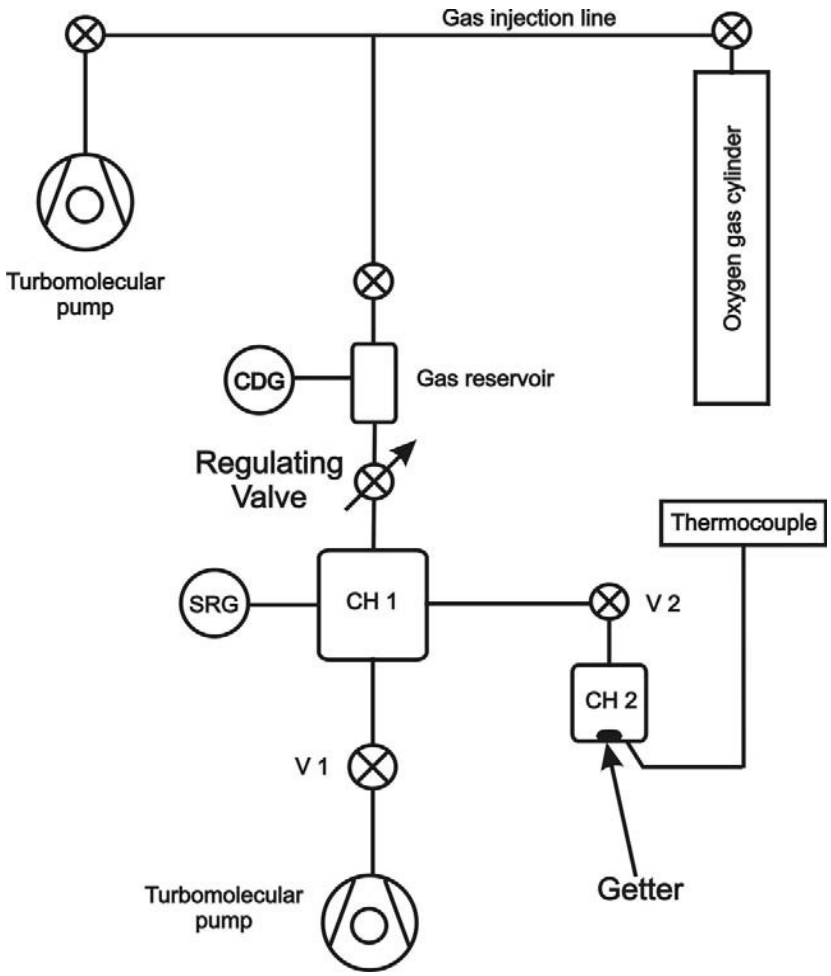

Figure 33: Scheme of the vacuum system. SRG is Spinning Rotor Gauge, CDG is Capacitance Diaphragm Gauge

4.4 Methods for characterization of NEGP

The characterization of the surface and bulk properties of NEGP include basic chemical and crystallographic structures.

4.4.1 Energy dispersive spectroscopy (EDS)

In our experimental work we used a JEOL JSM 650-F scanning electron microscope, with an add-on retractable backscatter electron detector and equipped with the following analytical techniques: energy dispersive spectroscopy (EDS), wavelength dispersive spectroscopy (WDS) and electron backscatter diffraction (EBSD).
Energy Dispersive X-Ray Spectroscopy (EDS or EDX) is a chemical microanalysis technique used in conjunction with scanning electron microscopy (SEM). The EDS technique detects x-rays emitted from the specimen during bombardment by an electron beam to characterize the elemental composition of the analyzed volume. By EDS method the information of analyses are from 1.5 to 3 micrometers. So as a result of a primary electron beam bombardment, X-ray radiation of characteristic wavelengths is emitted from a specific material.
Elemental constituents are identified with the aid of Mosley's law that relates the wavelength of each observed spectral line to a specific element through the relationship:

$$\frac{1}{\lambda} = k\sqrt{(Z-\sigma)} \tag{24}$$

where λ is the X-Ray wavelength, *k* is a constant for each spectral-line series, *Z* is the atomic number of the element from which the X-Rays originate, and σ is a constant associated with the atomic screening effects.
EDS identifies the elemental composition of materials imaged in an SEM for all atomic numbers greater than that of Boron. Elements are typically detected at concentrations as low as 0.1%.

4.4.2 Auger electron spectroscopy (AES)

AES is a common analytical technique used specifically in the study of surfaces and, more generally, in the area of material sciences. AES is used as an analytical technique for obtaining information about the chemical composition of solid surfaces. The surface sensitivity, namely the ability of AES to detect elements in the outermost (0.4 to 5 nm) region of the sample surface, as well as the rapid acquisition speed are among some of the advantageous characteristics of this technique. All elements except hydrogen and helium in principle can be detected by AES. An advantage of AES over XPS as another surface analysis technique is the ability to focus the probing electron beam in AES down to about 10 nm or less and thus achieve high spatial resolution, something that cannot be achieved in XPS due to the inability to focus X-rays. The sampling depth in AES is about three monolayers, and the sensitivity is of the order of 0.1% [72, 73, 100-102].
The radiative (X-Ray emission) or nonradiative (Auger) processes are the standard routes for an excited atom to achieve relaxation. In AES the atomic core levels are ionized by the incident electron beam and the resulting Auger electrons are detected with an electron spectrometer. These electrons form small peaks in the total energy distribution function.
By considering the ionization process of an isolated atom under electron bombardment the Auger process can be understood. The incident electron with sufficient primary energy E_1 ionizes the core level, such as a K level. The vacancy thus produced is immediately filled by another electron from L_1, Figure 34.

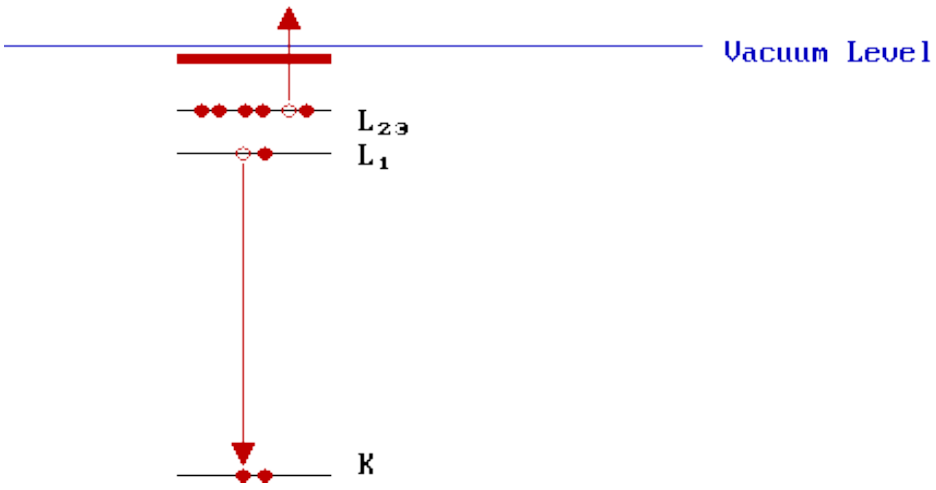

Figure 34. Energy level diagram in an Auger process. Electron from L_1 drops into the K level, which causes the emission of an L_2 electron.

The energy (E_k-E_{L1}) released from this transition can be transferred to another electron, as in the L_2 level. This electron is ejected from an atom as an Auger electron. We can make an estimate of the energy of the Auger electron:

$$E = E_K - E_{L1} - E_{L2} \quad (25)$$

It is obvious that at least two energy states and three electrons must take part in the Auger process. Therefore, H and He atoms cannot give rise to Auger electrons. The excitation process from the equation (25) is denoted as a KL_1L_2. Several transitions (KL_1L_1, KL_1L_2, LM_1M_2, etc) can occur with various transition probabilities. The Auger electron energies are characteristic for the target material and independent of the incident beam energy.

Except qualitative and quantitative analyses, depth profiling is one of the most important applications of the AES because it provides a convenient way of analyzing the composition of thin surface layers. It is a destructive technique. In this technique the specimen is eroded by ion sputtering. The specimen is bombarded with ions accelerated in an ion gun to energies in the range of 1 to 4 keV. As these energetic ions strike the specimen, a small amount of energy is transferred to the surface atoms, which causes them to leave the specimen. The ion beam is scanned on the surface for a known time to remove a uniform layer of the specimen. Under controlled conditions the thickness of the layer removed can be calculated. The residual surface is then analyzed by AES, giving the depth distribution of different species in the specimen. Inert gases (usually Argon) are commonly used as ion sources.

4.4.3 X-ray diffraction (XRD)

X-Ray powder diffraction analysis is a powerful method by which X-Rays of a known wavelength are passed through a specimen to be identified in order to identify the crystal structure. This technique, based on Bragg's law, is described in reference [74]. The wave nature of the X-Rays means that they are diffracted by the lattice of the crystal to give a unique pattern of peaks of "reflections" at differing angles and of different intensities, just as light can be diffracted by grating of suitably spaced lines. The diffracted beams from atoms in successive planes cancel unless they are in phase, and the condition for this is given by Bragg's relationship:

$$k \cdot \lambda = 2d \sin \alpha \quad (26)$$

where λ is the wavelength of X-rays, d is the distance between different planes of atoms in the crystal lattice, α is the angle of diffraction. The X-Ray detector moves around the specimen and measure the intensity of the peaks and the position of these peaks.
The X-ray diffraction pattern of a pure substance is like a fingerprint of the substance. The powder diffraction method is thus ideally suited for characterization and identification of polycrystalline phases. Today about 50,000 inorganic and 25,000 organic single components, crystalline phases, and diffraction patterns have been collected and stored on magnetic or optical media as standards. The main use of powder diffraction is to identify components in a sample way by a search/match procedure. Furthermore, the areas under the peak are related to the amount of each phase present in the specimen [74].

4.5 Oxygen diffusion in St 707 non evaporable getter material

4.5.1 EDS analyses

The compositions of the constituents of the as-received St 707 specimen and after their oxidation in the vacuum system were investigated by EDS.

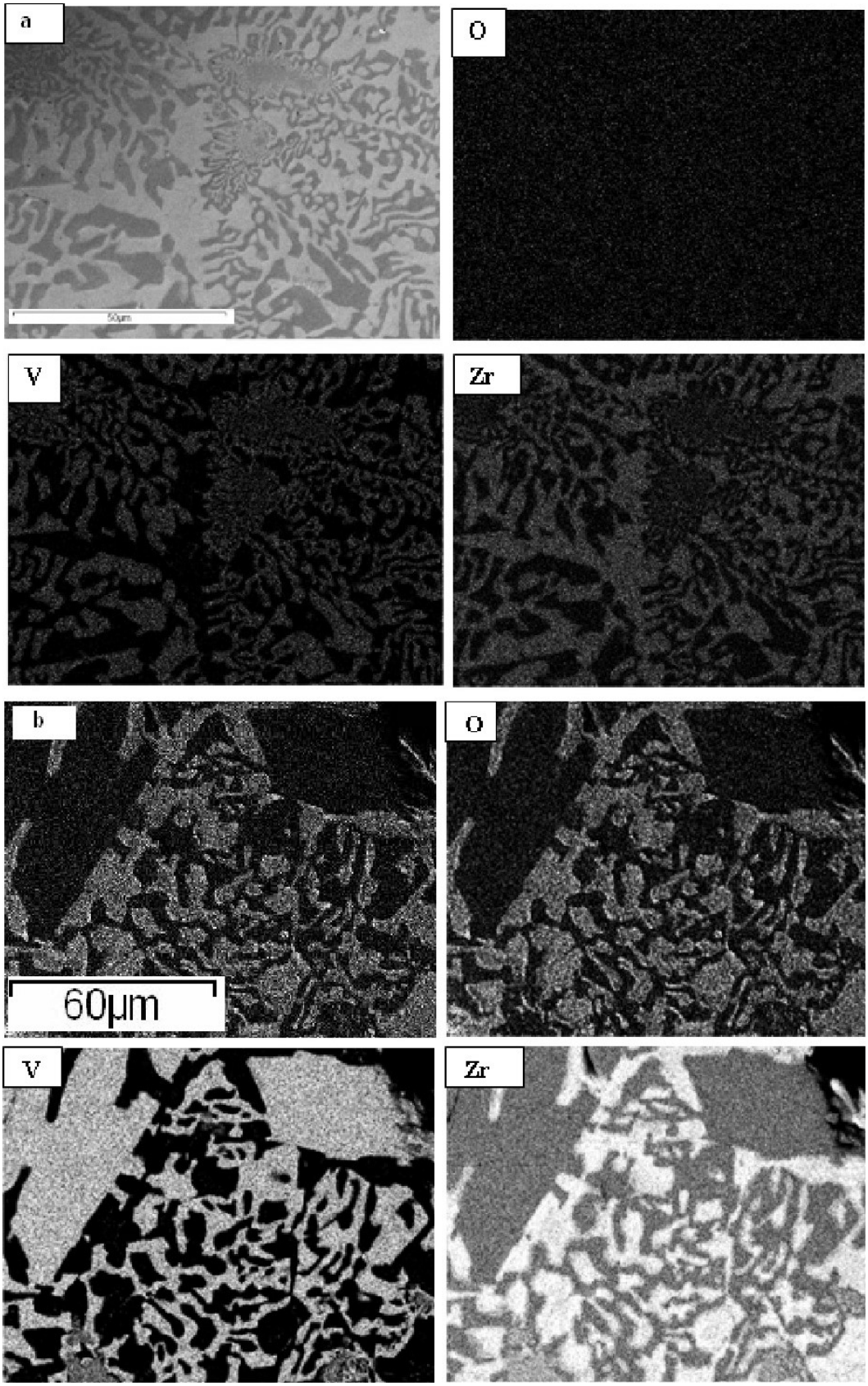

Figure 35: (a) SEI of a polished surface of the "non-oxidized" specimen St 707 and EDS elemental map images of O, V, and Zr. (b) SEI of a polished surface of the oxidized specimen St 707 at temperature T = 450 °C, pressure P = 1.2 × 10^{-6} mbar, and time t = 1 h and the EDS elemental map images of O, V, and Z.

The results of the EDS investigations are summarized in Table 9 and Figures 35 and 36. The specimen in the "not-oxidized" state contained particles which consisted of two different compositions of zirconium-rich phase and Laves phase, as can be seen from Figure 36a. Areas rich in zirconium are surrounded by those with which vanadium is the major component. It was found that iron is present only in the vanadium-rich areas [69]. According to Figure 35 and Figure 36, the bright areas in the secondary electron images could be assigned to areas rich in elemental zirconium, whereas the dark ones indicate the dominance of the Laves phase.

When the getter is exposed to air, it absorbs oxygen and the gases present in the atmosphere. As consequence, a layer is formed at its surface which prevents further adsorption. For further use of the getter it should be activated, which is achieved through increasing the temperature. For this reason, a small amount of oxygen will be found in the "not-oxidized" getter, Figures 35a and 36a. The presence of oxygen in the "non-oxidized" specimen is barely noticeable compared to the oxygen presence in the oxidized specimen Figures 35b and 36b, and Table 9. Also in the "not-oxidized" specimen the presence of oxygen is almost similar in all phases, the zirconium-rich phase and the Laves phase.

From the EDS spectra as well as the EDS elemental maps images of the "non-oxidized" getter material it is obvious that the amount of oxygen is almost the same in the both phases, the zirconium-rich phase and the Laves phase Figure 36a. On the other hand, through the same techniques we observed a larger oxygen content in the zirconium-rich phase compared to the Laves phase (Figure 36b). Also from Figure 36 and Table 9 it is evident that there is more oxygen in the zirconium-rich phase than in the Laves phase. The spectrums 1, 2, 3 are of the zirconium-rich phase and spectrums 4, 5, 6 are of the Laves phase. Measured oxygen concentration in spectrums 1, 2 and 3 of oxidized specimen is close to 60%. This happened due to the fact that close to 500 °C the formation of ZrO_2 bond occurred [69], and also the solubility values indicate that metals of the 4B group (in our case zirconium) have higher storage capacities for oxygen than those of the 5B group (V), or, putting it another way, that hcp crystalline structures have in general higher storage capacities than the bcc ones [36].

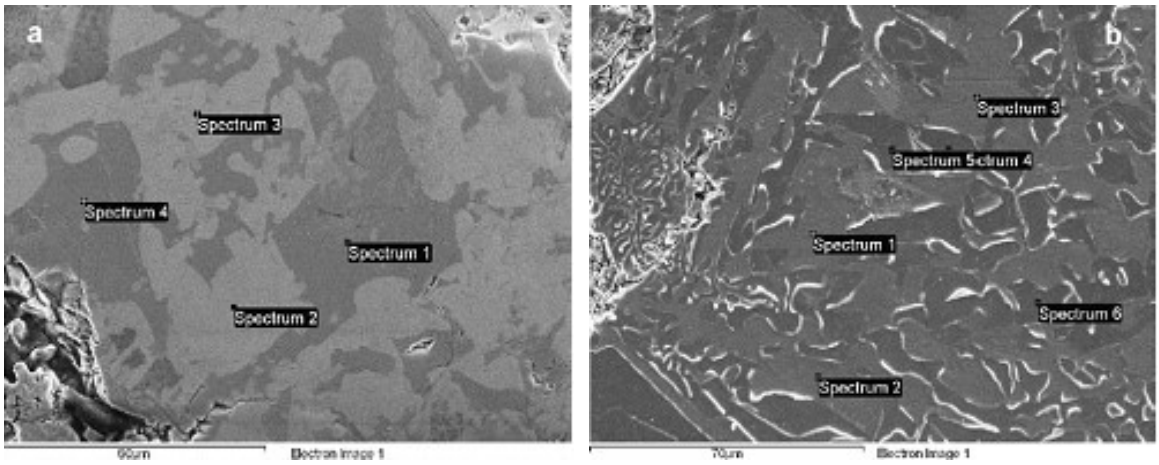

Figure 36: SEI of the locations were EDS was performed: a). "non-oxidized" specimen, the presence of oxygen is almost the same in both phases b). For "oxidized" specimen in different phases, oxygen is more present in the zirconium than in the Laves phase.

Table 9: Composition of "non-oxidized" specimen and "oxidized" specimen using EDS

Spectrum “non-oxidized” specimen	O	V	Fe	Zr	Total
Spectrum 1	13.32	45.28	9.31	32.09	100
Spectrum 2	14.94	4.93	0.00	80.12	100
Spectrum 3	12.52	8.99	0.00	78.48	100
Spectrum 4	18.82	42.07	8.99	30.12	100
Spectrum “oxidized” specimen					
Spectrum 1	59.75	4.47	0.00	35.78	100
Spectrum 2	60.99	0.45	0.00	38.56	100
Spectrum 3	60.48	1.81	0.00	37.70	100
Spectrum 4	19.29	40.69	9.07	30.95	100
Spectrum 5	16.46	41.41	9.85	32.28	100
Spectrum 6	0.00	51.88	10.86	37.25	100

4.5.2 AES analyses

The surface of the getter materials is particularly difficult to analyze because of their high chemical reactivity. The results obtained can, therefore, be strongly influenced by the experimental set-up and the procedures [75, 76] as recently confirmed through our measurements. The results from the AES, Figures 37 and 38 are similar to those obtained with EDS (Figure 36). Again, we can observe that oxygen is more present in the Zr-rich phase than in the Laves phase.

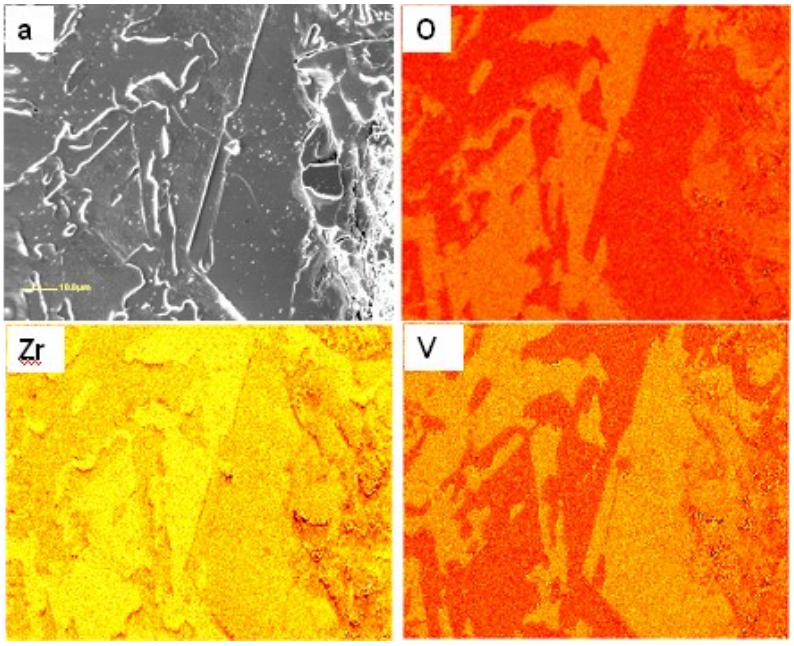

Figure 37: a). SEI- Scanning Electron Image of the Oxidized St 707 alloy, and SAM – Scanning Auger maps show the distribution of O, V, and Zr on a polished surface of the oxidized St 707 alloy

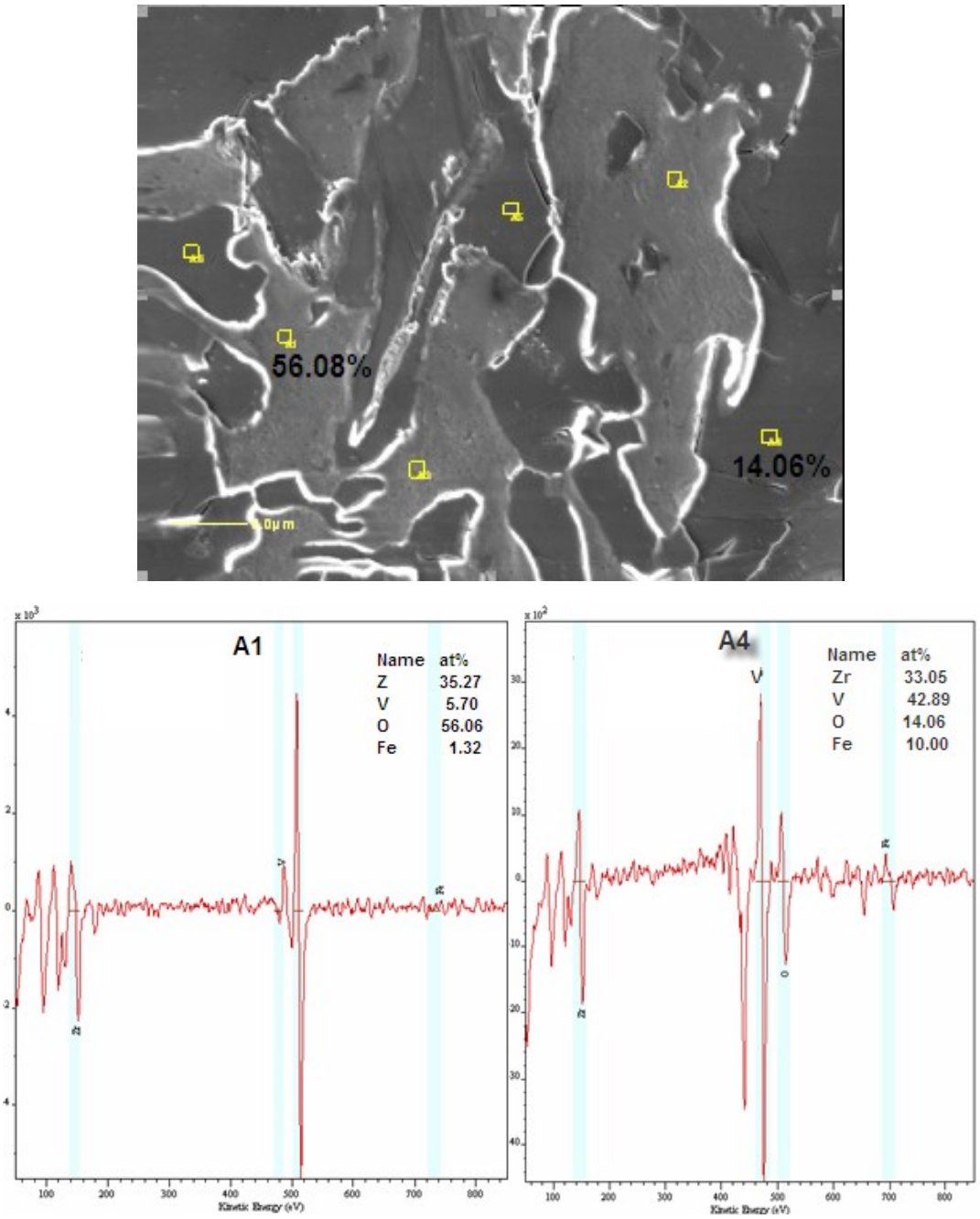

Figure 38: SEI of indicated locations of AES analyses of "oxidized" specimen in different phases, more oxygen is present in Zr phase, shown in spectrum A1-56.08 % than in the Laves phase, spectrum A4-14.06 %.

From Figure 38 we see that the content of oxygen in atomic percent (in the depth 153 nm) in the Zr phase (spectrum A1) is 56.08 %, and in the Laves phase (spectrum A4) is 14.06 %. Also, from mapping, a larger oxygen content in Zr compared to the Laves phase (Figure 37) was observed. In addition, a larger amount of oxygen along the grain boundary and dislocations in crystal grains is observable, because the grain boundaries, as dislocations, are considered as short-circuits for atomic diffusion in metals [36].

AES depth profiling measurements were made at some points of the specimen in order to be able to estimate the penetration depth of the oxygen within the getter, concretely for the zirconium-rich phase, (Figure 39a) and the Laves phase (Figure 39b). This measurement technique makes it possible to distinguish the oxidized zone (the presence of ZrO_2) and the diffused zone (the zone where oxygen is dissolved). Because of the

formation of ZrO_2 chemical bond in the zirconium-rich phase there is the presence of the oxidized layer. This oxidized layer is absent in the Laves phase. On the other hand, the thickness of the diffused layers is higher for the Laves phase compared to the zirconium-rich phase.

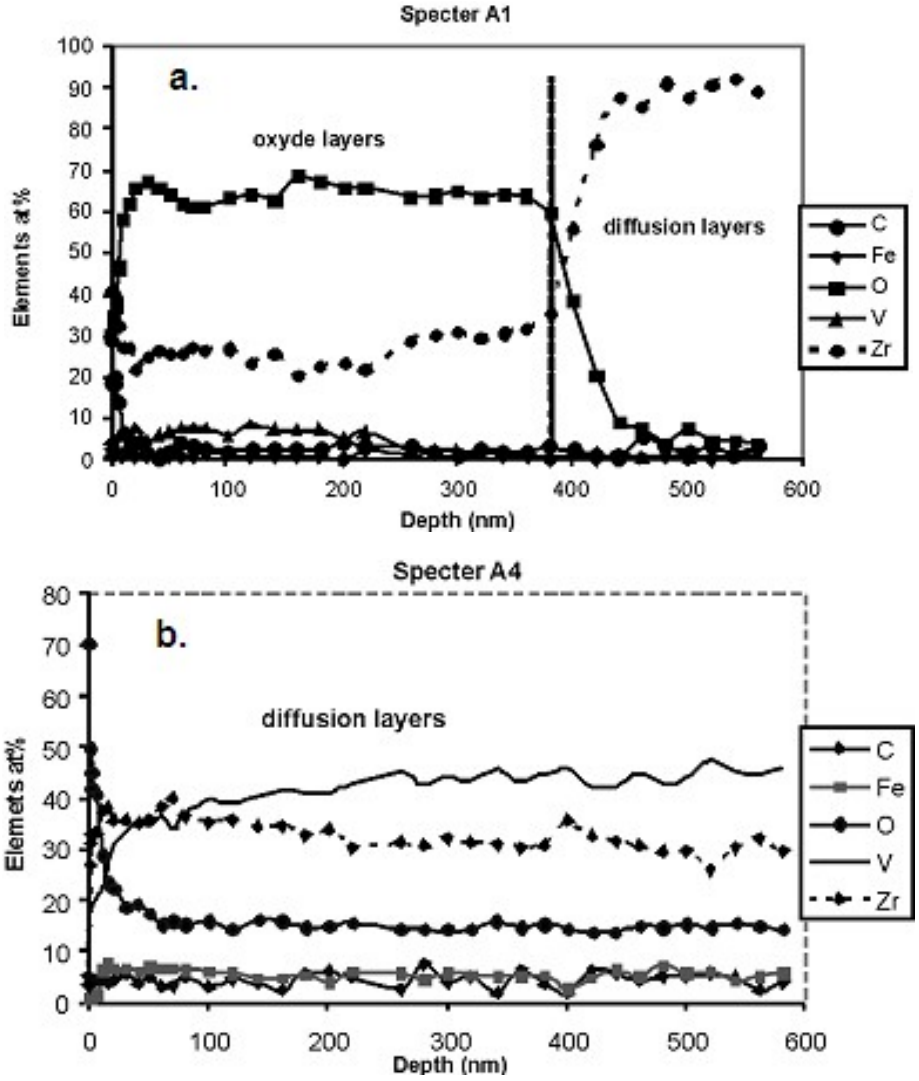

Figure 39: AES depth profiles for a) Zr phase and b) Laves phase of the oxidized sample at 450 °C for 60 min.

4.5.3 X-ray diffraction analysis

XRD analyses were carried out in order to determine the phases present in the materials. The phase composition was determined by X-ray powder diffraction (XRD) at Institute Jozef Stefan, Ljubljana, Advanced Materials Department, with a Bruker Axs D4 ENDEAVOR using CuK_a radiation (($\lambda = 0.15406$ nm).

We confirmed that the "non-oxidized" specimen alloy is biphasic at room temperature (300 K), consisting of hexagonal α-Zr and the cubic Laves phase $Zr(V_{1-x}Fe_x)_2$ as shown in Figure 40a and indicated in references [69, 77]. We can see in Figure 40b that for the specimen treated at 450 °C under oxygen partial pressure of 1.2×10^{-6} mbar the intensity of the Laves phase will decrease and, at the same time, a new phase of ZrO_2 will emerge. This new phase comes as consequence of ZrO_2 bond formation at high temperatures. The

ZrO_2 has a monoclinic structure. The "non-oxidized" specimen exhibits narrower XRD peaks, while with the oxidized specimen a certain broadening of the peaks (mainly Laves phase) due to lattice strains and distortions can be observed.

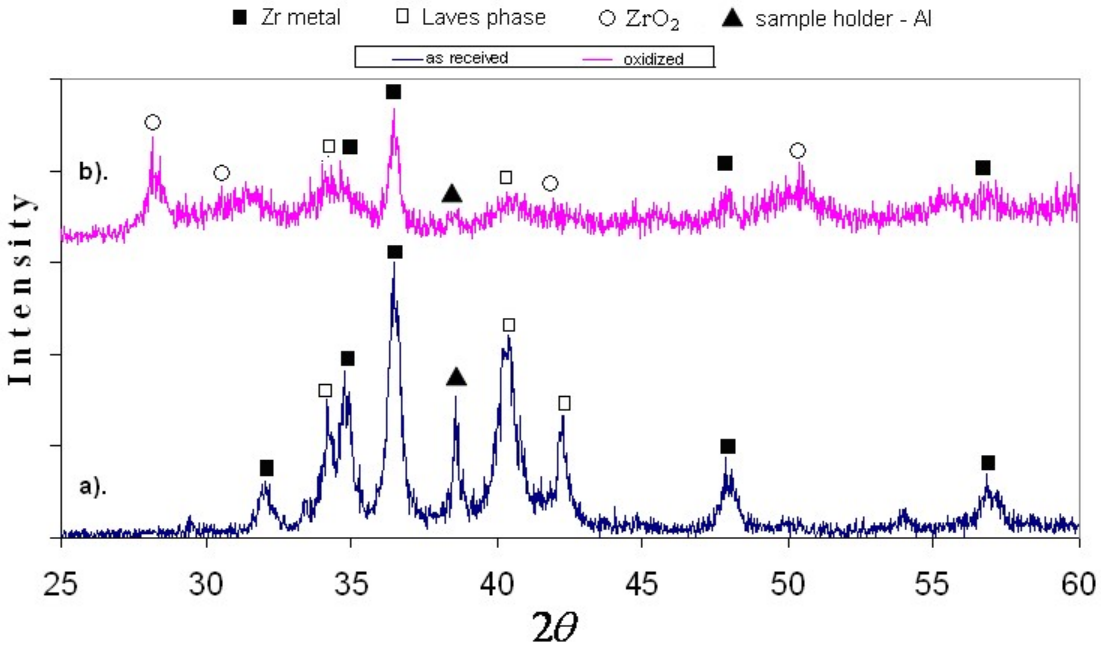

Figure 40: X-Ray diffraction spectra: a) "non-oxidized" specimen, b) oxidized specimen at 450 °C for 1h

4.6 Discussion about oxygen diffusion in NEG

The diffusion length during the time t and temperature T is given by:

$$L = \sqrt{D(t)\,t} \tag{27}$$

where L (cm) is the thickness, D (cm^2s^{-1}) is the diffusion coefficient and t (s) is the time. The diffusion coefficient (or diffusivity) in metal at the temperature T is:

$$D = D_0(t)\ \exp\left(-\frac{E}{RT}\right) \tag{28}$$

where D_0 is a constant, E is the activation energy for diffusion, and R is the universal gas constant. In the literature [78] we have found following values for hexagonal α-Zr (mean of two data): D_0 = 0.21 cm^2 s^{-1} and E = 184.1 kJ mol^{-1} K^{-1}, and for cubic V: D_0 = 0.013 cm^2 s^{-1} and E = 121.3 kJ mol^{-1} K^{-1}. Using these oxygen diffusion values we get for Zr: D (T = 723 K) = $1.3\times10^{-14}cm^2$ s^{-1} and for V: D(T = 723 K) = 2.6×10^{-11} cm^2 s^{-1}. The corresponding diffusion lengths for 1 hour treatment at 450 °C are 70 nm for Zr and 3050 nm for V. We can see from Figure 40a that in the diffusion layer in Zr phase the drop of oxygen concentration from 66 % to nearly zero occurs in approximately 100 nm. Because of almost 50 times larger diffusion length in V we can not see in Figure 40b a considerable change of oxygen concentration in Laves phase over the investigated depth of 600 nm. The data for the diffusivity and the solubility limit from the literature give us a global view about the diffusivity and solubility limit in single-crystal pure metals.

However, the NEG materials under investigation are alloys. The diffusivity and the solubility-limit values that can be found in the literature are valid for single crystals, so they are not very helpful to evaluate the diffusivity and the solubility limit in the case of alloy. It is known that the diffusivity and the solubility limit increase in the presence of grain boundaries. From the literature we find that metals of the 5B group (in our case vanadium) have a higher diffusivity for oxygen than elements of the 4B (in our case zirconium) group, whereas the solubility limit values indicate that metals of the 4B group (Zr) have higher storage capacities for oxygen than those of the 5B group [36]. This can be clearly seen from the results of our measurements, which are presented in Figure 39. There are two layers in the zirconium-rich phase, the first one is the oxidized layer, and the second is the diffused layer. On the other hand, in the Laves phase there is only the diffused layer. The appearance of the oxidized layer in the zirconium-rich phase is the consequence of the affinity of Zr to form chemical bonds with O_2 at elevated temperatures. As a consequence of the composition of ZrO_2, the presence of oxygen in the zirconium-rich phase in mole fractions (%) can be twice that of the zirconium atoms at most, which is evident in Figure 39a. By increasing the temperature or time of oxidation, we will observe an increase in the thickness of the oxidized layer, whereas the structure of diffused layer will remain similar. Thus we have a saturation of the zirconium-rich phase with oxygen in the oxidized layer. On the other hand, in the Laves phase the oxidized layer practically does not exist. Only the diffused layer is present there, which is in accordance with theory [36]. According to theory, the elements of the 5B group have a greater affinity for oxygen diffusion compared to those of the 4B group, whereas the solubility in these elements is quite small.

5 A study of hydrogen outgassing from Stainless Steel chamber with well defined wall thickness

Stainless steel (SS) is very important material for building vacuum systems. So the knowledge of outgassing and procedures to reduce outgassing of this material is important. In this section we will discuss only hydrogen outgassing from SS which is the dominant gas after the removal of adsorbed surface water vapor and other atmospheric gases.

Experience has shown that the typical outgassing rate of vacuum components made from SS is of the order of 10^{-11} mbar l $s^{-1}cm^{-2}$ without additional processing. An outgassing rate of 10^{-13} mbar l $s^{-1}cm^{-2}$ is achievable "routinely" with a sufficient bake-out treatment. Outgassing rates lower than 10^{-14} mbar l s^{-1} cm^{-2} are achievable only with exceptional care, particularly in thin-wall vessels [55]. Until now several experimental data have been published about reduction of outgassing rate of SS by conventional bake-out or vacuum firing, but the resulting outgassing rates are not consistent: similar bake-out temperature and time gave significantly different numerical values for outgassing rates.

In 1967 Calder and Levin published a paper on the reduction of outgassing of hydrogen from metals. They proposed a diffusion limited model (DLM), which means that atomic hydrogen concentration at the surface is zero and the hydrogen atoms desorb and recombine as molecules as soon as hydrogen reaches the surface. But their assumption was not correct for lower outgassing rates, whereas their assumption was reasonable for higher outgassing rates. The experimental values obtained by Calder and Levin were two orders of magnitude larger [53] than expected from DLM model. Their assumption in solving the diffusion equations, that the surface density of hydrogen is always zero, is therefore questionable. To overcome this problem, Moore [79] calculated outgassing rate using a recombination limited model (RLM). His assumption was that surface density can never be zero, and during solving the diffusion equation boundary conditions have to be included.

Another effort to reduce outgassing rate was given by Nemanic, Setina, Bogataj and Zajec [80, 81, 82] using very thin-wall vessels instead of using thicker materials. They introduced also a Fourier number (or dimensionless time) $F_0 = D\,t\,d^{-2}$ to describe the

heat treatment intensity. They reported the extremely low outgassing rates of about 10^{-17} mbar l s^{-1} cm^{-2} which were achieved using thinner materials [80]. Therefore the use of thin materials is more efficient and economically more suitable, because much shorter baking times than in the past can be used. However for the practical realization of a vacuum chamber the use of very thin walls may not be suitable because of insufficient mechanical strength.

5.1 Measuring of outgassing flux and outgassing rate

Outgassing flux of a SS sample can be measured by two general methods [12]. Applying the first method, the pressure rise with time is measured in a closed vacuum chamber after its evacuation to a low pressure. This method is called the rate-of-rise (RoR) method or gas-accumulation method. The outgassing flux Q is obtained as:

$$Q = V \frac{dP}{dt} \tag{29}$$

where V is the chamber volume and dP/dt is the measured rate of pressure rise in a closed chamber at a constant temperature.

Using the second method, the chamber under test is pumped through an orifice of known conductance and the pressure drop across the orifice is measured. This method is known as the throughput method or the orifice method. The outgassing flux Q is expressed as:

$$Q = C\,\Delta P \tag{30}$$

where C is the conductance and ΔP is the pressure difference.

In both cases the outgassing rate q of the sample is obtained by dividing measured outgassing flux Q with the surface area A of the sample: $q=Q/A$. The measured outgassing rate is a net rate being the difference between the intrinsic outgassing rate of the surface and the readsorption rate.

A common problem of both methods is also the fact that sample under test is placed in a vacuum measurement chamber whose walls also outgas during measurement. So it is necessary to measure the "background" outgassing flux of the empty chamber and subtract it from the measured flux with the sample in the chamber.

The presence of a hot cathode residual gas analyzer (RGA) or ion gauge in the test chamber can cause extra outgassing and also reactions of residual gas on hot filament can occur. Since they exhibit also a certain pumping speed, RoR measurements shall be only made using inert vacuum gauges such as a spinning rotor gauge (SRG).

5.1.1 Experimental setup and sample description

We have performed a study of time dependence of the outgassing rate of SS during bake-out at 250 °C and 350 °C. Main goal was to determine a necessary time to reach the outgassing rate below 10^{-13} mbar l $s^{-1}cm^{-2}$ at these bake-out temperatures.

We have made two simple cylindrical chambers to be used as outgassing samples. They are shown in Figure 41. Each chamber was assembled from CF 16 flanges, a short connection tube with an inner diameter of 16 mm and a wall thickness of 1.5 mm, circular end plates with a thickness of 2 mm and cylindrical body with an inner diameter d_i=108.7 mm and a wall thickness 2.62 mm. The only difference between two chambers was a different length. The length of cylindrical body of chamber V1 was only l_1=10 mm, while that of the chamber V2 it was l_2=210 mm.

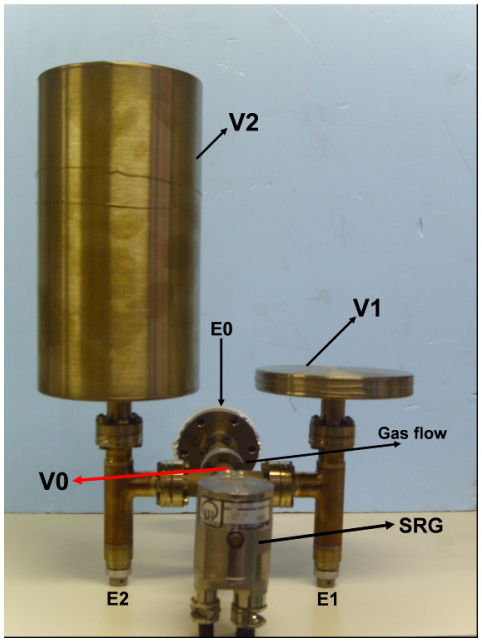

Figure 41: Photo of two SS cylindrical chambers being used for the outgassing rate study.

The chambers were connected to vacuum measurement system as shown in Figure 42. System was pumped with turbo pump and was equipped with a quadrupol mass spectrometer (QMS), a Bayard-Alpert gauge (BAG) and a spinning rotor gauge SRG. SRG is connected to a small chamber V0 which is composed of a standard CF16 4-way cross and a CF16 T-piece. The chamber V0 can be isolated from pump by valve E0. The chambers V1 and V2 are connected to V0 in symmetrical way through bakeable CF16 all all-metal valves E1 and E2, respectively. A calibration gas can be introduced into V0 through a valve E3.

For the modelling of outgassing behaviour of SS by DLM and RLM the thickness of the sample is a very important parameter. The same reduction of the outgassing rate of a plane sheet is achieved in a 4 times longer time if the sample is 2 times thicker. All parts of the measurement sample chamber were made of AISI type 304 L SS, but we were not able to make the whole chamber from the same sheet of SS. Also the thickness of different parts was different. However the measurement procedure was designed in such a way that we could easily calculate the outgassing rate of the cylindrical body (which has a well-defined thickness) from separate measurements of the outgassing flux of each chamber.

The chambers V0, V1 and V2 were placed in an oven where they could be uniformly heated up to 350 °C. Additional vacuum measurement instruments (BAG and QMS) were mounted outside the oven due to the limitation of their operational temperature. During the bake-out a SRG suspension head was removed and only a thimble with a rotor was baked together with other parts.

Outgassing flux measurements at ambient temperature were carried out by the RoR method, whereas outgassing flux measurements during baking the vacuum system (at the temperature of 250 °C and 350 °C) were performed using a throughput method which is described in paragraph 5.1.3.

5.1.2 Measuring outgassing flux using RoR method

By closing the valves E0, E2 and E3 and opening the valve E1 we can measure with SRG a pressure increase in the chambers V0 + V1 to calculate the outgassing flux

$Q_1 = (Q_{V0} + Q_{V1})$. With the same SRG we can also measure a pressure increase in the chambers V0 + V2 when the valve E1 is closed and E2 opened. This measurement gives us $Q_2 = (Q_{V0} + Q_{V2})$. In both cases Q_{V0} is the same because of symmetrical configuration of the connection of V1 and V2. By subtracting the two measured outgassing fluxes the outgassing flux of V0 can be eliminated: $Q_2 - Q_1 = Q_{V2} - Q_{V1}$ and the difference is exactly equal to the outgassing flux evolving from the part of the cylindrical body of the chamber V2 having an area $A = \pi d_i \times (l_2 - l_1)$.

To calculate the outgassing flux by the RoR method following Eq. (29) we need to know the volume of the measurement system. The volumes V1 and V2 can be calculated from a geometrical measurement because they are composed of simple cylindrical parts. The volume V0 has much more complicated geometrical shape because it includes also an inner volume of CF16 valves. Its volume can be determined by the static gas-expansion method. The calculated surface areas of V1 and V2 are quite accurate, but for a surface area of V0 we can only make a rough estimate. The values of volume and surface area for each of three parts of vacuum system are given in Table 10.

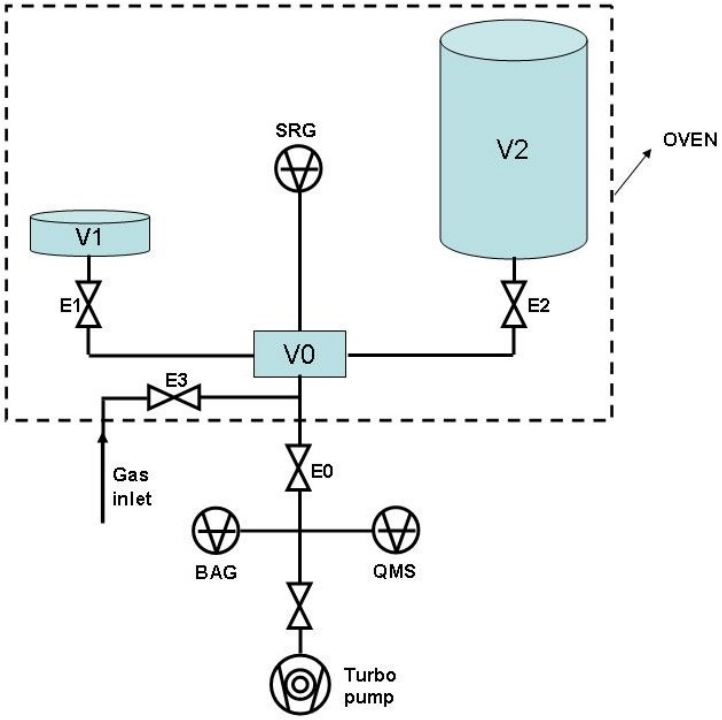

Figure 42: Schematic of the outgassing measurement system. QMS- quadrupole mass spectrometer, SRG - spinning rotor gauge, BAG – Bayard-Alpert gauge, E0, E1, E2 and E3 – bakeable vacuum valves, V0, V1 and V2 - measuring volumes

Table 10: Values of the geometrical surface area and volume including their ratio for each part of the vacuum measurement system

	Geometrical surface area [cm^2]	Volume [l]	Ratio V/S [l cm^{-2}]
V0	475 (rough estimate)	0.1206	$2.54 \cdot 10^{-4}$
V1	247	0.1046	$4.23 \cdot 10^{-4}$
V2	931	1.962	$2.11 \cdot 10^{-3}$
V_{Tot}	1653	2.1872	$1.32 \cdot 10^{-3}$

5.1.3 Measuring outgassing flux using throughput method

To measure the outgassing flux of test chambers during the baking the use of SRG is not possible because the operating temperature range for the measuring head of SRG is only from 10 °C to 50 °C [83]. As a consequence, it is also impossible to use the RoR method. Therefore, in this case an adapted throughput measurement method which differs from the orifice method has been applied.

The steady-state outgassing flux from the chamber V1 can be calculated by measuring the pressure difference ΔP_1, being indicated by BAG or QMS while opening and closing the valve E1. By knowing the effective pumping speed S at the point where BAG or QMS are connected to the vacuum system we can calculate the corresponding outgassing flux $Q_1 = S \times \Delta P_1$. Similarly, by opening and closing E2 we can get ΔP_2 and from it the outgassing flux $Q_2 = S \times \Delta P_2$. Also in this case the difference of two fluxes gives us the outgassing flux coming from the part of the cylindrical body of the chamber V2 having the area $A = \pi d_i \times (l_2 - l_1)$, like in the case of RoR measurements.

We were interested mainly in the outgassing of hydrogen from SS, so we used for the ΔP measurement a QMS tuned to the mass number 2 (H_2 peak). The basic output signal of QMS is an ion current of a particular gas. The ion current I_i^+ as a function of partial gas pressure P_i is given by $I_i^+ = g_i \times P_i$ where g_i is the sensitivity coefficient which depends on the type of gas, QMS geometry and settings of various operational parameters. For accurate measurements g_i has to be determined experimentally (calibrated *in-situ*) for each instrument and each gas separately. Therefore, to measure the outgassing flux of hydrogen it was necessary to determine the sensitivity coefficient of QMS g_{H2} and the effective pumping speed S_{H2}. For hydrogen the outgassing flux Q equals:

$$Q = \frac{S_{H_2} \cdot \Delta I^+_{H_2}}{g_{H_2}} \tag{31}$$

To make the determination of the outgassing rate $q = Q/A$ easier we can combine the effective pumping speed and the sensitivity coefficient into a single calibration coefficient K_{H2}:

$$K_{H_2} = S_{H_2} / g_{H_2} \tag{32}$$

The calibration coefficient K_{H2} can be determined quite straightforward experimentally as it will be described in the next paragraph.

5.2 Determination of Calibration Coefficient

We can introduce a known flow of a calibration gas through the valve E3 which is an adjustable leak valve. By closing the valves E0, E1 and E2 the flow rate of the calibration gas Q_{cal} into the volume V0 can be measured by the RoR method using the same SRG as for the outgassing flux measurement. After the flow of calibration gas is determined we can measure a difference in hydrogen ion current ΔI_{H2}^+ by opening the valve E0. Since the calibration gas flow was introduced to QMS from the same direction as the outgasing flux from measuring chambers, calibration coefficients for the calibration gas flow and the outgassing flux are of the similar value. It can be calculated by rearranging Eq. 31:

$$K_{H_2} = \frac{Q_{\text{cal}}}{\Delta I^{+}_{\text{H}_2}} \tag{33}$$

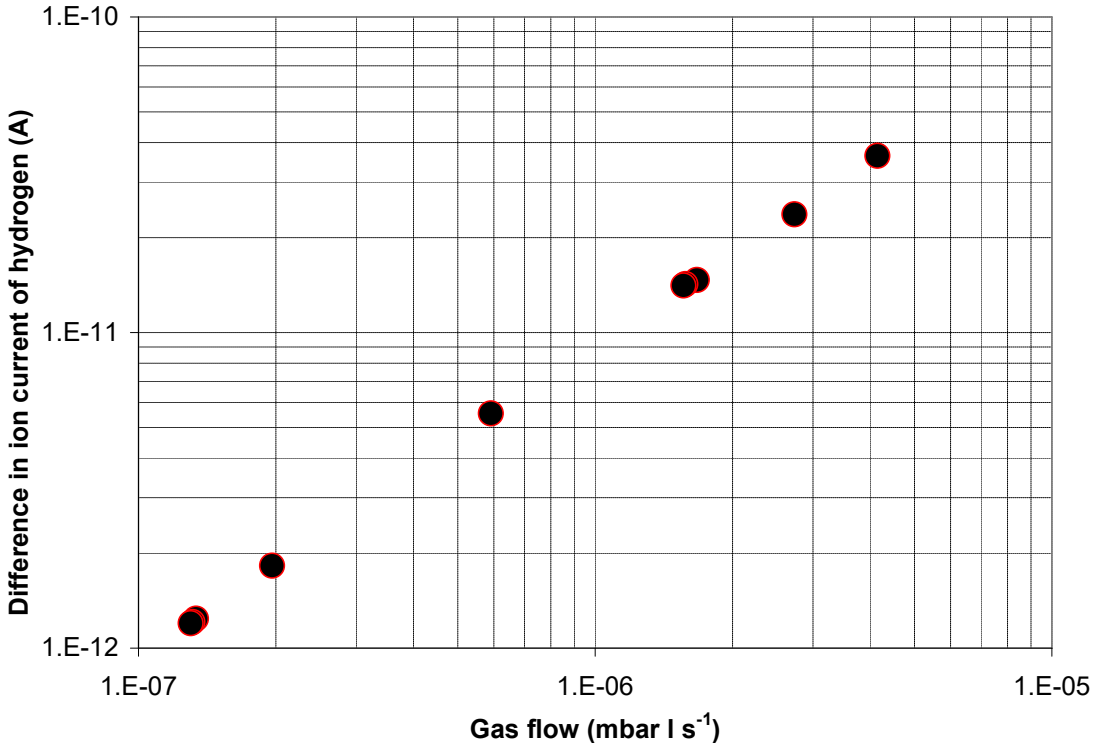

Figure 43: Difference in hydrogen ion current, measured by QMS vs. hydrogen gas flow, measured by SRG (using the RoR method)

The measurements of $\Delta I_{H2}{}^{+}$ have been done for a wider range of calibration gas flow Q_{cal} and it can be seen in Figure 43 that when the Q_{cal} (measured by SRG) increases, also the $\Delta I_{H2}{}^{+}$ (measured by QMS) increases proportionally.

Table 11: Values of calibration coefficient of QMS for hydrogen while measuring outgassing flux by the throughput method.

I^{+} (A)	K (mbar l A^{-1} s^{-1})
1.21E-10	116998
1.10E-10	118505
3.63E-11	114295
2.37E-11	115234
1.47E-11	113737
1.42E-11	110694
1.41E-11	110739
5.54E-12	106750
1.83E-12	107483
1.24E-12	107763
1.21E-12	108467
1.20E-12	108439

From the data in Figure 43 and using Eq. (33), we have calculated the calibration coefficient. The calculated values are given in Table 11. The mean value of the calibration coefficient K of QMS for hydrogen was 1.12×10^5 mbar l A^{-1} s^{-1} and the relative standard deviation was $\sigma(K)/K = 3.61\%$.

The final equation to calculate outgassing rate is the following:

$$q = \frac{K}{A}\left(\Delta I_{V2} - \Delta I_{V1}\right)$$

where ΔI_{V1} and ΔI_{V2} are the changes in hydrogen ion current when closing the valves E1 and E2, respectively.

5.3 Time dependence of H_2 outgassing during bake out at 250 °C

Measuring chambers were first baked at 250 °C for a total time of 380 h. After that bake-out was continued at 350 °C for another 140 h. The chambers were baked by keeping one side of the chamber wall in air while the other side was under vacuum.
During bake-out at 250 °C we have performed several measurements of the outgassing rate at the bake-out temperature using the throughput method. The heat treatment intensity expressed as a Fourier number, time of baking of the system and outgassing rate values during the heat treatment are given in Table 12.
The Fourier number (or dimensionless time) $F_0 = 4\,D\,t\,d^{-2}$ is a characteristic quantity or "dimensionless time" for describing and modeling diffusion and shall be used to compare outgassing rates obtained while performing different experiments. To determine the dimensionless time F_0 we should know: diffusion constant D for hydrogen at temperature T, processing time t and the thickness of wall. The last two parameters, the processing time and the wall thickness, are measured directly. The temperature dependence of D is given by,

$$D = D_0 \exp\left(-\frac{E_a}{KT}\right) \tag{34}$$

Typical values for diffusion pre-exponencial factor D_0 = 0.012 cm^2 s^{-1} and activation energy E_a=0.57 eV [84] were used to calculate F_0 values.

The bake-out at 250 °C was interrupted few times to cool-down the chambers down and measure outgassing rate at room temperature. The time course was the following: bake-out at 250 °C for 24 hours followed by interruption for room temperature measurement - bake out at 250 °C for 73 hours followed by interruption for room temperature measurement and again bake out at 250 °C for 284 hours followed by the room temperature measurement. After this temperature was raised 350 °C and baking was performed for additional 140 hours. System was then cooled down again and last measurement at room temperature was performed. Results of hydrogen outgassing rate measurements at room temperature, which were performed using RoR method, are summarized in Table 13.

A comparison of our result of room temperature outgassing rate with the results obtained by Park et. al.[85] is shown in Figure 44. Fourier numbers for the data from the paper of Park et. al. were recalculated using our activation energy for the diffusion E_a=0.57 eV (instead of E_a=14.5 kcal mol^{-1} ~0.622 eV which was used by Park, et al). We can say that our results and results of Park et al. roughly agree within a factor 3 to 4.

Table 12: Measured hydrogen outgassing rate of stainless steel chamber during bake out; all outgassing rates are measured at a temperature of 250 °C.

ΣF0	t(h)/250 °C	q (mbar l s^{-1}cm^{-2})
0.20	24	$2.6\cdot10^{-8}$
0.77	95	$1.10\cdot10^{-8}$
0.77	95.2	$1.12\cdot10^{-8}$
0.78	96	$1.19\cdot10^{-8}$
0.88	108	$8.20\cdot10^{-9}$
0.89	110	$8.40\cdot10^{-9}$
0.91	112	$8.80\cdot10^{-9}$
1.54	190	$4.20\cdot10^{-9}$
1.59	196	$3.90\cdot10^{-9}$
1.71	211	$2.90\cdot10^{-9}$
1.72	211.5	$2.95\cdot10^{-9}$
1.72	212	$3.00\cdot10^{-9}$
1.84	227	$2.50\cdot10^{-9}$
1.86	228.5	$2.40\cdot10^{-9}$
1.87	230	$2.30\cdot10^{-9}$
2.06	254	$2.00\cdot10^{-9}$
2.07	255	$2.05\cdot10^{-9}$
2.08	256	$2.08\cdot10^{-9}$
2.26	278	$1.80\cdot10^{-9}$
2.27	279	$1.85\cdot10^{-9}$
2.84	350	$1.00\cdot10^{-9}$
2.85	351	$1.05\cdot10^{-9}$
3.06	376	$6.90\cdot10^{-10}$
3.07	378	$7.30\cdot10^{-10}$

Table 13: Hydrogen room temperature outgassing rate after receiving given bake-out treatment.

T (°C)	incremental time Δt (h)	$F_0(\Delta t)$	$\sum F_0$	q (mbar l s^{-1}cm^{-2})
250	24	0.19	0.19	2.10×10^{-12}
250	73	0.59	0.78	7.90×10^{-13}
250	284	2.31	3.09	2.86×10^{-13}
350	140	8.66	11.75	5.70×10^{-14}

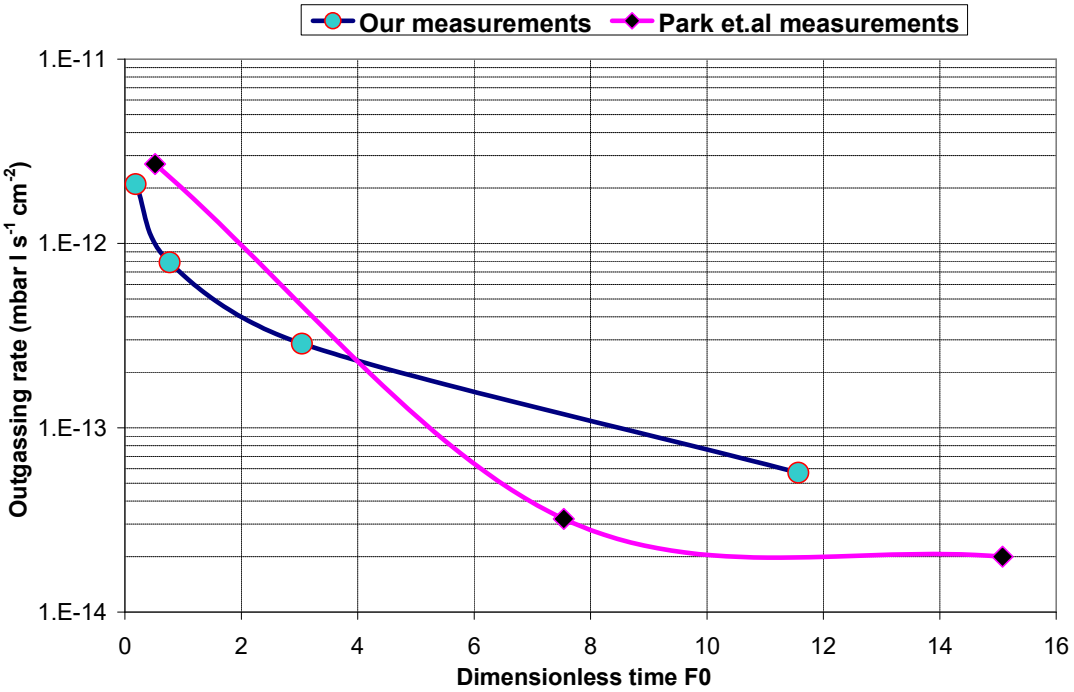

Figure 44: Comparison of hydrogen outgassing rates between our measurements and the measurements of Park et.al [85]; the latter were done after the system was cool down at room temperature.

A graphical representation of results of outgassing rate measurements at 250 °C (taken from Table 12) as a function of dimension less time F_0 is shown in Figure 45.

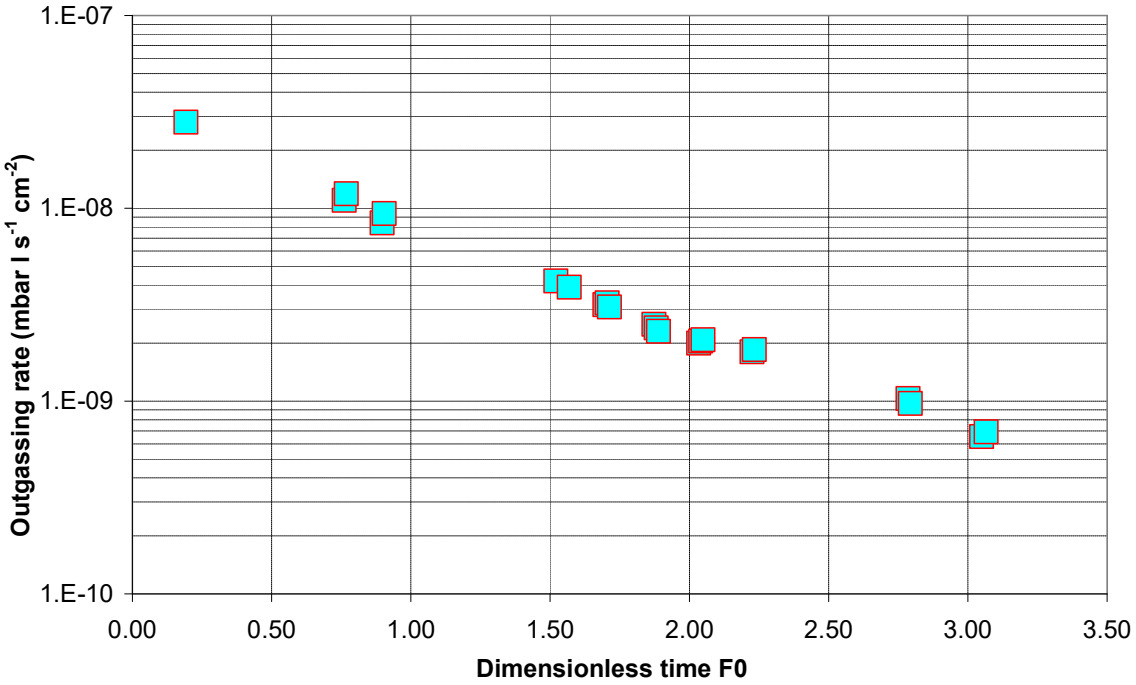

Figure 45: Hydrogen outgassing rate of stainless steel in dependence on the dimensionless time measured during the heat treatment at 250 °C.

In Figure 46, the same measured outgassing rate data as a function of bake-out time are presented and compared with calculations based on diffusion limited (DLM) [44,54]. It can be concluded that the outgassing rate predicted by diffusion theory for t = 380 h is $q = 5 \times 10^{-11}$ mbar l s^{-1} cm^{-2} which is 15 times lower than measured value $q = 7 \times 10^{-10}$ mbar l s^{-1} cm^{-2}.

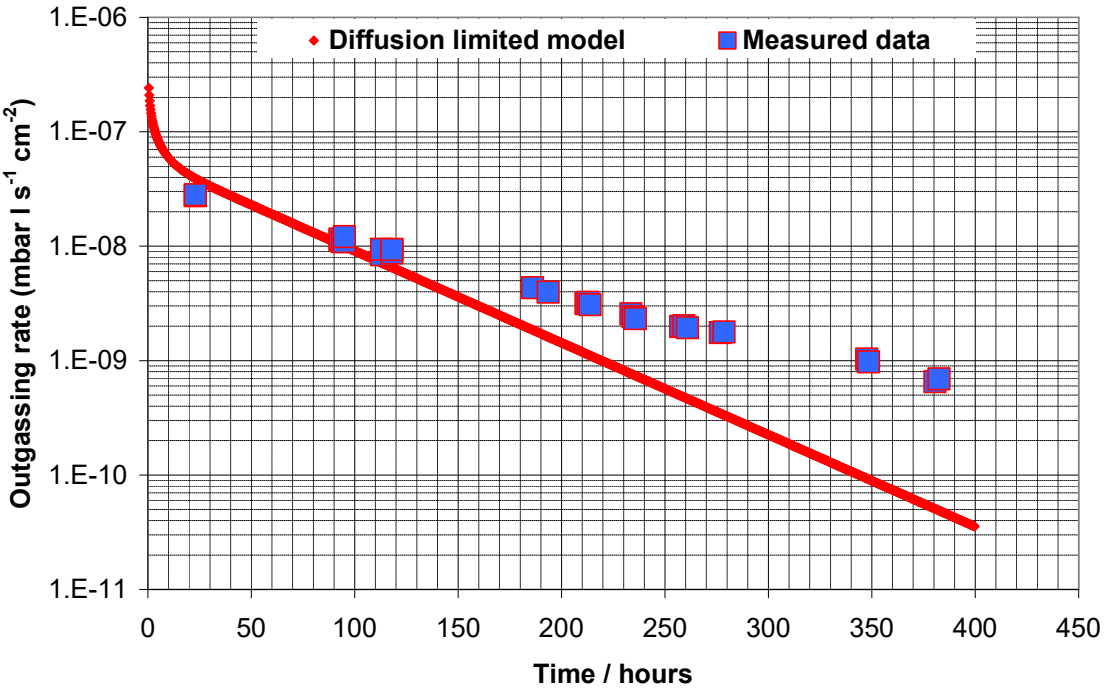

Figure 46: Hydrogen outgassing of stainless steel in dependence on bake-out time calculated by DLM and compared to the measured data during the heat treatment at 250 °C.

In the early stage of bake-out, approximately up to 100 h at temperature 250 °C, a curve obtained by DLM and measured data still agree to each other. But after 100 h the discrepancy starts to emerge. It is assumed that for a Fourier number $F_0 > 0.8$ the atomic hydrogen recombination on the stainless steel surface becomes a rate limiting step. When a hydrogen atom from the bulk has moved to the surface/vacuum interface, it needs to find another hydrogen atom on the surface to recombine. The smaller the number of freely-movable hydrogen surface atoms, the less probable is recombination. So, when the diffusion of hydrogen atoms to the surface become small, the recombination of the hydrogen atoms might be the rate limiting step i.e. the outgassing from the surface is then no longer given by the bulk diffusion rate, but by the rate at which the hydrogen atoms can be recombined.

5.4 Intermediate conclusions about outgassing

The determination of calibration coefficient K for BAG and QMS gave us the opportunity to measure the outgassing rate during the heat treatment without a need to stop heating. Diffusion limited model governs the initial removal of hydrogen from stainless steel, whereas it is assumed that hydrogen surface recombination plays an important role in the outgassing rate at lower hydrogen concentration. In order to compare a particular

treatment with another, the F_0 number seems to be a good choice since it can be accurately calculated for any processing time and temperature. Fourier number F_0 is a parameter which shows the level of heat treatment of stainless steel and it is related to the hydrogen diffusion in the stainless steel.
An outgassing rate $q = 2.86 \times 10^{-13}$ mbar l s^{-1} cm^{-2} at room temperature was achieved in the case of AISI type 304 L SS after baking the system at 250 °C for 380 h (conversion to dimensionless time gives F_0=3.09). This outgassing rate was reduced even further to $q = 5.7 \times 10^{-14}$ mbar l s^{-1} cm^{-2} by baking for another 140 h at T=350 °C ($\Delta F_0 = 8.66$, total dimensionless time $F_0 = 11.75$).

6 Application of getters for precise volume ratio measurements in static expansion system

Several methods have been used in vacuum metrology for volume determination. Measurements of volume ratios using the gas expansion methods below 10^{-4} mbar are influenced by hydrogen outgassing from the chamber walls. To reduce the increase in pressure in the expansion chambers during measurements, we have installed nonevaporable getter (NEG) pumps. Scheme of our experimental static expansion system with built-in getters is shown in Figure 47.

The system consists of stainless steel chambers and all-metal vacuum valves. An SRG that is attached to a small chamber is used for precise measurements of gas pressure before and also after the expansion. The SRG is an inert vacuum gauge and operates entirely at room temperature; therefore, no temperature gradients were introduced. Using a single gauge for the pressure measurement before and after the expansion, the SRG calibration constant (accommodation coefficient) cancels out while calculating the pressure ratio. Therefore, one can use an uncalibrated SRG rotor for such measurements. In contrast to previous reports on the use of SRGs for volume ratio determination [1, 6], we have also introduced NEG pumps in our expansion chambers. In chamber CH0, we used a St122 getter strip from SAES Getters. The St122 is an alloy consisting of Ti-Zr-V-Fe. In CH1, we mounted an SAES NEG cartridge pump Capacitor D 400-2, based on St172 getter material (consisting of Zr-V-Fe).

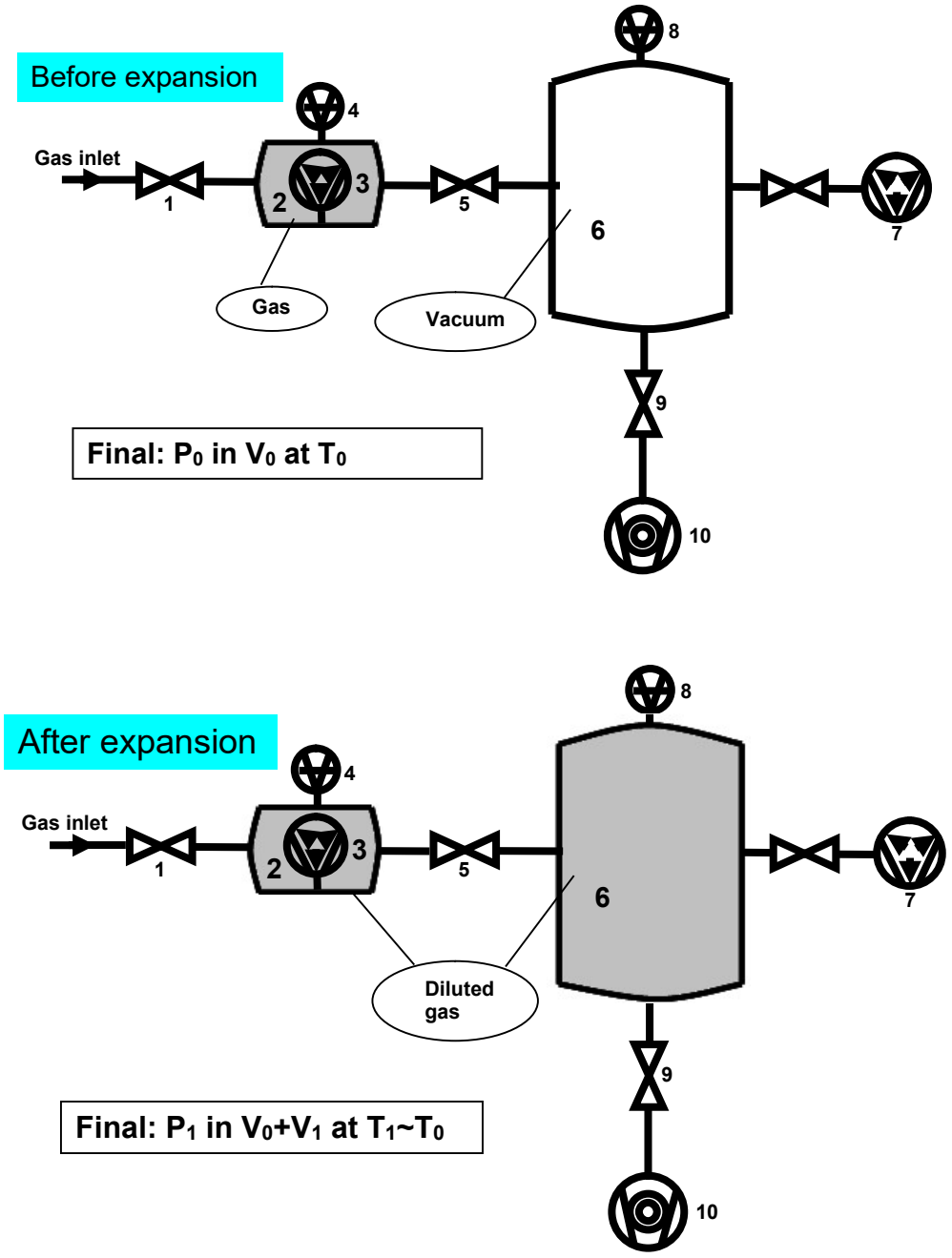

Figure 47: Scheme of our experimental static expansion system with getters. 1,5,9 valves; 2 small volume; 3,7-NEGP; 4,8-Spining Rotor Guage; 6-large volume; 10-turbopump

Basic principle of static expansion method has been already described in the introduction 1.1.1, where Eq. (6) describes relation between gas pressure and temperature before and after expansion. Taking into account that we make expansion at relatively low initial pressure, ($P_0 << 1$ mbar), we can neglect the virial correction, so Eq. (6) simplifies to:

$$p_1 = p_0 \frac{V_0}{V_0 + V_1} \frac{T_1}{T_0} \tag{35}$$

The volume ratio $R_V = \frac{V_0 + V_1}{V_0}$ is a crucial parameter of the expansion system, and it has to be determined with the highest possible accuracy.

We can define an isothermal pressure ratio R_{PI} as

$$R_{PI} = \frac{P_0}{P_1}\frac{T_1}{T_0} \tag{36}$$

It is obvious that $R_V = R_{PI}$. In the simplest case, when $T_1 = T_0$, we get the isothermal pressure ratio as a ratio between the initial and the final pressure.

The volume ratio of static expansion chambers can be determined from the ratio between pressures before and after expansion only when the total amount of gas remains unchanged. Because of the outgassing from the chamber walls, it becomes difficult to fulfill this condition in practice when the gas pressure after expansion is reduced below 10^{-5} mbar. Using getters and inert gases, the effect of outgassing can be eliminated. We have determined the volume ratio in our experimental static expansion system using inert gases, such as helium, argon and krypton. Assuming a zero pumping speed of NEGs for inert gases, Eq. (36) can be satisfied.

The use of a spinning rotor gauge (SRG) for volume ratio measurements was first proposed by Berman and Fremerey [86]. The idea is based on the fact that the response of an SRG is linear in the molecular flow regime. However, the useful dynamic range of the linear response that can be used for volume ratio measurements is quite limited. The linearity of the measured signal of an SRG as a function of nitrogen pressure becomes better than 0.1% at pressures below 0.05×10^{-2} mbar. SRG readings at a constant pressure have a Gaussian distribution, with a standard deviation decreasing in proportion to $\tau^{-2.5}$, where τ is the sampling interval [86]. For high-precision measurements with an SRG, a sampling interval of 30 s is usually selected. The standard deviations of readings (equal to type-A uncertainty) at τ=30 s are typically on the order of 1×10^{-8} mbar. This means that the type-A relative uncertainty of individual SRG readings becomes larger than 0.1 % at pressures below 1×10^{-5} mbar.

Consequently, one can perform volume ratio measurements within the linear range of an SRG with an uncertainty better than 0.1% only for volume ratios R_V <50. To overcome the problem of linearity and enable the measurement of volume ratios several times larger, Berman and Fremerey [6] proposed a series of measurements with an initial pressure P_0 distributed over the range from 0.1×10^{-2} mbar up to several 10^{-2} mbar. In such a series, the ratio between the measured SRG signal before and after expansion is not constant, but it decreases with increasing P_0. Berman and Fremerey fitted pressure-dependent ratios of the measured SRG signal (rotor deceleration rate) with a second-order polynomial function. An extrapolation of the fitting polynomial to zero pressure gives the volume ratio for the limiting case of a pure molecular flow regime. The same procedure was used in a more recent study by Jousten et al. [1]. However, in their experiment, they identified a problem associated with measurement of SRG offset and were able to obtain good agreement with another independent method of volume ratio determination only after using a fitted value of the offset instead of the measured value. They also pointed out that a small change in the offset on the order of 3×10^{-8} mbar (nitrogen equivalent) would change the extrapolated volume ratio by 0.1 % (in the case of R_V =109). This indicates that the procedure of extrapolating the fitting polynomial could lead to erroneous results in the volume ratio R_V for the case in which the measured pressure ratio obtained by the

gas expansion would be pressure dependent, as such pressure dependence would be hidden in the fitting polynomial. This can happen when the volume ratios are measured at very low pressures and, consequently, the outgassing of the chamber walls can contribute to additional gas being introduced during the expansion process.
In our experiments, we tried to avoid Berman and Fremerey's extrapolation procedure [1, 6]. Commercial SRG controllers use a linearization algorithm (embedded in the measurement software) to compensate for the decreasing measured signal due to gas viscosity effects in the transition flow regime (above 0.1×10^{-2} mbar). In a study of the reliability of these algorithms [87], we have found that their accuracy is better than 0.2% for pressures up to 10^{-2} mbar (in nitrogen gas), providing that correct gas parameters (temperature and viscosity) are entered into the controller. Therefore, we have decided to use the linearization algorithm from the SRG controller and to calculate the volume ratio using the pressure displayed by the SRG instrument (according to Eq. 36).

For temperature measurements, we attached one temperature sensor to each expansion chamber. A better temperature correction in Eq. (36) could be made using more temperature sensors, but we estimated that these two sensors were sufficient because our experimental system was quite small (volume V_1=10 l) and the whole experiment was performed under well-controlled ambient conditions. To reduce temperature drifts and transient local heating during the working day, we kept all electrical equipment (pumps) and lights switched on at all times (24 h/day). Temperatures measured by the two sensors were within 0.12 K during experiments, and the average temperature drift was less than 0.1 K/h. Such stability of the ambient temperature is also necessary for good offset stability of the SRG [88, 89]. In addition to creating stable temperature conditions, it is also necessary to ensure low vibrations [90]
As the viscosity correction factor in the linearization procedure and its uncertainty increased with pressure, we limited the gas pressure before expansion to $P_0 < 10^{-2}$ mbar in the case of N_2 and Ar, and to $P_0 < 3\times10^{-2}$ mbar in the case of He. Measurements with Kr were performed with $P_0 < 0.2\times10^{-2}$ mbar. This means that in our case of $R_V \approx 212$, the pressure after expansion P_1 was below 5×10^{-5} mbar in most measurements, so we used the sampling interval of 30 s. To further reduce the type-A uncertainty of P_1, we made 10 consecutive readings and used a mean value instead of a single measured value. The type-A uncertainty of the mean value was thus reduced by a factor of $10^{1/2}$ compared with the uncertainty of the single value. A drawback of this procedure is the prolonged total measurement interval spanning more than 360 s after the expansion (we also had to wait for two additional sampling intervals before we obtained the first reliable SRG reading after the mechanical disturbance of the system when the valves were manipulated for the gas expansion). As can be seen from our results, the outgassing from the chamber walls can significantly influence the measured expansion ratio during such a long measurement interval.
The system was evacuated from atmosphere to its base pressure (in the 10^{-9} mbar range) after several days of pumping. It was not baked in order to work under similar conditions to those encountered during regular calibrations with static expansion systems. Most capacitance diaphragm gauges are calibrated using the static expansion method, and almost all of them cannot be baked. In the case of the calibration of SRG rotors, baking is not recommended to avoid changes in the accommodation coefficient [86]. Another reason for omitting the system baking was to avoid partial activation of the getters before the first series of measurements.

At atmospheric pressure, an NEG surface is instantly covered by a protective oxide layer. To achieve gettering properties, NEG materials have to be activated in vacuum by heating at a high temperature (usually over 300 °C) for a certain amount of time. During the

activation, oxygen from the surface oxide layer diffuses into the bulk of the NEG, leaving a fresh surface composed of chemically active metals. Our St122 getter consists of a high-porosity, thick getter film (100 μm) sintered to a 50 μm–thick supporting metal strip. It was mounted to an electrical feed-through so it could be resistively heated. The Capacitor D 400-2 is a commercial getter cartridge with a built-in electrical heater.

According to general recommendations from SAES Getters, the total pressure during activation of NEGs should be less than 10^{-6} mbar. Malyshev et al. [91] have pointed out the importance of keeping the partial pressure of gases such as CO, CO_2, H_2O, O_2, and N_2 as low as possible during activation. Because our chambers were not baked, we introduced a pre-heating phase in order to degas the getters and their housing prior to activation. Pre-heating was done at a temperature of approximately 200 ºC for a period of 1 h.

The St122 getter strip was activated by heating at approximately 400 °C for 30 minutes. The Capacitor D 400-2 was activated at a temperature of 350 °C for a period of 8 hours.

After the activation of NEG pumps, only inert gases can be used for calibrations because any other "active" gases, including nitrogen, would be selectively pumped. Special care has to be taken not to poison the getter surface with residual gas molecules [91]. We were not operating any type of ionisation gauge in the expansion chambers, as pressure bursts caused by switching on the ionisation gauge or the residual gas analyser can poison the getter surface.

At first, we measured the pressure ratio without conducting the getter activation. A few measurements were done using nitrogen in order to compare them with subsequent measurements using argon. In the second series of measurements with the activated getter in CH1 only, we used argon. After the second series, we re-activated the St122 getter strip and performed the first activation of the capacitor pump. In the third series of measurements, we used argon, helium and krypton. Measurements with each gas lasted several days, and to maintain sufficient pumping capacity, both getters were re-activated before the change to another gas.

6.1 Volume ratio of a model static expansion system using NEG

Figure 48 shows the measurement with argon before the activation of the NEG pumps. Pressure readings in chamber CH0 before expansion (P_0) and readings of pressure P_1 after expansion (in chambers CH0 and CH1) are shown. We can see that the pressure readings are increasing in both cases because of the outgassing from the chamber walls. We can compare the importance of increases in pressures P_0 and P_1 on the same scale if we define "a relative increase in pressure" as the pressure reading divided by the mean value of 10 consecutive readings. We can see that because of the much higher P_0 pressure, the relative increase in pressure before the expansion was significantly smaller than the relative increase in the P_1 pressure after the expansion (Figure 49a).

After activation of the getter in CH1 (second series of measurements), the relative increase in the P_1 pressure was completely eliminated (Figure 49b) because the active residual gases released from the inner surfaces of the chamber were pumped by the NEG pump. We observed only random fluctuations of P_1, but the relative increase in P_0 remained unchanged. For the third series of measurements, we also activated the getter in CH0, and with this, we eliminated the increase in P_0 (Figure 49c).

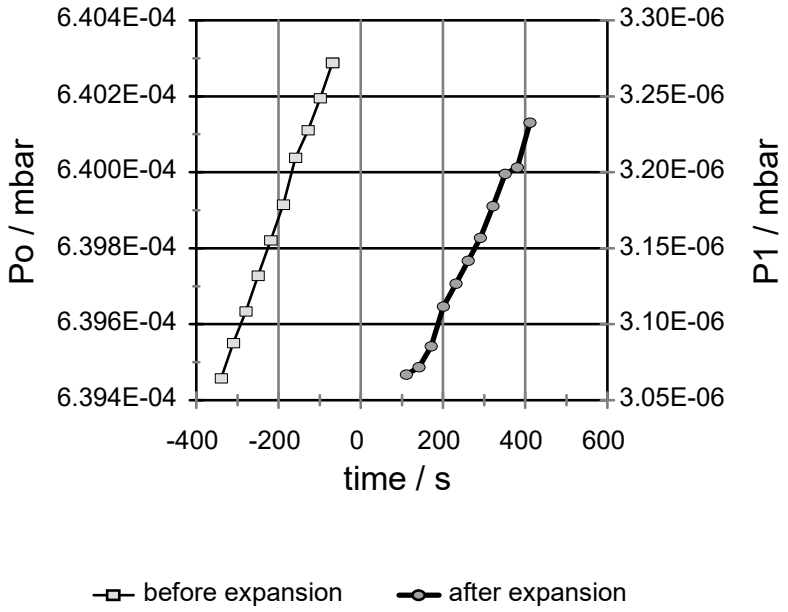

Figure 48: SRG pressure readings: P0 before expansion and P1 after expansion (volume ratio R=212). Getters not activated.

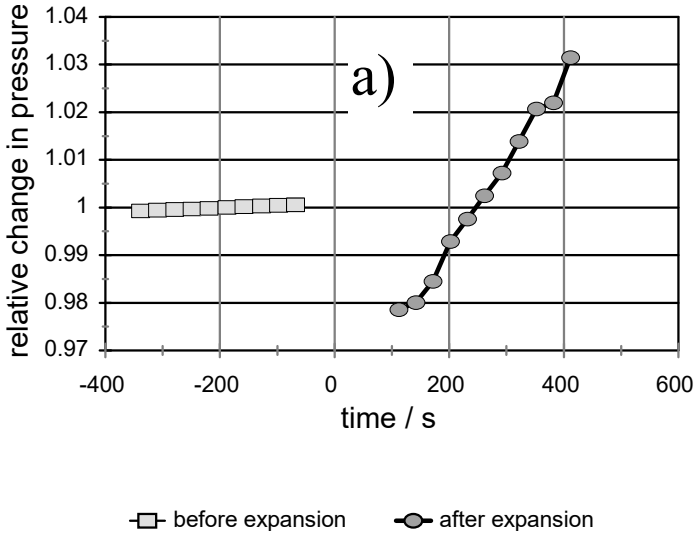

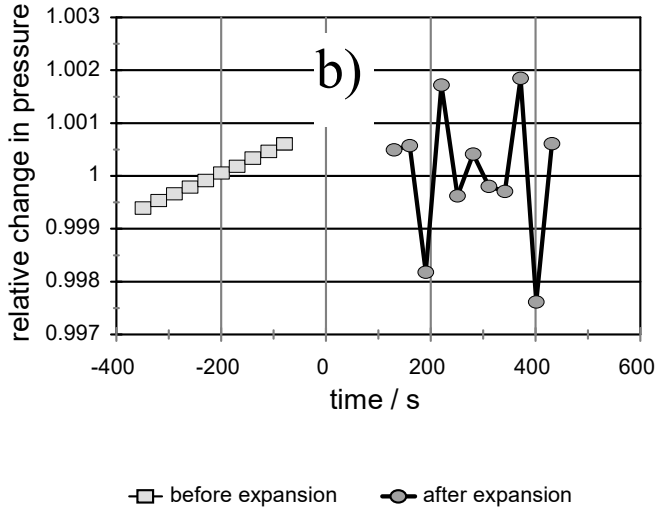

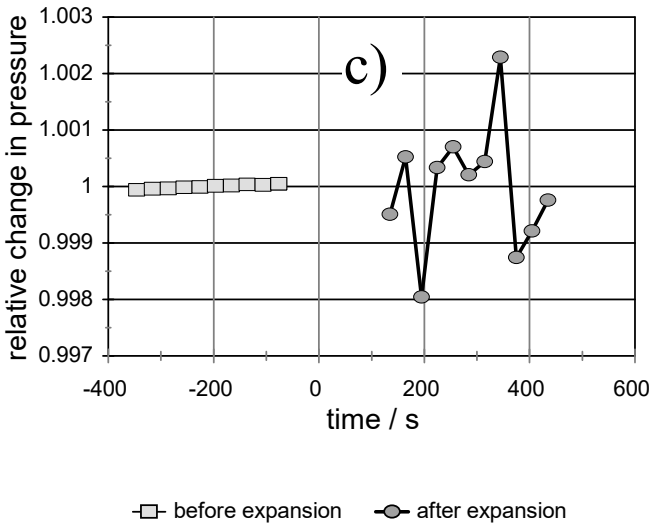

Figure 49: Relative increase in pressure before and after expansion: a) getters not activated (P_0 = 0.064×10^{-2} mbar), b) after activation of the getter in CH1 (P_0 = 0.066×10^{-2} mbar), c) after activation of getters in both chambers CH1 and CH0 (P_0 = 0.064×10^{-2} mbar).

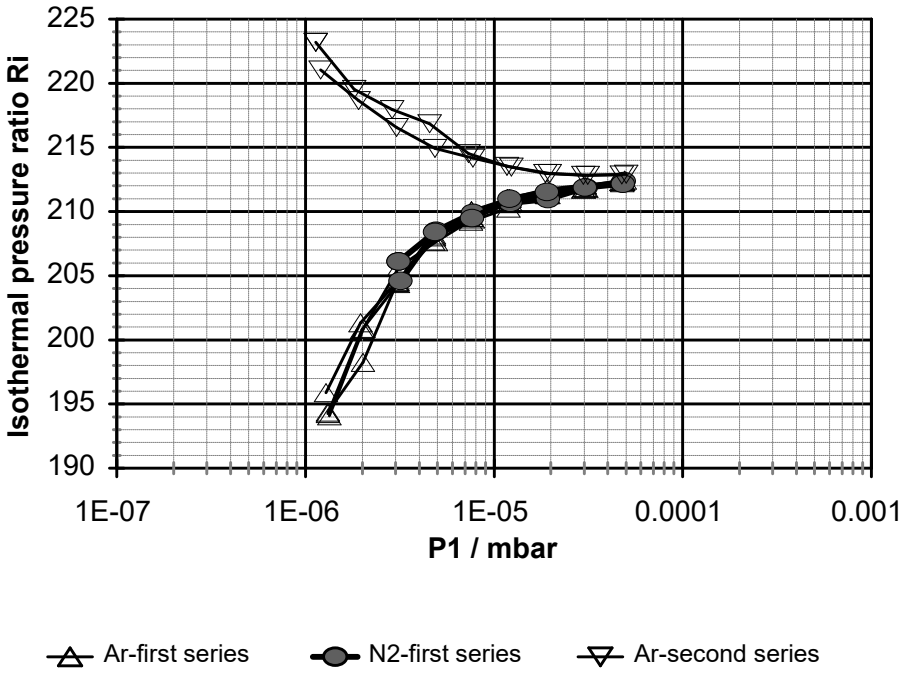

Figure 50: Calculated isothermal pressure ratio R_{PI} for He, AR and Kr before getter activation and for Ar after activation of getter in CH1

The calculated isothermal pressure ratios R_{PI} for the first and second series of measurements are shown in Figure 50, which shows a significant pressure dependence for R_{PI}. The outgassing rate does not depend on the pressure of an inert calibration gas. So, the relative concentration of a contaminating gas is higher when the expansion is done at lower pressures, and the calculated R_{PI} increasingly deviates from the volume ratio R_V when the pressure P_1 decreases.

The results for the third measurement series are shown in Figure 51. Getters were activated in both expansion chambers, so the effect of outgassing and the contamination

of expansion gas were eliminated, and the calculated pressure ratios became pressure independent. In this case, we can say that the R_{PI} equals the volume ratio R_V.

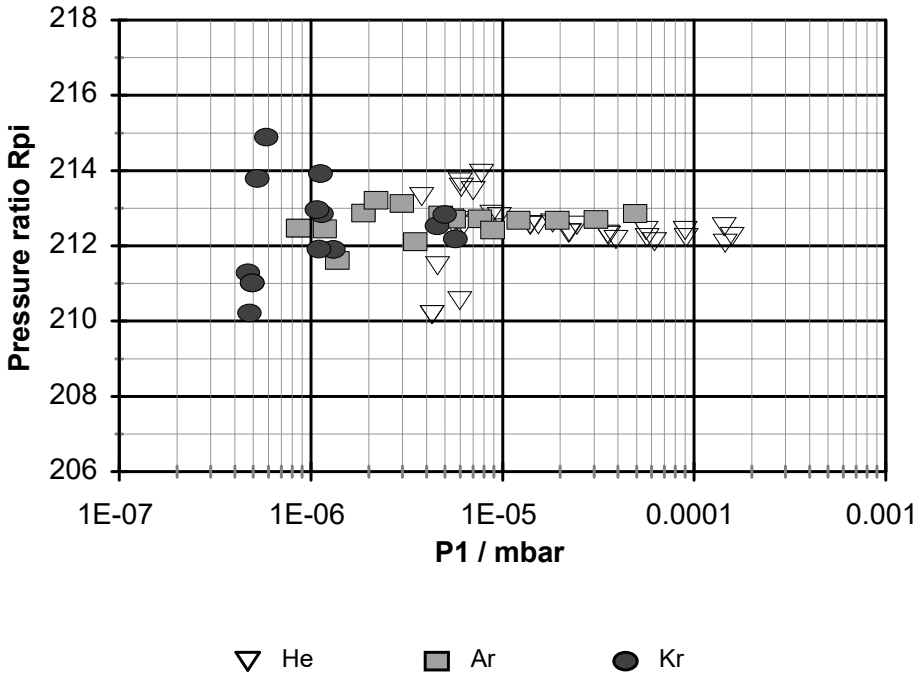

Figure 51: Calculated isothermal pressure ratio R_{PI} for He, Ar and Kr after activation of getters in both chambers CH1 and CH0.

When we close or open a valve on the system, we always cause a mechanical disturbance to the SRGs and we have to wait for a period of at least two sampling intervals (2×30 s) before we can obtain an undisturbed reading. It is also necessary to wait for some time in order to equilibrate the gas temperature in the system after the expansion. In addition, it is desirable to reduce the type-A uncertainty of SRG measurements by averaging 10 consecutive readings and using a mean value in the calculation of the pressure ratio. Because of this measurement procedure, there is a time delay for a "mean pressure reading" Δt = 250 s to 300 s after the expansion. This time delay is long enough for the outgassed gas species to make a significant contribution to the total gas amount after the expansion.

From Figure 48, it can be seen that the chamber pressure increased steadily because of the outgassing from the chamber walls before and after the expansion (when the NEG pump was not activated). As a result, the calibration gases, such as nitrogen and argon, in the first measurement series became contaminated by the outgassing, and the mean values of P_0 and P_1 were always larger than the pressure of the calibration gas itself. This means that the condition required by Eq. (36) of having the same amount of gas before and after expansion cannot be fulfilled. Because R_{PI} is the ratio of two pressures, the larger contribution to the uncertainty of R_{PI} arises from the uncertainty of the pressure reading that has the larger relative increase, which was P_1 in the case of the first measurement series (Figure 49a). The measured value of P_1 is the sum of the expanded gas and the outgassing contribution. The relative content of the outgassed gas species becomes progressively higher with decreasing P_1; therefore, one can expect a decreasing isothermal pressure ratio R_{PI} in the first measurement series.

In the second measurement series, the NEG pump was activated in CH1 only. In this case, we dealt with contamination of the calibration gas before expansion from outgassing in CH0 during the measurement of the initial pressure P_0. Therefore, the measured value of

P_0 is the sum of the partial pressures of argon and outgassed gas species. After expansion, the contaminating gas species were pumped by the getter, and P_1 was equal to the partial pressure of the expanded argon only. The calculated volume ratio in this case became progressively higher when the expansion was done at lower pressures.

In addition to possible contamination of gas by the outgassing in CH0 during the measurement of the initial pressure P_0, other sources of contamination of the calibrating gas are possible. At the beginning of our experiments, we filled a small gas reservoir (GR) with a calibration gas introduced from a gas cylinder. After each gas expansion, CH0 was evacuated and re-filled from the GR. We always started the particular set of measurements with the highest initial pressure P_0, followed by P_0 reduced by a factor 1.6 at each successive step. We did not refill the GR between the steps. Because of this, the outgassing contamination of gas in the GR also increased with time. The same thing can happen if the gas intended for expansion is kept in supply tubing for a longer time or when contamination is already present in the gas cylinder. This means that before the getter activation CH1, we were practically always measuring an initial pressure P_0 of the gas that was already contaminated with some getterable impurities. After the expansion into CH1 when it contained an activated getter (second series of measurements), these impurities were removed. As a result, the measured P_0 was too high (inert gas + contamination), so the isothermal pressure ratio R_{PI} calculated by Eq. 36 became significantly higher than the volume ratio R.

After activating both NEG pumps (third measurement series), all contamination was effectively pumped away before and after the expansion. The measured values of P_0 and P_1 represented the pressure of a pure calibrating gas, and in this case, the calculated isothermal pressure ratio became pressure independent. This proves that by using an NEG pump in both chambers, the gas quantity during expansion was unchanged.

The sensitivity of an SRG is inversely proportional to the square root of the molecular mass of the gas, so it is almost 5 times smaller for He than for Kr. This means that we can measure a pressure 5 times smaller with Kr with the same type-A relative uncertainty. At higher pressures, we are limited in our measurements to the values for which the uncertainty of the implemented viscosity correction remains within acceptable limits. The same value of the viscosity correction appears at a pressure approximately 3 times higher for He than for Ar and at a pressure 4 times higher for Kr. According to this, we performed measurements at an initial pressure P_0 of He ranging from 0.08×10^{-2} to 4×10^{-2} mbar and of Ar ranging from 0.02×10^{-2} to 1×10^{-2} mbar. Using Kr, we performed measurements at even lower P_0 pressures ranging from 0.01×10^{-2} to 0.12×10^{-2} mbar.

6.2 Statistical evaluation of results

The statistical evaluation of all calculated R_V in the third measurement series is given in Table 14. The standard uncertainty of the mean value $<R_V>$ for each gas was calculated by

$$u(<R_V>)=\frac{s(R_V)}{\sqrt{n}} \tag{37}$$

where s(R_V) is the experimental standard deviation and n is the number of measurements. The weighted mean of three gases and its uncertainty was calculated by taking into account the fact that the mean values for different gases have different standard uncertainties.

Table 14: Statistical evaluation of volume ratio measurements for three inert gases (He, Ar and Kr) in the third measurement series with getters activated in both chambers

Gas name	Number of measurements	SD of measured value $s(R_v)$	Mean value $\langle R_v \rangle$	Standard uncertainty (type-A) of mean value	Relative standard uncertainty $u(\langle R_V \rangle)/\langle R_V \rangle$
He	33	0.73	212.47	0.13	0.06%
Ar	15	0.38	212.63	0.10	0.05%
Kr	13	1.23	212.49	0.35	0.17%
Weighted mean of three gases			**212.57**	**0.08**	**0.04%**

6.3 Intermediate conclusions about applications of NEG in volume ratio measurements

The selective pumping characteristics of NEG pumps, i.e., the negligible pumping of inert gases and the high pumping speed for active gases, can be successfully employed in static expansion vacuum calibration systems when an inert calibration gas is used. We have shown that the contamination of the inert calibration gas by outgassing was the main reason for the pressure dependence of the calculated volume ratio when the expansion was done at lower pressures. The use of an NEG pump in the small and large volume of the static expansion system can diminish the influence of outgassing and offers the possibility to reliably generate lower calibration pressures. The NEG pump facilitates the condition of having the same amount of gas in the calibrating chambers before and after the expansion, which is the basis for the use of Eq. 2 to calculate the gas pressure after the expansion. It has been shown that it is important to "purify" the inert calibration gas before the expansion, so it is necessary to also use the getter in the small chamber of the static expansion system during the measurement of the initial pressure.

7 Construction of flowmeter for very low gas flows of inert gas

The schematic of a flow meter for very low gas flows which was constructed at IMT is shown in Figure 52. Measurement principle of the flow meter is based on the constant volume-variable pressure method. This design is relatively simple and has no precisely movable parts compared to the constant pressure-variable volume method.

When designing the system we followed the established practice for building UHV/XHV systems. It is built from SS parts with Con-flat flanges and bakeable all-metal valves. The flowmeter can be evacuated by a turbomolecular pumping station having a nominal pumping speed of 60 l s^{-1} for N_2 (Pfeiffer Economy TSU-071).

Main part of a flowmeter is a vacuum chamber V1 with a precisely calibrated volume. A spinning rotor gauge SRG2 is connected to V1 which enables gas flow measurement by the constant volume-variable pressure method.

The system has another two vacuum chambers: V0 and V_B which are used as gas reservoirs. Gas is introduced from a gas cylinder (not shown in Figure 52) through a SS gas supply line and a vacuum valve VV4 into a previously evacuated ballast volume V_B = 0.35 l. Gas fill pressure can be measured with two capacitance diaphragm gauges, connected to V_B: a 1 mbar full scale CDG1 and a 1000 mbar full scale CDG1000. After filling V_B we close VV4, V_0 is filled with the gas from the ballast volume V_B through vacuum valve VV2. A 100 mbar full scale capacitance diaphragm gauge CDG100 is connected to V0. These three gauges enable precise measurement of the fill pressure in the range from 0.001 mbar to 1000 mbar.

From V0 the gas flow can be generated by opening a variable leak valve (VLV). The gas flow at a given gas fill pressure in V0 can be regulated by a variable conductance of VLV. We have selected the VLV instead of a fixed conductance in the form of a very small orifice or capillary to have a higher dynamic range of gas flow generation.

After setting the desired conductance of the VLV, the gas flow through the VLV depends on the fill pressure in V0. Since V0 is quite small (only 0.039 l) the pressure drop due to the loss of gas at higher gas flows can be significant, causing a steady reduction of gas flow with time. To minimize a drop in the fill pressure we usually keep VV2 opened to increase the volume by V_B. Main motivation to install VV2 between V_B and V0 was to get a small well defined volume V0 with CDG100 for precise determination of the measuring volume V1 using the gas expansion method (see section 7.3).

The important factors for the accuracy of the determined gas flow are the accuracies of the measuring volumes and pressure measurements and also the stability of the conductance of the VLV.

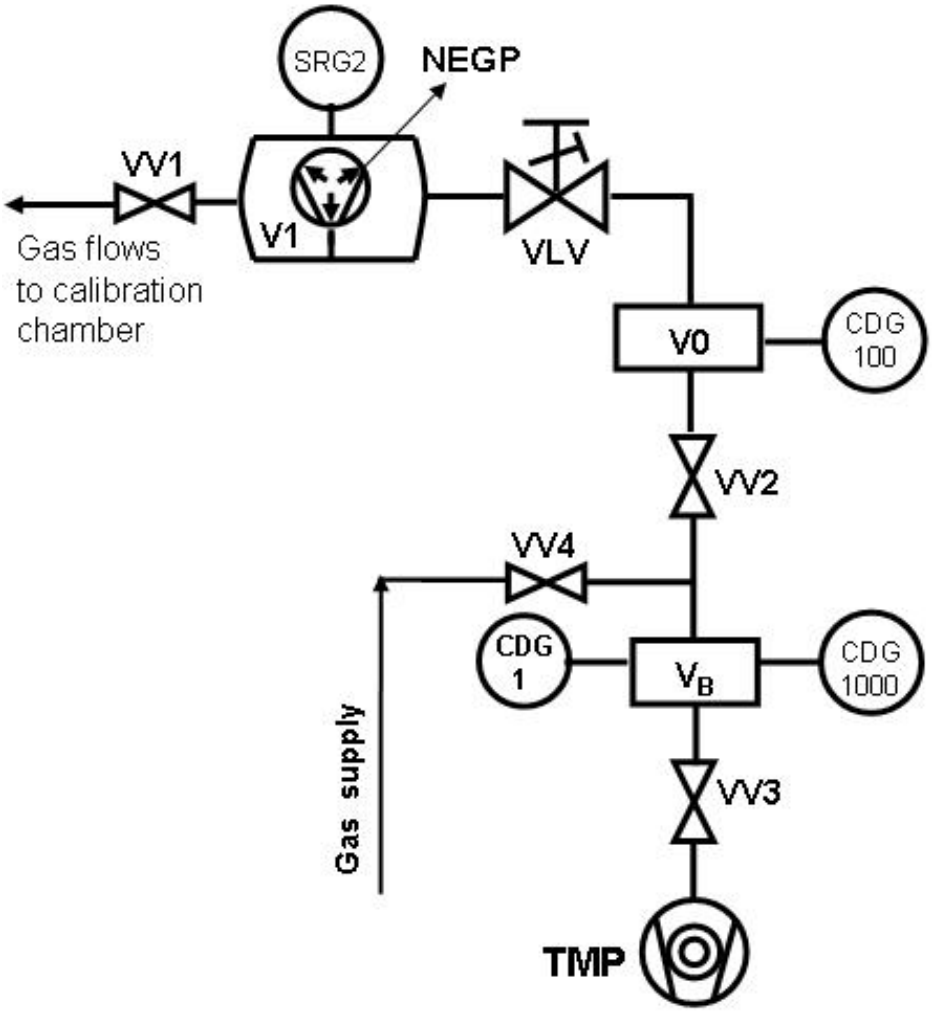

Figure 52: Flow meter constructed at IMT. VLV–Variable Leak Valve, VV1, VV2-Valves, V_0, V_1 – are volumes

Our flowmeter enables measurement of gas flows by the constant volume-variable pressure method in the range from 10^{-10} mbar l s^{-1} to 5×10^{-5} mbar l s^{-1}. The gas flow is measured by the pressure rise method using SRG2 which is connected to V1.

Experiments showed that when the conductance of VLV was reduced below 10^{-9} l s^{-1} the

gas flow through the variable leak valve became proportional to the upstream pressure (gas pressure in V_0) for $P_0 < 100$ mbar (Figure 54). This means that the gas flow is in molecular flow regime and the conductance of VLV is constant (see section 7.4). The described behavior of VLV enables extension of precise flow generation below 10^{-10} mbar l s^{-1} down to 10^{-12} mbar l s^{-1} by the so called "constant conductance method". This value is lower by almost two orders of magnitude compared to other reported flowmeters [92]. This extremely low limit of gas flow enables generation of calibration pressures below 10^{-12} mbar in our dynamic expansion system directly, without using the flow division technique.

7.1 Measurement of gas flow by pressure rise method using SRG2

The pressure rise method for gas flow measurement in our flowmeter is essentially the same as the RoR method for the outgassing rate measurement, which was used in experiments described in section 5.1.2. The only difference is that in the flowmeter we introduce the flow of a calibrating gas through VLV.

Procedure is following:

- The VLV is opened to the desired conductance which is determined in the preliminary measurement. The setting of VLV is kept unchanged for the period of 2 hours or more for mechanical stabilization of VLV. Experiments showed that this is necessary to reach a stable value of conductance (changes less than 1% in a period of 1 h).
- the reservoir (volume V0) is filled with a 5 N purity noble gas (Ar or He) at a predetermined pressure which is measured by CDG100 (it can be measured also by CDG 1 or CDG1000 when VV2 is opened).
- The VV1 is shut off and the gas pressure in V1 starts to increase, due to the gas flow. The SRG2 keeps on reading the pressure value at fixed time periods, preset by the sampling interval (from 5 s at high gas flow to 60 s at low gas flow). The rate of pressure rise (pressure versus time measurements) is carried out automatically by means of a PC based data acquisition system (Figure 53).

- The flow rate is calculated from this relation:

$$Q = \mathrm{V1}\left(\frac{dP}{dt}\right) \tag{38}$$

As it can be seen from Figure 52 we have placed in the volume V1 a NEGP. In this case NEGP diminish the influence of the outgassing from chamber walls of volume V1. Because NEGP has no pumping speed for noble gases, the gas flow rates for Argon and Helium are not affected and extremely low flow rates of these gasses can be measured by the rate of rise method.

Figure 54 shows the example of the measured gas flow over the range of reservoir pressure from 1 mbar to about 10^3 mbar at a set conductance for argon of around 5×10^{-10} l s^{-1}. For low reservoir pressures (less than 100 mbar) the gas flow through the VLV is in the molecular flow regime whereas for higher pressure the transitional flow regime and viscous flow regime is obtained. More results of conductance measurements of VLV are given in section 7.4.

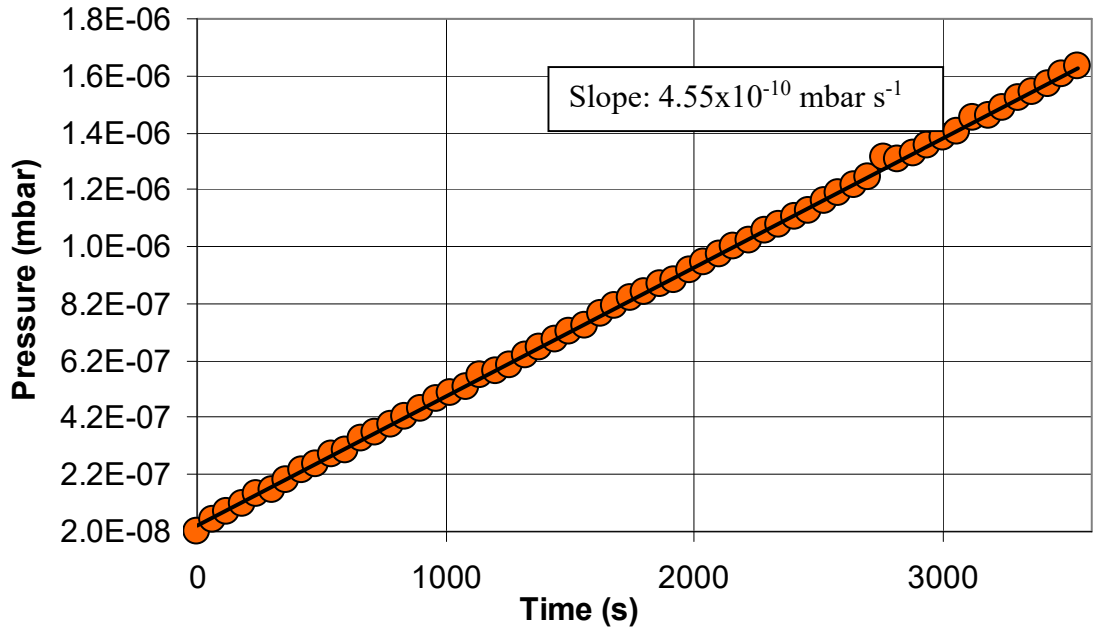

Figure 53: Example of a pressure rise during time measured by SRG2 and calculated linear regression line. The gas flow for a given slope is $Q = 1.59\times10^{-10}$ mbar l s^{-1}.

The highest pressure of SRG2 during pressure rise measurements in V1 shall be kept below 1×10^{-2} mbar as the uncertainty of SRG above this pressure increases rapidly due to the possible errors in viscosity correction algorithms [87]. This sets the upper limit of gas flow measurement by SRG2 in our flowmeter to approximately 5×10^{-5} mbar l s^{-1}, when the slope is calculated from 10 consecutive SRG readings at sampling interval 5s.

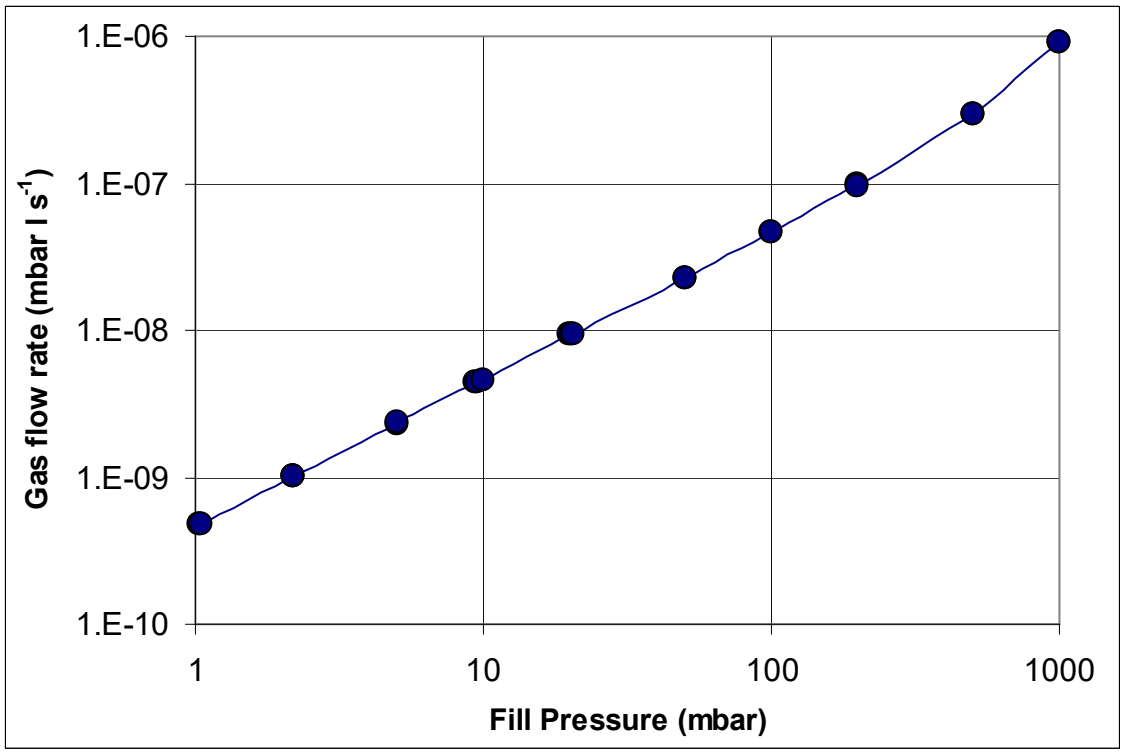

Figure 54: Plot of gas flow versus the reservoir pressure for argon.

7.2 Measurement of gas flow by "constant conductance" method

For generated gas flows lower than 5×10^{-10} mbar l s^{-1}, the adjustment of the gas flow is done by the “constant conductance” method. The “constant conductance” of VLV is calibrated in the molecular flow region by pressure rise measurements in the range between 1 mbar and 100 mbar. After that the gas pressure in V0 is reduced below 1 mbar (measured by CDG1) and gas flow rate is calculated using relation:

$$Q = C_{\mathrm{VLV}}\, P_{\mathrm{upstream}} \tag{39}$$

where C_{VLV} is constant conductance and $P_{upstream}$ is gas pressure at the high pressure side of VLV.

The lowest gas flows for inert gases which can be generated in this way are down to 1×10^{-12} mbar l s^{-1}.

7.3 Determination of volumes V0 and V1

Volumes V1 and V0 were determined using static expansion method using a well-known volume V3. The well-known volume means the volume which has regular geometrical form (in our case a cylinder). The setup of this system is shown in Figure 55, whereas the form and dimensions of the volume V3 can be seen in the Figure 56.

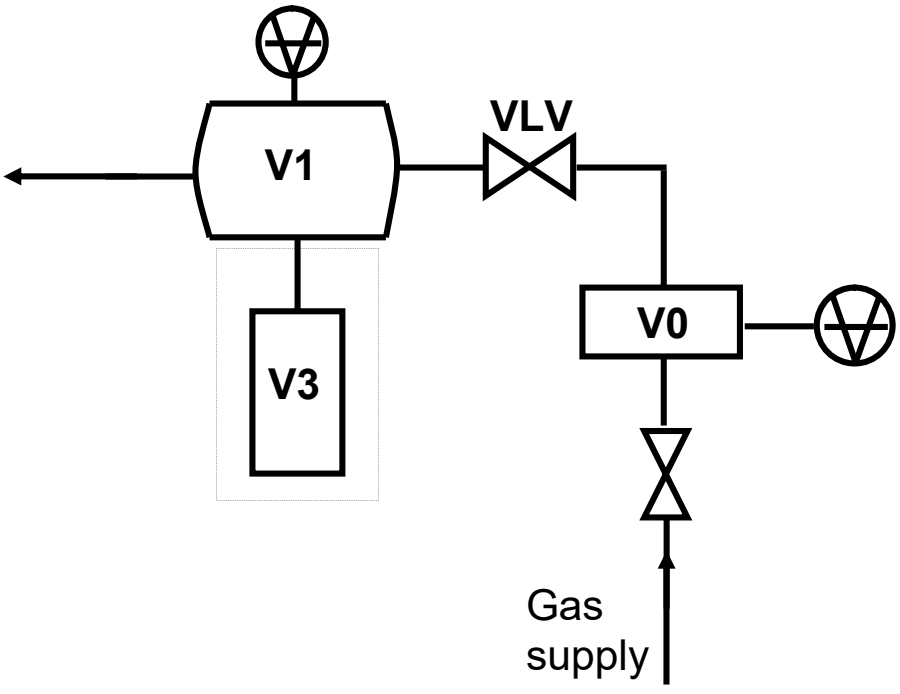

Figure 55: Schematic of the static expansion system used for determination of volumes V1 and V0

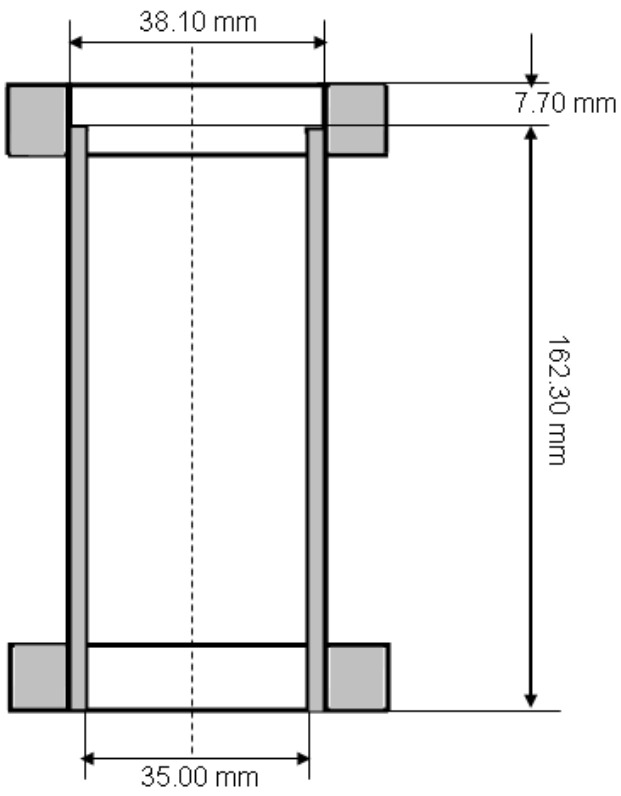

Figure 56: Dimensions of volume V3, which is used as a calibration volume.

We measured the geometrical dimensions of the known volume V3 by a calibrated caliper. Using the dimensions of the volume V3, the calculated value of the volume is $V3 = 0.165$ l.
To determine volumes V0 and V1, the gas was expanded using two different setups. Relating to Figure 55, in the first setup the volume V3 was connected to V1 and closed with a blank flange at the other side. Volume V0 was filled with gas at a pressure close to 100 mbar and expanded afterwards into V0+V1+V3. Gas pressure before and after expansion was measured using CDG100.

In the second setup volume V3 was removed from V1. A blank flange was placed instead, and the gas was expanded from V0 to V0+V1.

By expanding the gas from volume $V0$ to V0+V1+V3 and from V0 to V0+V1 we obtained volume ratios given in the Table 15. From this data and using Eqs. (40, 41):

$$R_1 = \frac{V0 + V1 + V3}{V0} = 14.34 \tag{40}$$

$$R_2 = \frac{V0 + V1}{V0} = 10.06 \tag{41}$$

it is possible to calculate the volumes V0 and V1:

$$V0 = \frac{V3}{R_1 - R_2} \tag{42}$$

$$V1 = V0(R_2 - 1) \tag{43}$$

So the volume V0 = 0.0385 l and V1 = 0.3468 l.

Table 15: Values of the volume ration (pressure ratio) during expansion of the gas from V0 to V0+V1+V3 and from V0 to V0+V1, SD - standard deviation, RSD – relative standard deviation

(V0+V1+V3) / V0	(V0+V1) / V0
14.37	10.05
14.35	10.06
14.35	10.06
14.36	10.05
14.34	10.06
14.33	10.06
14.32	10.04
14.31	10.06
14.33	10.07
14.32	10.07
Mean value	Mean value
14.34	10.06
SD	SD
0.018	0.009
RSD	RSD
0.13%	0.09%

The calculated uncertainty of volume V3 obtained from geometrical measurements is: u(V3)=0.54%, whereas the calculated uncertainties of the volumes V0 and V1 obtained from gas expansion measurements are: u(V0) = 0.73% and u(V1) = 0.74%.

7.4 Conductance of the variable leak valve (VLV)

An important factor for the accuracy of the determined calibration pressure is the accuracy by which the conductance can be determined. Highest accuracy is achievable only in the molecular flow regime. Therefore, the dynamic expansion method is mostly limited to the pressure where flow is molecular. First task here is to confirm that gas flow is in molecular flow regime.

We measured conductance of the VLV using the schematic in the Figure 52 for the flow meter. Gas supply is measured by tree different gauges CDG1, CDG100 and CDG1000 depending upon the magnitude of the gas flow. This gas is expanded through the VLV to the volume V1. This is done for different setting of the VLV (for example we opened VLV for 1, 1.5, 2, 2.5, 3 turns). Argon and helium are used as the test gases. Examples of conductance measurements for argon are shown in the Figures 57 and 58 and for helium in Figure 59.

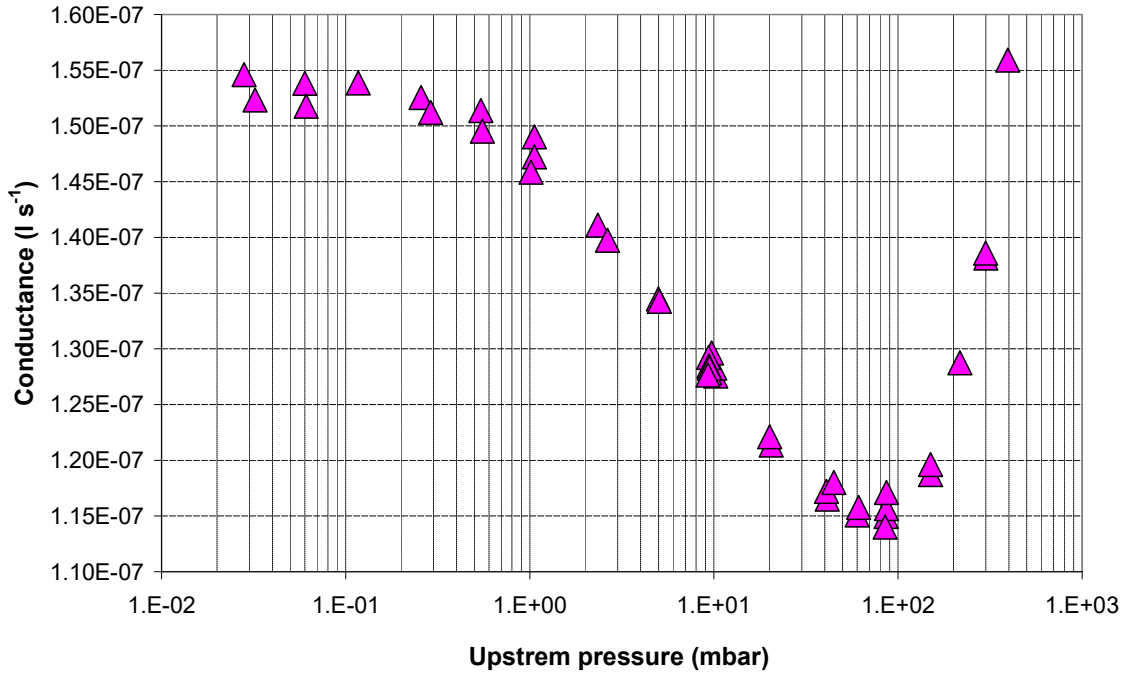

Figure 57: Conductance of the VLV versus upstream pressure for argon.

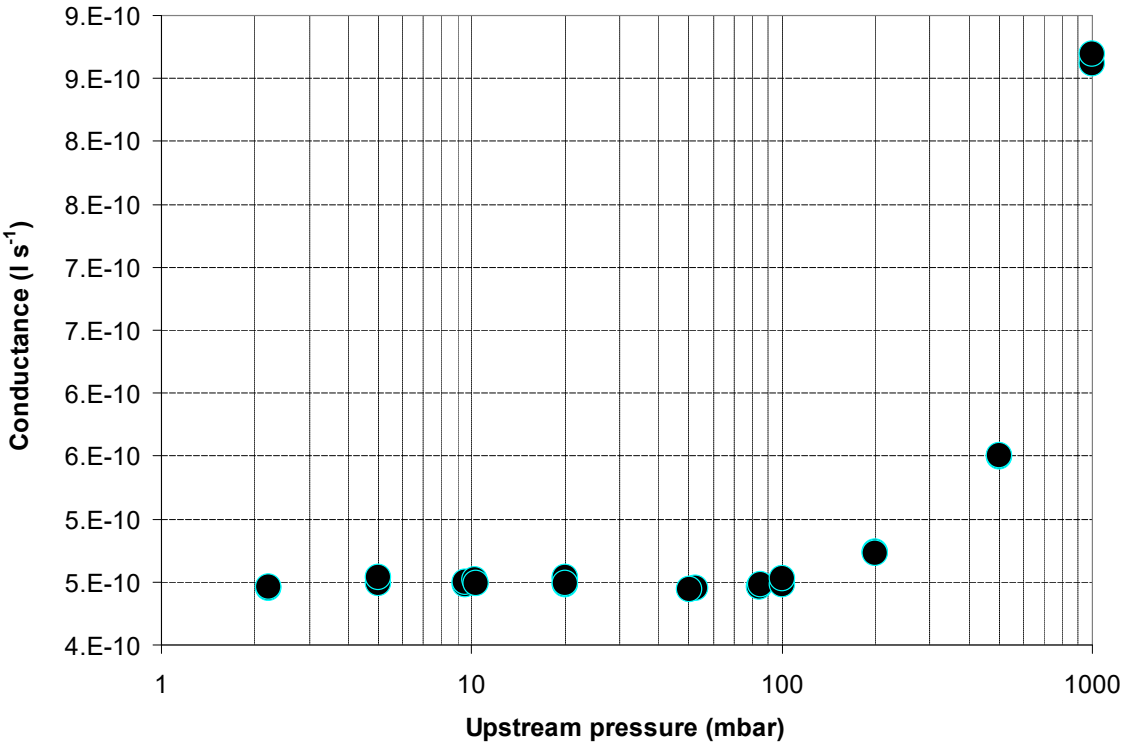

Figure 58: Conductance versus upstream pressure of the VLV for argon

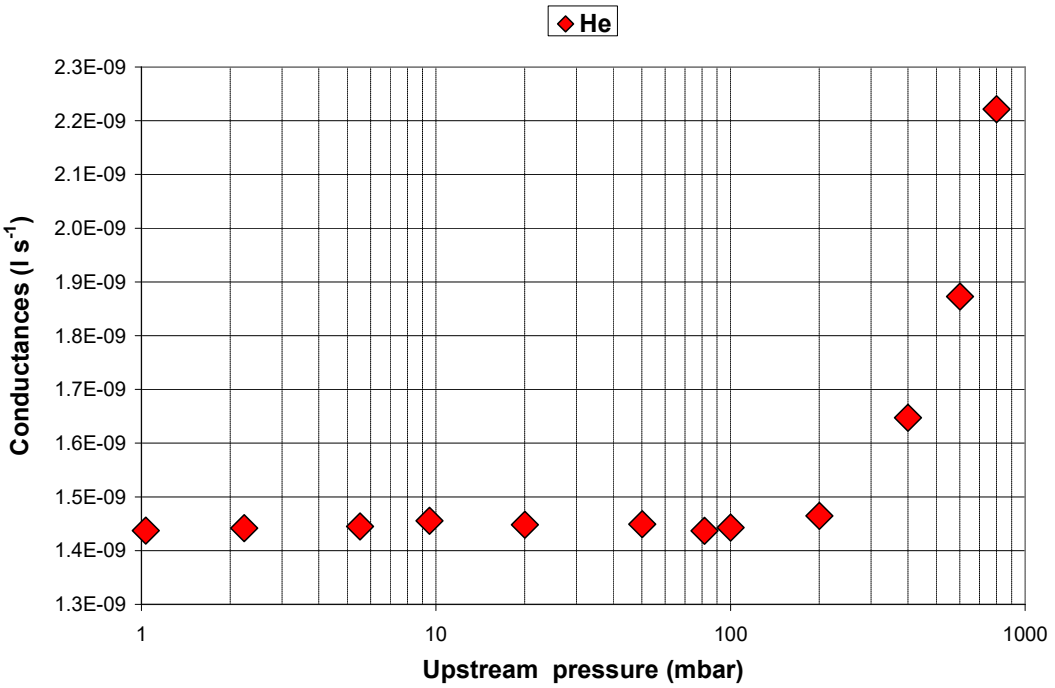

Figure 59: Conductance versus upstream pressure of the VLV for helium.

In Figure 60 are given conductances for different settings (open turns of the variable valve) for argon as the test gas, while in the Figure 61, those conductances for different settings are given as a relative conductance, which means each conductance is divided by the value of conductance when the upstream pressure is 85 mbar.

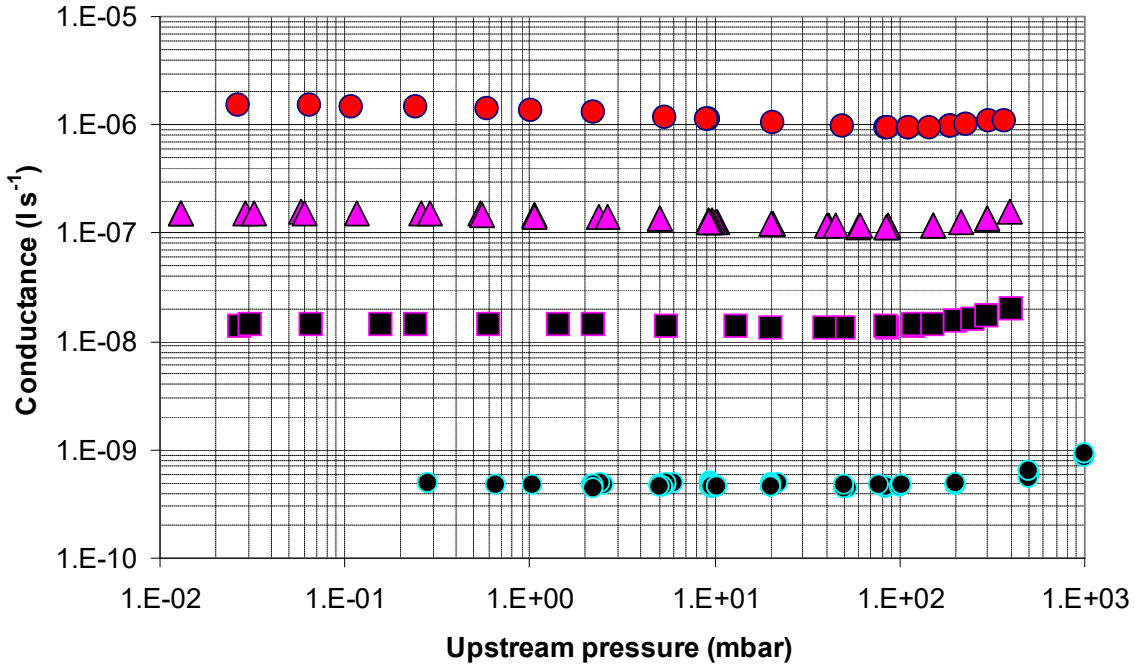

Figure 60: Conductance of the VLV for argon for different settings

It can be seen from the results (Figure 61) that the conductance is constant (it is in molecular flow regime) for different upstream pressures. The conductance 2×10^{-6} l s^{-1} is constant for the upstream pressure $p < 0.2$ mbar, 2×10^{-7} l s^{-1} for $p < 0.6$ mbar, and 2×10^{-8} l s^{-1} for $p < 3$ mbar. Conductance 5×10^{-10} l s^{-1} is in molecular flow regime for the upstream

pressure p < 50 mbar, while for the pressure above 50 mbar this conductance is in transition or viscous regime. This means that conductance 5×10^{-10} l s^{-1} or smaller can be used for generation of gas flow by "constant conductance" method using upstream pressure from the reservoir up to 50 mbar.

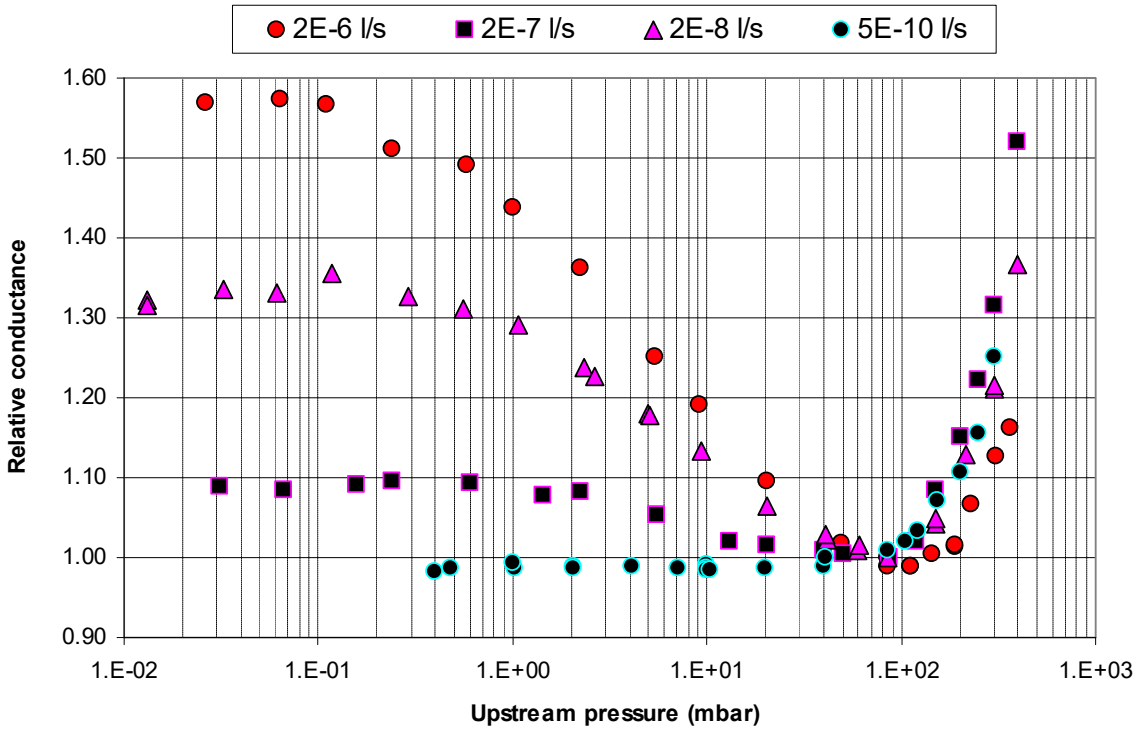

Figure 61: Relative conductance of the VLV for argon for different settings

Figure 62 and Figure 63 shows the comparison of the VLV conductance for argon and helium for the same setting. The mean value of conductance of VLV for molecular flow region for Ar is $C_{Ar} = 4.2\times10^{-10}$ l s^{-1} and for He is $C_{He}=1.4\times10^{-9}$ l s^{-1}. The ratio of these values is in agreement with the theory,

$$\frac{C_{He}}{C_{Ar}} = 3.32 \tag{44}$$

because according to the theory the orifice conductance for a particular gas is:

$$C = 3.64\sqrt{\frac{T}{M}}\,A \tag{45}$$

where M and T are the molecular weight and temperature of the gas used respectively and A is area of the orifice. For our case the temperature and area of the orifice are the same, therefore the ratio of conductances for two different gases it will be,

$$\frac{C_{He}}{C_{Ar}} = \sqrt{\frac{M_{Ar}}{M_{He}}} \tag{46}$$

Now the conductances ratio can easily be calculated by knowing the molecular weight of Ar and He. Molecular weight for Ar is M_{Ar}=39.948, whereas for He is M_{He}= 4.0026. The ratio is:

$$\frac{C_{He}}{C_{Ar}} = 3.16 \quad (47)$$

So the calculated value of the ratio between conductances for argon and helium is in agreement with the ratio obtained from theory.

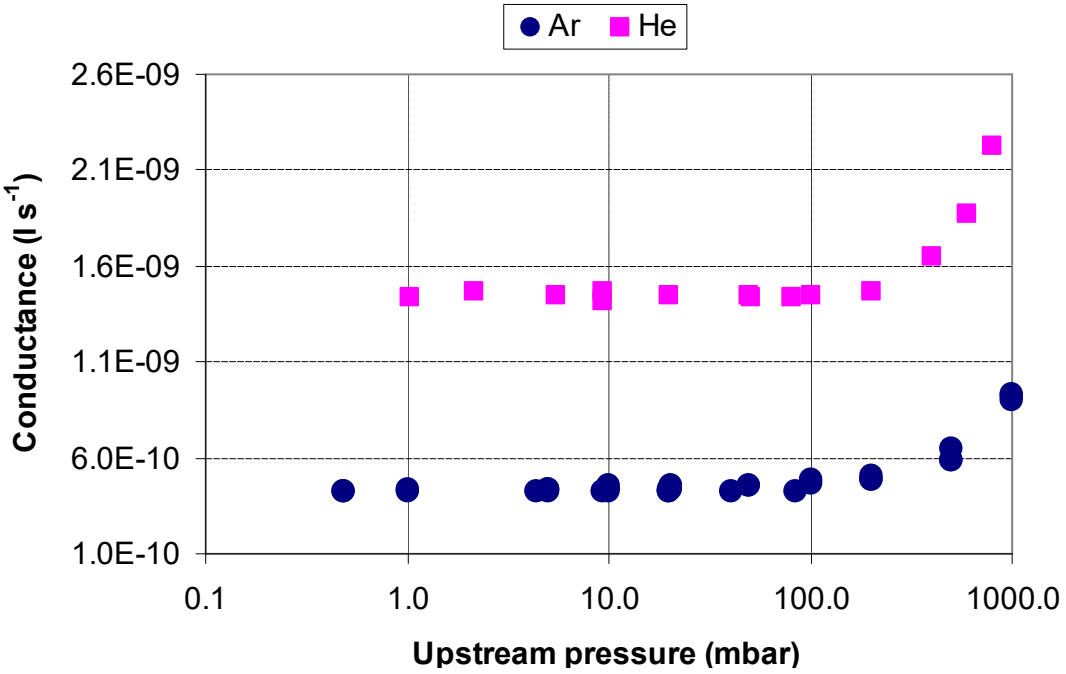

Figure 62: Comparison of conductance of the VLV for argon and helium for the same setting.

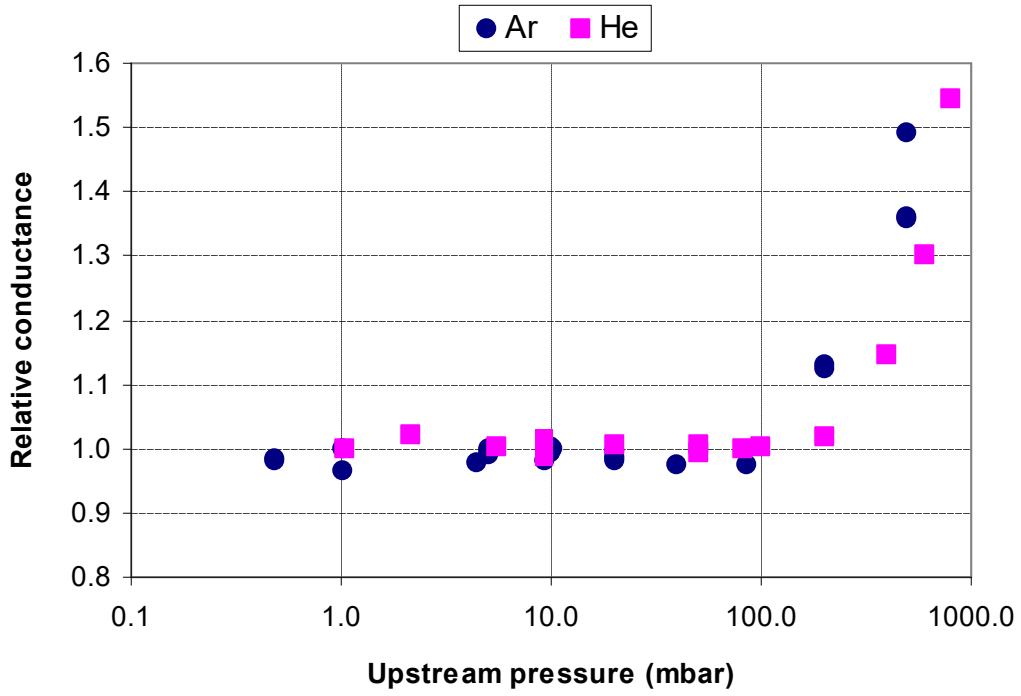

Figure 63: Comparison of relative conductance of the VLV for argon and helium for the same setting.

Conclusion about the conductance of the variable leak valve

From all of these measurements we can conclude that for conductance setting of the VLV below 5×10^{-10} l s^{-1}, the molecular flow regime is for upstream pressures in the range less than 50 mbar. We can determine the precise value of conductance from measured gas flow by pressure rise method for several values of upstream pressures in the range from 2 mbar to 20 mbar.

7.5 Extensions to lower flows by constant conductance method

After "calibrating" the value of conductance for the selected setting of VLV in molecular flow regime it can be used to calculate gas flow by "constant conductance" method and we can determine a lower gas flow compared with the rate of pressure rise method used before (Figure 54).

To calculate the gas flow by "constant conductance" method we used the Eq. 39. Calculated values of the gas flow against upstream pressure are given in Figure 64. It can be seen from the Figure 64 that the range of gas flow is extended down to 10^{-12} mbar l s^{-1}, when the upstream pressure is reduced below 0.01 mbar. With this low gas flow we can generate pressure below < 1×10^{-10} mbar in the calibration chamber.

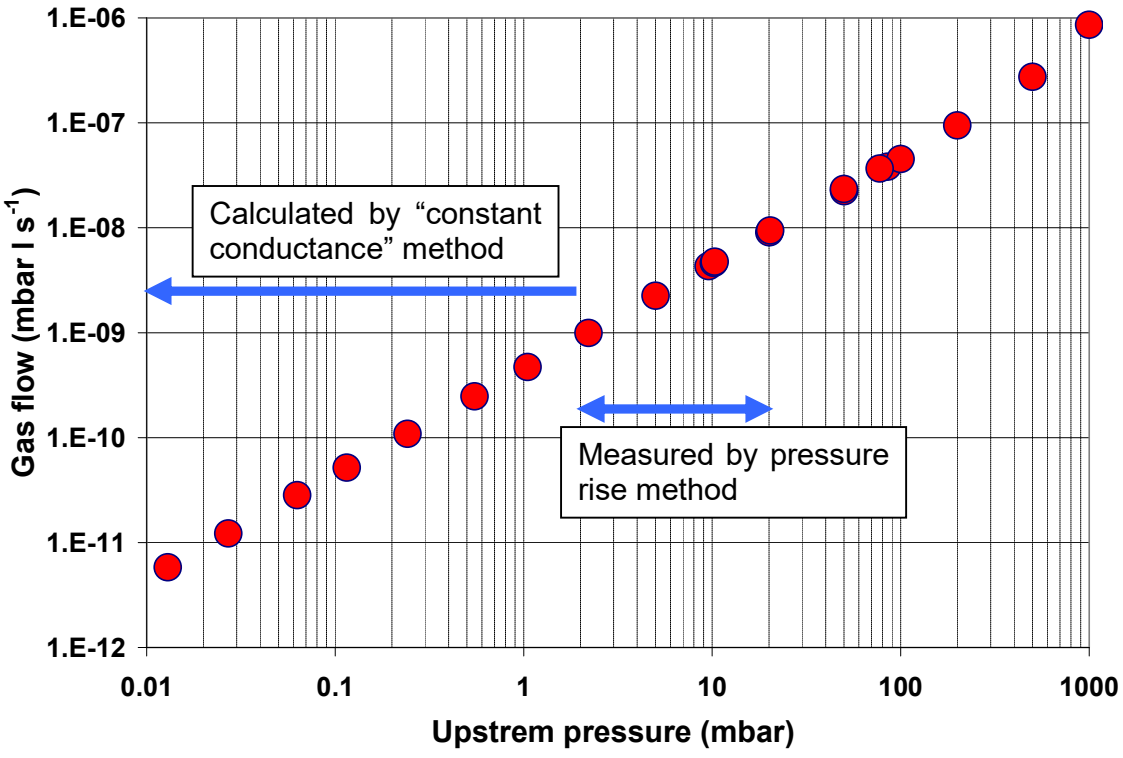

Figure 64: Extension to lower flows by constant conductance method

7.6 Time stability of the setting of the variable leak valve

Another important thing is if the conductance of the VLV is stable over time. The time stability of conductance of VLV is given in the Figure 65. This stability of the conductance over time is given for 5 different upstream pressures (2, 5, 10, 20, 50 mbar). All of those fill pressures lie in the range of molecular flow regime. From Figure 65 it can be seen that the valve is almost stable over the time.

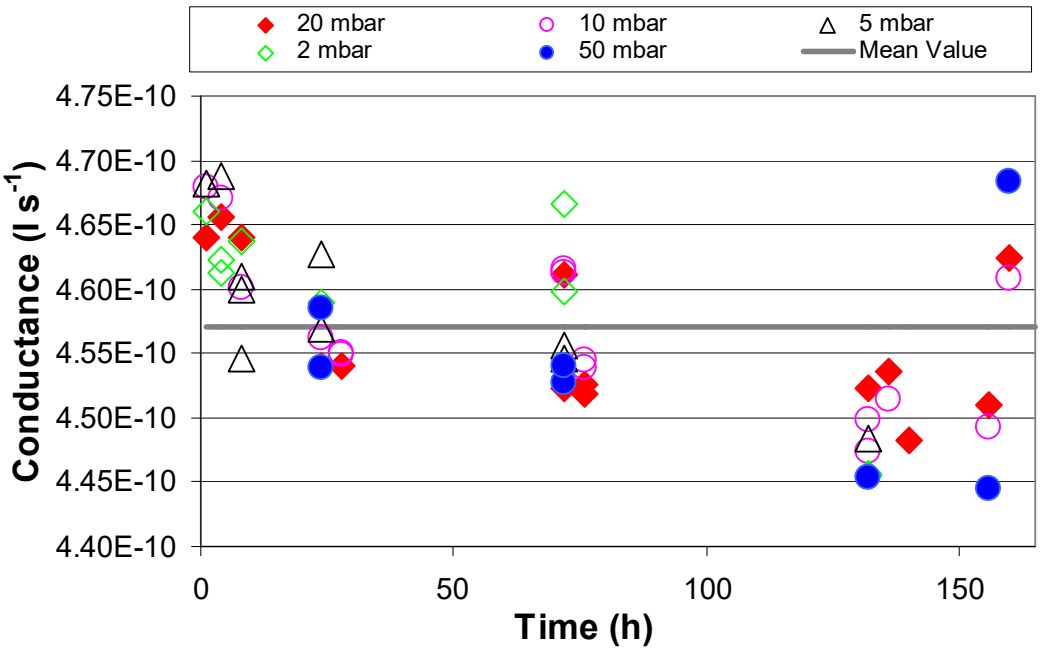

Figure 65: The time stability of conductance of the variable valve

A mean value of the measured conductance in the Figure 65 is 4.57×10^{-10} l s^{-1}, and relative standard deviation is 1.45%.

7.7 Analyses of measurement uncertainty of flow measurements

7.7.1 Pressure rise method

As mentioned above we use the pressure rise method for the gas flow determination higher than $Q > 5\times10^{-10}$ mbar l s^{-1}. The gas flow is calculated using Eq.(38). The uncertainty associated with its measurements is a combination of uncertainty associated with the different terms appearing in this expression (volume V1, pressure P and time t). For uncertainty analysis the time derivative dP/dt can be replaced by $\Delta P/\Delta t$ where ΔP *is* measured pressure increase in time interval Δt, so the uncertainty of gas flow can be calculated as:

$$\frac{u(Q)}{Q} = \sqrt{\left(\frac{u(V)}{V}\right)^2 + \left(\frac{u(\Delta P)}{\Delta P}\right)^2 + \left(\frac{u(\Delta t)}{\Delta t}\right)^2} \qquad (48)$$

The volume of the flowmeter chamber was determined by expansion method (in section 7.3) to be V1 = 0.3468 l with a relative uncertainty of 0.74%. The pressure increase ΔP is

measured with SRG that was previously calibrated at IMT.
For lowest flow Q = 5×10^{-10} mbar l s^{-1} the pressure increase $\Delta P=2\times10^{-6}$ mbar is obtained in Δt =25 minutes. For $\Delta P > 2\times10^{-6}$ mbar a one sigma relative uncertainty of 0.5% can be achieved. The time interval Δt was measured with reference to a PC internal clock with an uncertainty 0.1 s, so for Δt >100 s we have the relative uncertainty $u(\Delta t)/\Delta t < 0.1\%$ which is negligible in comparison with other uncertainties. Combining these uncertainty components, the total relative uncertainty in the gas flow is estimated to be $u(Q)/Q = 1.1\%$.

7.7.2 Constant conductance method

Based on the Eq. 39, the uncertainty of the gas flow Q_{CC} in this case is combination of the uncertainty of »constant conductance« and fill (upstream) pressure in the reservoir which is measured by CDG 1. From Eq. 39, the relative uncertainty of the gas flow rate can be calculated using this equation:

$$\frac{u(Q_{CC})}{Q_{CC}} = \sqrt{\left(\frac{u(C)}{C}\right)^2 + \left(\frac{u(P_{upstream})}{P_{upstream}}\right)^2_{CDG1}} \tag{49}$$

The relative uncertainty of the upstream pressure can be calculated by using uncertainty of the CDG100 which is 1×10^{-3} mbar. Another parameter used in this equation is »constant conductance« which is determined using this equation:

$$C = \frac{Q_{VdP}}{P_{upstream}} \tag{50}$$

Conductance of the leak valve is determined by measuring gas flow using the pressure rise method Q_{VdP} at a given upstream pressure in the range from 10 to 100 mbar which is measured with the CDG100
Using Eqs (50) and (51) and adding an additional contribution δ_{stab} for the time stability of the set conductance of the leak valve the equation for total uncertainty of the gas flow rate generated using the "constant conductance" method is:

$$\frac{u(Q_{CC})}{Q_{CC}} = \sqrt{\left(\frac{u(Q_{VdP})}{Q_{VdP}}\right)^2 + \left(\frac{u(P_{upstream})}{P_{upstream}}\right)^2_{CDG100} + \left(\frac{u(P_{upstream})}{P_{upstream}}\right)^2_{CDG1} + \delta_{stab}} \tag{51}$$

The relative uncertainty of the gas flow $\underline{u}(Q_{VdP})/Q_{VdP} = 1.1\%$ has been already determined in 7.7.1. Time stability of the conductance of the leak valve has been determined in paragraph 7.6 and is δ_{stab} = 1.5%. Relative uncertainty of pressure measurements with CDG100 is 0.2% for pressures between 1 mbar and 100 mbar. The relative uncertainty of CDG1 is 0.3% for pressures between 0.005 mbar and 1 mbar.

Using these estimates for individual uncertainty contributions in Eq. (51) we obtain the resulting uncertainty of gas flow for the constant conductance method $\frac{u(Q_{cc})}{Q_{cc}} = 1.9\%$.

7.8 Outgassing of chamber V1

Outgassing of chamber V1 was measured by the RoR method using SRG. Results are shown in Figure 66a. A calculated outgassing flux before activation of the getter was $Q = 2.9\times10^{-10}$ mbar l s^{-1}. An estimated surface area is of approximately 500 cm^2, so the outgassing rate is $q = 5.8\times10^{-13}$ mbar l s^{-1} cm^{-2}. This result was obtained after baking assembled V1 at 250 °C for 140 hours. A pressure rise in V1 after the activation of getter is shown in Figure 66b. A slope of linear regression line is of 7×10^{-14} mbar s^{-1} which gives outgassing flux of 2.5×10^{-14} mbar l s^{-1}. So by using NEGP in the volume of the flowmeter we reduced the outgassing flux for four orders of magnitude, which is in full accordance with the hypothesis given in Chapter 2.

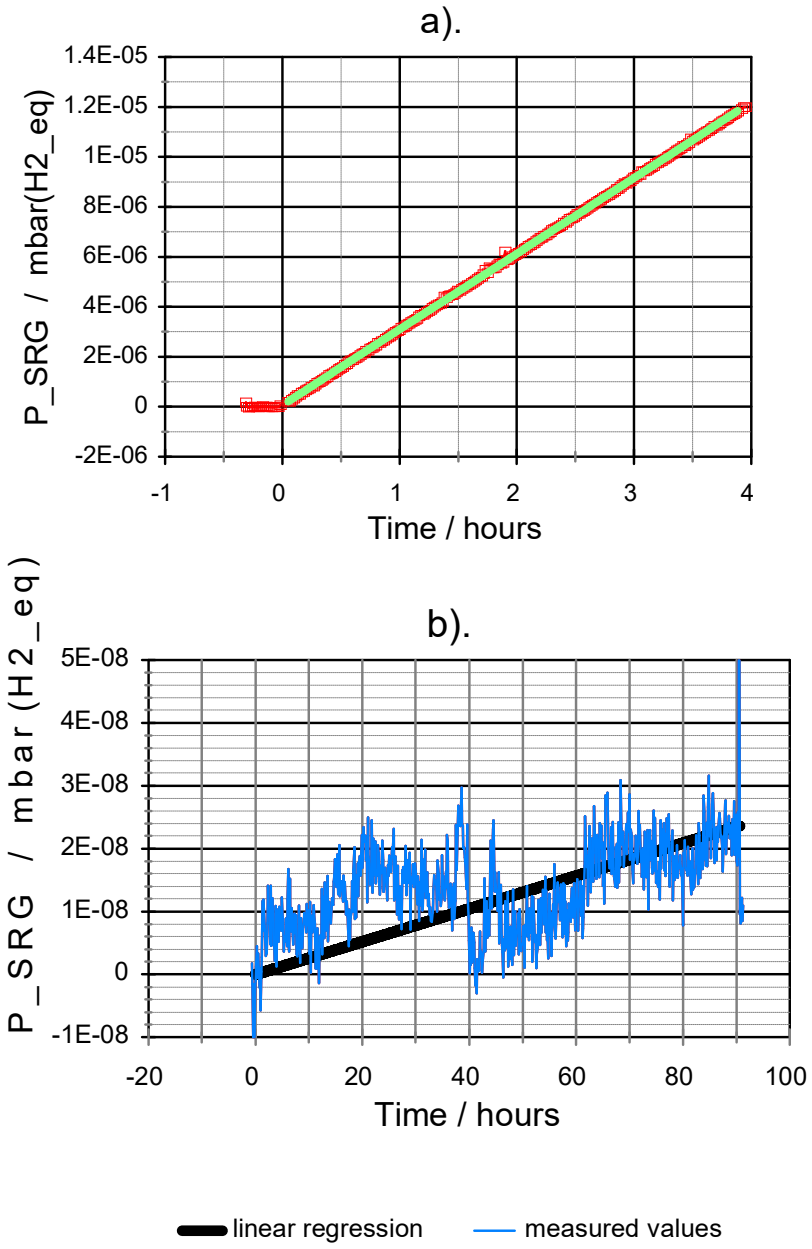

Figure 66: Pressure rise in V1. a). Outgassing of the flow meter chamber V1 before activation of getter. b). Pressure rise in V1 after activation of getter. Slope of linear regression line is 7×10^{-14} mbar s^{-1} which gives outgassing flux of 2.5×10^{-14} mbar l s^{-1}.

8 Construction of extremely high vacuum calibration system at the Institute of Metals and Technology

In the preceding sections the limitation to the measurement and attainment of the UHV/XHV are discussed. Based on those limitations we have constructed our extremely high vacuum calibrated system.

Working principle of our XHV calibration system is a dynamic (continuous) expansion of gas. Main components of the system are:

- Gas flow meter (described in previous chapter)
- Calibration chamber V2
- Gas flow restriction (orifice)
- Pumping system

8.1 Description of a construction of XHV calibration system

Our extremely high calibration system which is constructed at IMT is given in Figure 67. The material of the calibration chamber V2 and other interconnecting tubes is stainless steel 304 L. All connections are equipped with CF type flanges and all valves are bakeable all metal angle valves. The exceptions are interconnections between TMP1 outlet and TMP2 inlet and between TMP3 outlet and rotary vane forepump which are made by KF type metal bellows using Viton O-rings and an ordinary Viton sealed angle valve.

The calibration chamber has a cylindrical shape. Geometrical characteristics are presented in Table 16. The chamber has eight CF35 connection ports for vacuum gauges. They are arranged radially to the cylinder axis in two groups of four. One group is located in a plane at 1/3 of the length, the other at 2/3 of the length of the cylinder. In addition there are two CF35 connection ports located axially on each end of the cylinder.

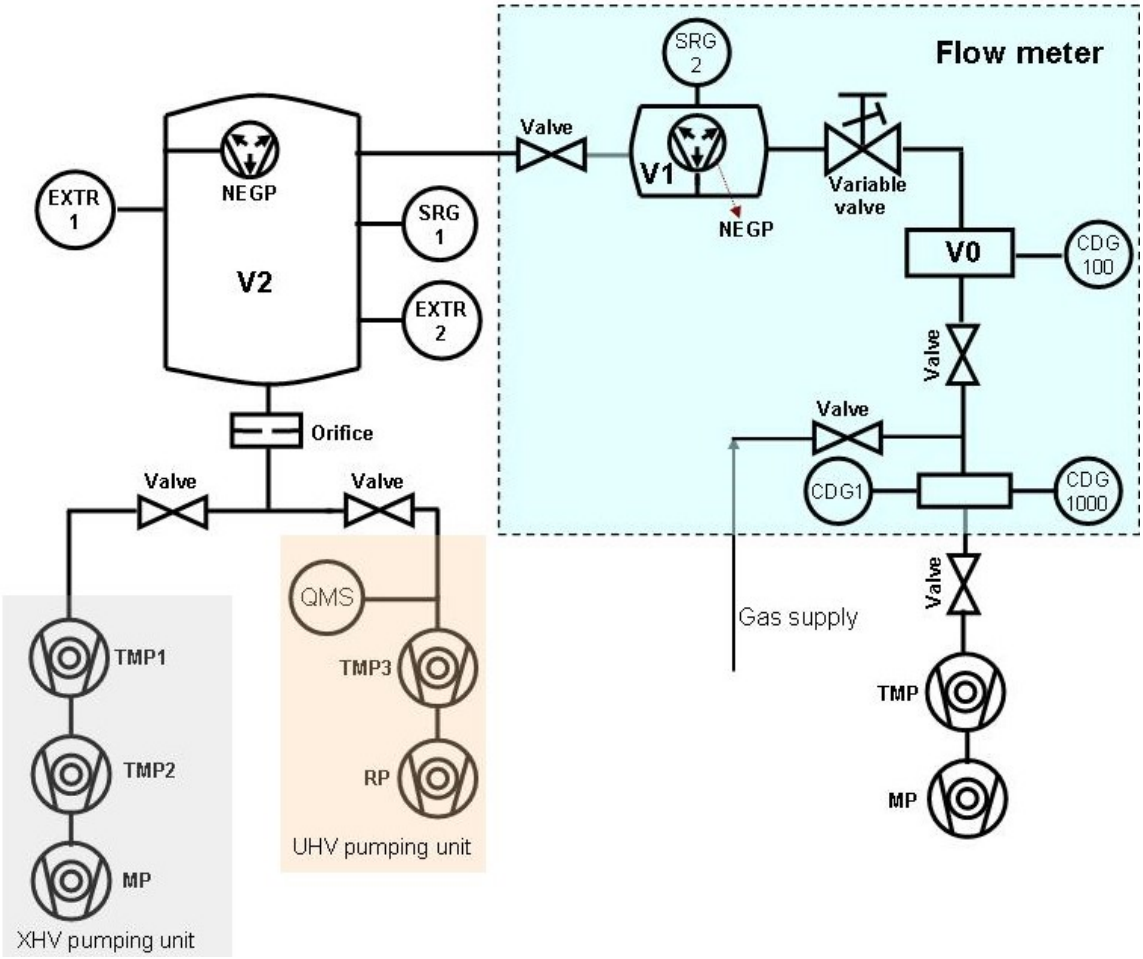

Figure 67: Schematic of the UHV system constructed in IMT

Table 16: Geometrical data for XHV calibration chamber

Inner diameter	Length	Volume (including connection tubes)	Inner surface area	Wall thickness
150 mm	300 mm	5.71 l	2200 cm^2	2 mm

A gas flow restriction in the current stage of the system was realized by a simple conduction reduction inside the connection tube from calibration chamber to the pumping units. This connection tube has an inner diameter of 35 mm (a standard for CF 35 flange) and a length of 225 mm. This long connection tube was initially designed in order to have a calibration chamber inside bake-out oven, while the pumping units which cannot be baked could be located outside. So the conductance of this tube is already limited to 20 l s^{-1} for argon in the molecular flow regime. We have decided to place in the tube a further restriction to reduce molecular conductance for argon to about 5 l s^{-1}. The geometry of this restriction inside the tube is not well defined, so it is not possible to calculate the conductance with required precision. Instead we have decided to measure the effective conductance using our flowmeter and a calibrated spinning rotor gauge (SRG1). This will be described in more detail in section 8.5.

There are two pumping units for evacuation of the calibration chamber:

- UHV pumping unit
- XHV pumping unit

Main characteristics of pumps mounted in the UHV and XHV pumping units are presented in Table 17. The UHV pumping unit is shown on the right hand side of Figure 67, and consists of a small compact turbo – drag pump TMP3 backed with a dual stage rotary vane pump. The UHV pumping unit also contains a Bayard-Alpert gauge and a quadrupole mass spectrometer for system diagnostics and leak checking.

Table 17: Pumping speed and compression ratio of pumps of UHV and XHV pumping units. All pumps were manufactured by Pfeiffer Vacuum

	TMP1	TMP2	TMP3
model	TMU 521 P	TMU 071 P	TMU 071 P
pumping speed for			
N_2	300 l/s	60 l/s	60 l/s
He	400 l/s	55 l/s	55 l/s
Hydrogen	400 l/s	45 l/s	45 l/s
compression ratio for			
N_2	$>1\times10^{12}$	$>1\times10^{11}$	$>1\times10^{11}$
He	5×10^{7}	1×10^{7}	1×10^{7}
H_2	5×10^{6}	1×10^{5}	1×10^{5}
backing pump	TMP2	diaphragm pump 0.9 m^3/h (MVP 015-2)	rotary vane pump 2.5 m^3/h (DUO 2.5)

The XHV pumping unit consists of a two turbomolecular pumps in series. A model TMU 521 P from Pfeiffer was selected for TMP1 because of its very high compression ratio for H_2. Also a TMP2 has quite high compression ratio, so the combined compression ratio of both pumps is expected to be 5×10^{11} for H_2.

For comparison, the turbo pump in the LIP system (described in Section 2.2.2) uses a magnetically levitated turbo pump Oerlicon/Leybold MAG W 2200, which has a compression ratio for N_2 of only 10^8 (4 orders of magnitude less than our pump) and a compression ratio for H_2 is even not specified by the manufacturer. A backing turbopump TW 70 has a compression ratio of 4×10^3 for H_2 which is 20 times smaller than that of our TMP2. So one of the reasons why the ultimate pressure in the LIP system was only 8×10^{-12} mbar may be the insufficient compression ratio of turbopumps for H_2.

Both pumping units can be isolated from the calibration chamber by all metal valves. The UHV pumping unit is used for initial evacuation and during bake-out. At the end of bake out pumping is switched over from the UHV to the XHV pumping unit. This procedure was introduced to avoid adsorption of water vapour inside TMP1, which cannot be baked.

The XHV pumping unit is kept running all the times, also during venting of the calibration chamber, when it is isolated by a valve. It is used for pumping of the calibration chamber only after it is baked and during calibration by the orifice flow method, when dry inert gases are used. So the XHV pumping unit is never exposed to a moist residual gas.

An additional pumping of active gases in the calibration chamber is provided with a NEG pump NEGP2. We use »CapaciTorr-D 400-2 pump from SAES Getters, which has a

nominal pumping speed of 400 l s^{-1} for hydrogen. We have tested several possible configurations of attachment of NEG pump (see section 8.4.1) and only by mounting the NEG pump directly on the chamber we can get enough effective pumping speed to reach XHV.

8.2 Preliminary test of XHV pumping unit

The XHV pumping unit was pre-conditioned and tested for ultimate pressure before it was mounted to the calibration system. The test configuration is shown in Figure 68.

Figure 68: A system for testing ultimate pressure of turbo pump TMP1

A standard transition piece CF 100/CF35 was attached to the inlet flange of TMP1. On the transition piece a CF 35 standard cross piece, a CF 35 all metal angle valve from Varian and a 150 mm long CF 35 nipple was attached. Two unused ports of the cross piece were closed with blank flanges. At the end of the nipple an extractor gauge was mounted. To reduce hydrogen outgassing from bulk material, the individual parts of the setup (transition piece, cross, valve and nipple) were baked prior to assembly at 300 °C to 350 °C for more than 100 hours and the extractor gauge was pre-baked at 200 °C for approximately one week.

After assembly of the system to the turbo pump, thermal outgassing was performed. Figure 69 shows temperatures and the pressure readings of extractor gauge during the thermal outgassing. First the cross piece, valve, nipple (= vacuum tubing) and extractor gauge were heated by a heating tape to 120 °C for 20 hours followed by increasing temperature to 145 °C for another 70 hours. At the same time the connection flange of turbo pump was heated to a temperature between 75 °C and 80 °C. In the first part of thermal outgassing the extractor gauge was switched off. It was turned on at t = 90 hours

after start of pumping. Just before turning on the extractor gauge, temperature of vacuum tubing was reduced to 105 °C. At t=112 hours the extractor gauge was degased for 10 minutes and at t=117 hours the heaters were turned off and system cooled down to room temperature. 20 hours after cool down of the setup (at t=140h), the extractor reading dropped to 1.96×10^{-11} mbar and was still decreasing slowly.

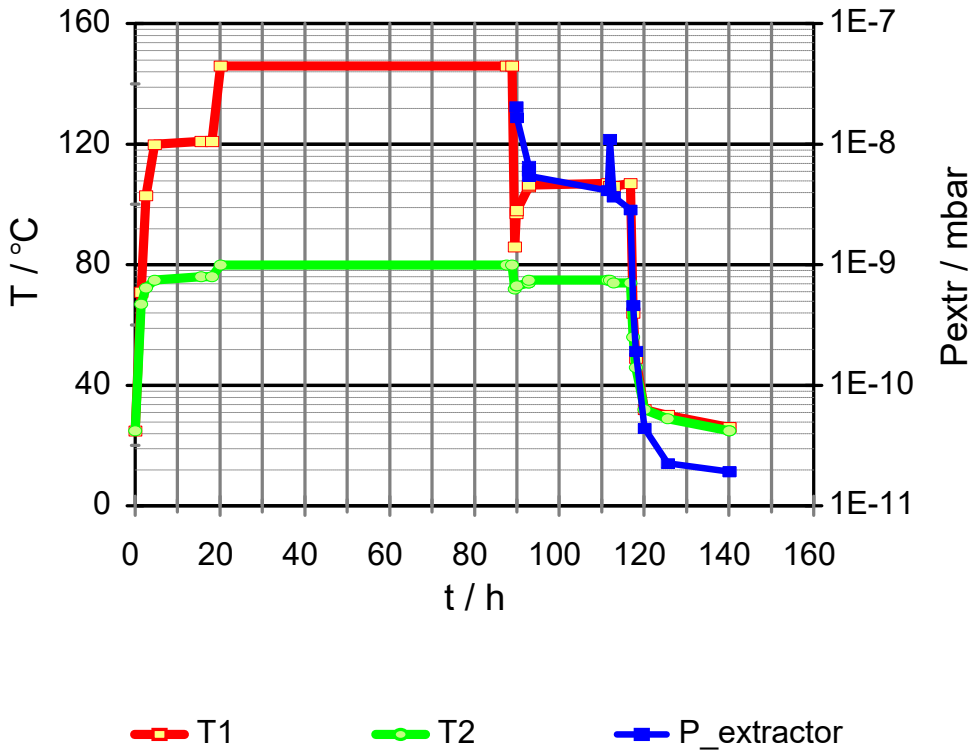

Figure 69: Extractor gauge readings of the ultimate pressure of XHV pumping unit during thermal degassing. T1 – temperature of CF35 nipple, T2 – temperature of intake flange of turbo pump.

8.3 Outgassing of XHV calibration chamber

In section 8.1 the XHV calibration chamber was already briefly described and its geometrical data are given in Table 16. A picture of the chamber is shown in Figure 70. It was manufactured by a local company under our supervision. The cylindrical body was made from a SS tube (AISI 304L) with an inner diameter of 150 mm and a wall thickness of 2 mm. End plates are were made from a sheet of AISI 304L with the same thickness. Connection tubes with CF 35 flanges were made from a tube with an inner diameter 35 mm and a thickness of 1.5 mm. The CF 35 flanges on connection ports are made from AISI 316 L SS.

Inner surfaces of all parts were mechanically polished before welding. Final cleaning after welding was done with a hot water and detergent followed by rinsing in deionized water.

The XHV calibration chamber has been thoroughly outgassed before the assembly to the calibration system. Figure 70 shows the chamber V2 connected to an UHV pumping system for bake-out. A spinning rotor gauge thimble was mounted to one of the radial connection ports, and all other ports were closed by blank CF 35 flanges which were made from 316 L, and were previously vacuum fired at 900 °C for 4 hours.

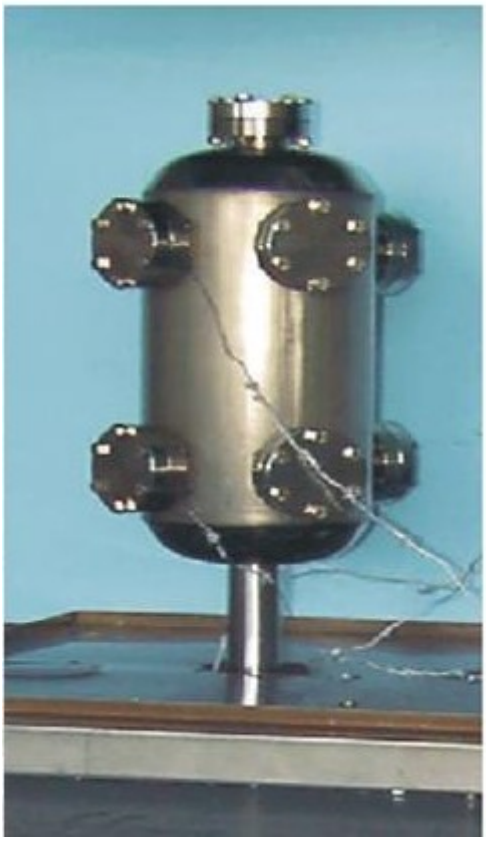

Figure 70: Picture of the XHVcalibration chamber on a bake-out system.

The chamber was baked in a bake-out oven at different temperatures from 100 °C to 350 °C. Table 18 shows measured outgassing rates by the rate of pressure rise method using SRG. Measurements were done at room temperature after the chamber was cooled from the indicated bake-out temperature for a minimum of 1 day. Unfortunately it is not possible to calculate a characteristic Fourier number (see also Chapter 5) for given temperatures and times, because the chamber was made of parts with a different wall thickness and also a certain surface area was represented by massive parts (blank flanges) with a thickness of 12 mm.

Table 18: Outgassing rate of chamber V2 calculated from the rate of pressure rise after different bake-out treatments.

Temperature	Time	Outgassing flux	Outgassing rate
°C	h	mbar l s^{-1} (H_2 equivalent)	mbar l $s^{-1}cm^{-2}$ (H_2 equivalent)
100	50	1.56×10^{-08}	7.1×10^{-12}
150	95	8.8×10^{-09}	4.0×10^{-12}
250	160	3.5×10^{-10}	1.6×10^{-13}
250	160+160	1.08×10^{-10}	4.9×10^{-14}
350	145	4.8×10^{-11}	2.2×10^{-14}

After bake-out the XHV chamber was vented, removed from the bake-out system and kept at atmospheric pressure for several months before it was finally mounted to the calibration system.

In the final assembly of the XHV calibration chamber there are few additional parts which were necessary for the connection to the XHV and UHV pumping units: a CF35 T-piece and two bakeable CF 35 valves. Two blank flanges were replaced with extractor gauge heads, but other connection ports were still closed with blank flanges. The additional parts also contribute to the final outgassing of chamber V2, so its outgassing rate was checked again after final assembly. The chamber with the additional parts was baked at 250 °C for 90 hours. After cooling down to room temperature (for 24 hours), a pressure rise test at room temperature was performed. Results are shown in Figure 71.

Outgassing flux $Q_{out} = 4.4 \times 10^{-10}$ mbar l s^{-1} was obtained, which is 10 times more than for the chamber itself. This means that addition of new components significantly increased the outgassing.

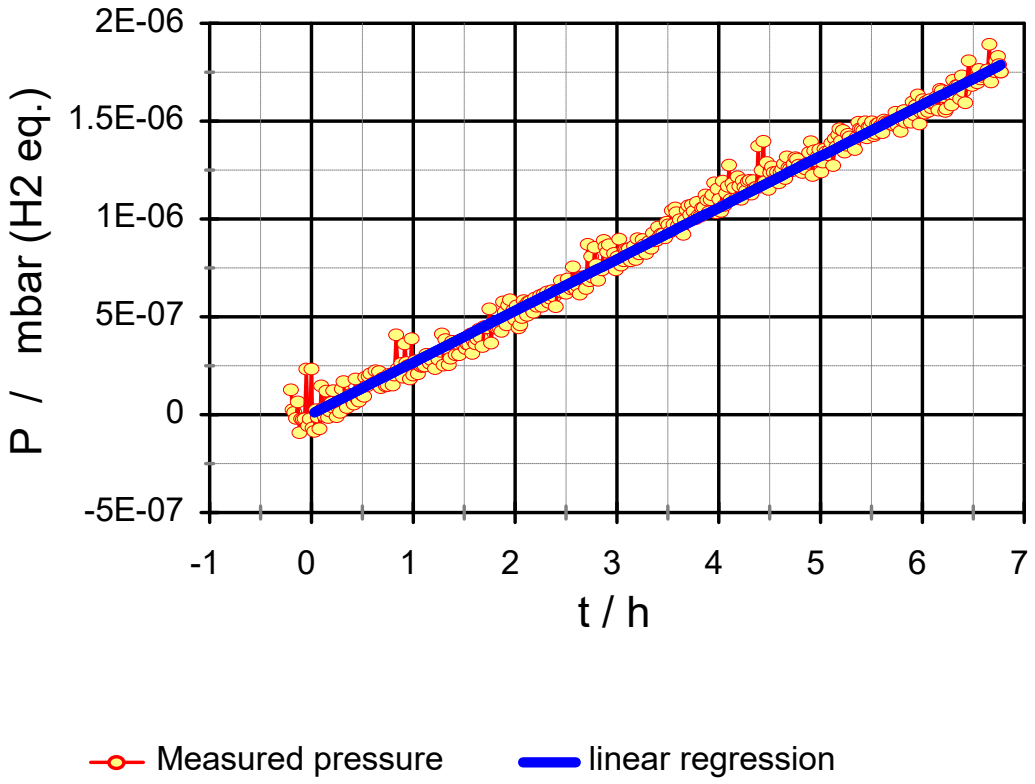

Figure 71: Pressure rise measurement in chamber V2 after final assembly. two extractor gauge heads were also connected to V2.

8.4 Testing of NEG pump for XHV calibration chamber

Our XHV calibration chamber utilizes a NEG pump to reduce hydrogen partial pressure, which is a result of residual hydrogen outgassing from chamber walls.

In order to mitigate the influence of hydrogen outgassing in XHV and to reach ultimate pressure in 10^{-12} range we need a large pumping speed for hydrogen. To boost pumping speed for the hydrogen in the XHV calibration chamber we use a NEG pump CapaciTorr D400. The specified pumping speed by the manufacturer of this pump is 400 l s^{-1} for hydrogen.

We have tested two possible configurations of connection of NEGP to the XHV calibration chamber:

a. the NEGP was connected to the chamber via an all metal valve, like in the LIP system (Figure. 72a - "out-of-chamber" configuration)
b. the NEGP was mounted directly in the chamber (Figure 72b – "nude" configuration)

Good feature of configuration:
a) is that NEGP can be isolated by the valve, when the system has to be vented. So it remains activated during exchange of test gauges. In case of configuration
b) NEGP is completely passivated during venting and has to be reactivated each time after opening XHV chamber to the atmosphere. Although NEGs can be re-activated several times, the number of possible reactivations is limited and the pumping speed of NEG as well as the sorption capacity gradually decreases with an increasing number of reactivations.

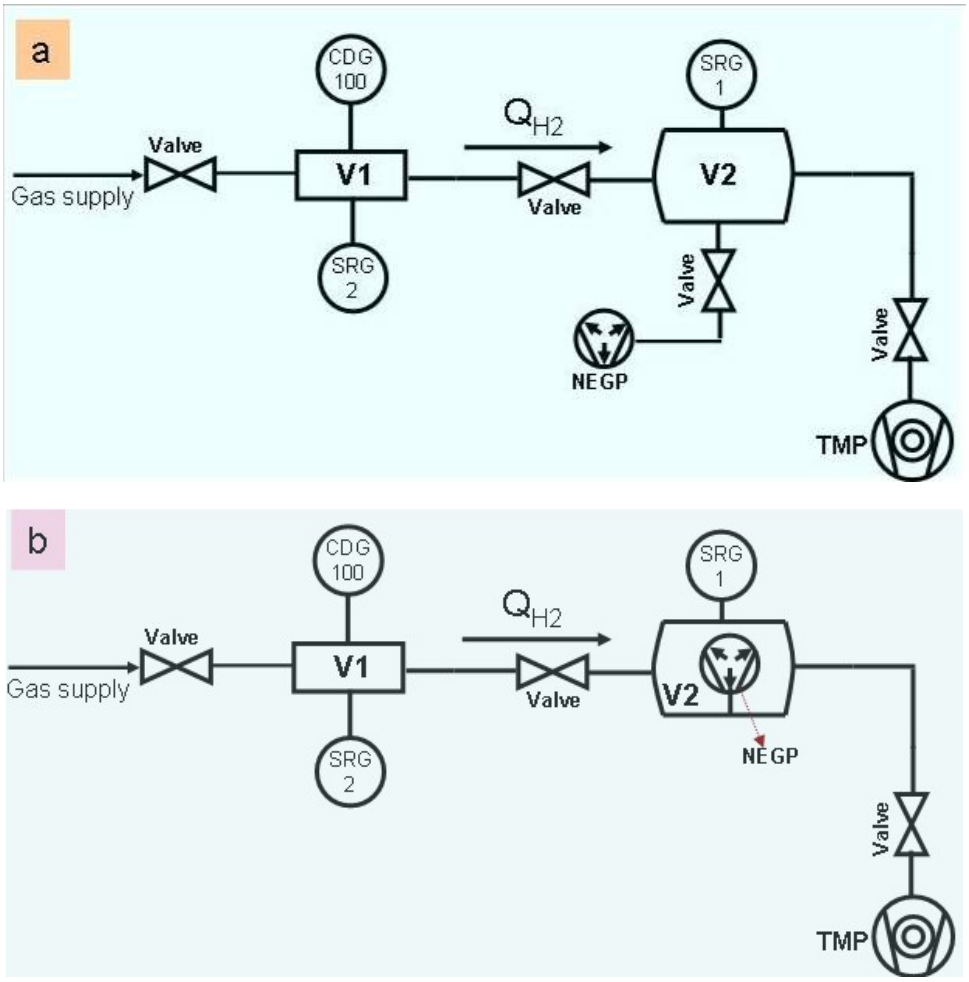

Figure 72: Scheme of the measurement procedure of pumping speed of the NEGP a) NEGP is connected to the calibration chamber (volume V2) by valve, b) NEGP is placed inside calibration chamber (volume V2).

In the CapaciTorr D400 a NEG cartridge is mounted to an electrical feedthrough on the CF 35 flange. The NEG cartridge fits into a tube with an inner diameter of 35 mm or more. In the case of the out-of-chamber geometry the NEGP was mounted to a standard

CF 35 intermediate piece (nipple) which was directly connected to a bakeable CF 35 valve.
In the molecular flow regime the effective pumping speed S_{eff} of the out-of-chamber geometry shown in Figure 72a is given approximately by

$$\frac{1}{S_{\text{eff}}} = \frac{1}{S_{\text{getter}}} + \frac{1}{C_{\text{getter}}} + \frac{1}{C_{\text{valve}}} + \frac{1}{C_{\text{port}}} \tag{52}$$

where S_{getter} = 400 l s^{-1} is the pumping speed of the NEGP and C_{getter} is the average conductance to the NEG elements inside getter cartridge, C_{valve} conductance of the valve and C_{port} the conductance of the connection port. Manufacturers specify for this type of valve a conductance of 34 l s^{-1} for nitrogen. In the molecular flow regime the conductance for hydrogen is by the factor of $\sqrt{M_{N_2}/M_{H_2}} \approx \sqrt{28/2} = 3.47$ higher, so it is $C_{valve}(H_2)$ = 127 l s^{-1}. Conductance C_{port} (H_2) = 220 l s^{-1} can be estimated from geometrical dimensions of the connection port, but it is difficult to calculate C_{getter} because of complicated geometry.

Even if C_{getter} would be very high, the resulting effective pumping speed would be limited to $S_{eff}(H_2) < 67$ l s^{-1}. With this pumping speed it would not be possible to reach ultimate pressure below 6×10^{-12} mbar in the XHV chamber.

In the case of the "nude configuration" the gas conductance to NEG elements is not limited so we can get maximum pumping speed.

8.4.1 In-situ measurement of NEGP effective pumping speed

Since pumping speed of the NEGP is constant from about 10^{-5} mbar down to UHV/XHV [93, 94] we can determine a pumping speed of the NEGP (S_{getter}) as a ratio between the injected gas flow Q and the equilibrium pressure P_{eq}.

$$S_{\text{getter}} = \frac{Q}{P_{\text{eq}}} \tag{53}$$

We have measured the pumping speed of CapaciTorr D400 for hydrogen for both possible configurations. We had to perform these measurements before we activated NEG in the flowmeter, since after activation only gas flow of inert gases could be measured.

8.4.2 Effective pumping speed of the "out–of-chamber" configuration

First we performed measurements of the "out-of-chamber" configuration. NEGP was activated at 450 °C for 1 hour. The gas flow of hydrogen in the range between 5×10^{-5} mbar l s^{-1} and 1×10^{-4} mbar l s^{-1} was generated and the equilibrium pressure P_{eq} in V2 was measured by SRG1. Measured effective pumping speed of NEG is shown in Figure 73. Mean value is S_{eff} = 20.1 l s^{-1}.
From Eq. (53) we can estimate that the effective conductance to getter elements was only C_{getter} = 33 l s^{-1}, when we placed NEG cartridge inside the tube with an inner diameter of 35 mm.

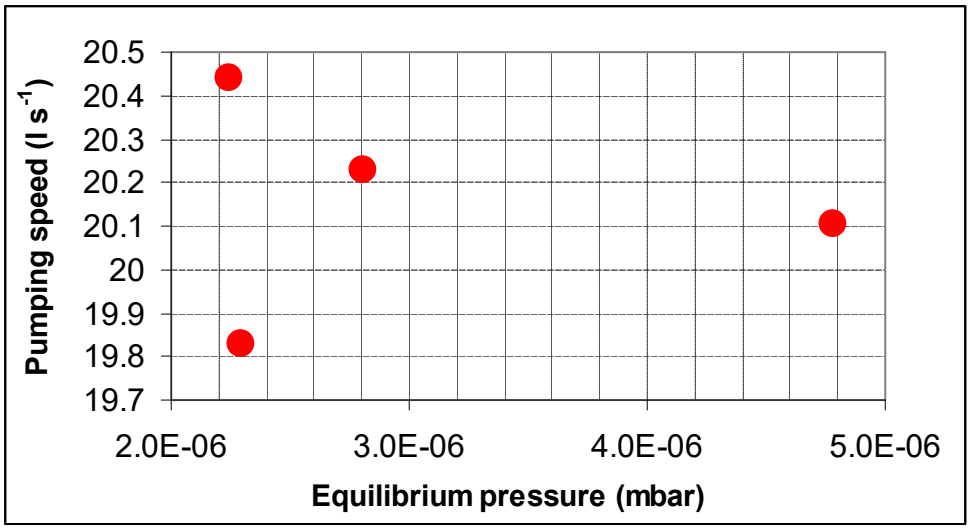

Figure 73: Pumping speed of the NEGP for hydrogen when NEGP is connected to the calibration chamber like in the Figure 72a.

From the measured outgassing flux of chamber V2 (see section 8.3) and measured effective pumping speed of the NEGP for this configuration, we can calculate achievable ultimate partial pressure of hydrogen in the XHV calibration chamber:

$$P_{u,H_2} = \frac{Q_{out}}{S_{eff}} = \frac{4.4 \cdot 10^{-10}\,\text{mbar}\,\frac{\text{l}}{\text{s}}}{20.1\,\frac{\text{l}}{\text{s}}} = 2.19 \cdot 10^{-11}\,\text{mbar} \qquad (54)$$

8.4.3 Effective pumping speed of the "nude" configuration

The conductances C_{getter}, C_{valve} and C_{port} in Eq. (52) can be ignored if the NEGP is placed directly in the calibration chamber. For this case the effective pumping speed is actually the pumping speed of the NEGP, $S_{eff} = S_{getter}$.

Measurement of pumping speed of the NEGP in this case was done with the same procedure like for the first case. As the NEGP was removed from the nipple and reinstalled directly into XHV calibration chamber, which was done under atmospheric conditions, a reactivation was necessary. Reactivation procedure was the same as first activation: 450 °C for 1 hour.

Because of much larger effective pumping speed we could not measure in our flowmeter the gas flows of hydrogen that would be high enough to give equilibrium pressures measurable by SRG. So we have used for pressure measurements two extractor gauges that were connected to V2. The gas flow rate of hydrogen was kept in the range between 2×10^{-8} and 1×10^{-6} mbar l s^{-1}, which produced an equilibrium pressure from 2×10^{-11} to 1×10^{-9} mbar.

Extractor gauge controllers displayed nitrogen equivalent pressure readings. So the readings were multiplied with a correction factor 2.4 (a typical value for ionization gauges, see section 3.5.2, Table 6) to get true hydrogen pressure in the system. The results of a measured NEG pumping speed for hydrogen are shown in Figure 74.

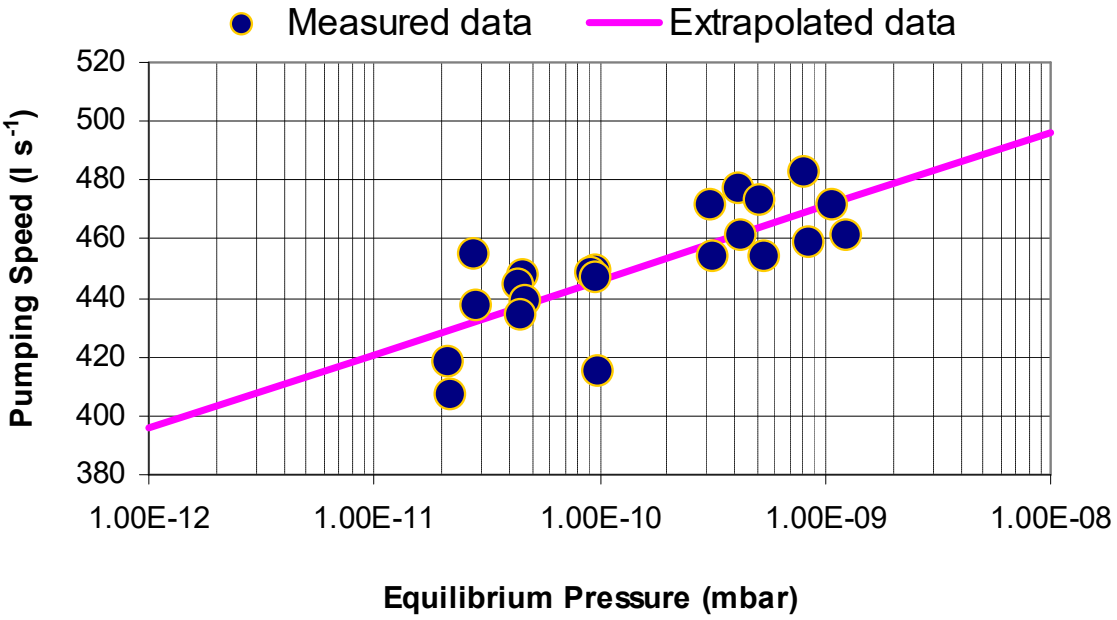

Figure 74: Hydrogen pumping speed of the NEGP when it was mounted directly in the calibration chamber

Measured pumping speed was more than 400 l s^{-1} in a pressure range from 2×10^{-11} to 1×10^{-9} mbar. Results also indicate a slight decrease in pumping speed with decreasing pressure. An estimated pumping speed at 1×10^{-12} mbar from regression analysis is of around 395 l s^{-1}.

We can see that by mounting NEGP directly in the chamber V2 we can achieve significantly lower ultimate pressure. Using measured outgassing fluxes $Q_{out} = 4.4\times10^{-10}$ mbar l s^{-1} and pumping speed S_{eff}=390 l s^{-1} we get:

$$P_{u,H_2} = \frac{Q_{out}}{S_{eff}} = \frac{4.4\cdot10^{-10}\,\text{mbar l s}^{-1}}{395\,\text{l s}^{-1}} = 1.1\cdot10^{-12}\,\text{mbar} \qquad (55)$$

8.5 Effective conductance of orifice

For calculation of the generated pressure in an orifice flow calibration system the effective conductance C_{eff} of the orifice in the molecular flow regime must be well known.

The equation for calculation of the generated pressure has been given in Chapter 1 (Eq. (8)). If we define $C_{eff} = C(1–R)$ then Eq. (8) becomes:

$$P = \frac{Q}{C_{eff}} \qquad (56)$$

In primary orifice flow systems the conductance of the orifice is calculated from geometrical dimensions of the orifice opening and its thickness. The geometry of the

mounting must be also taken into account. The conductance can be calculated with a sufficient accuracy only for very thin orifices and if all relevant dimensions are known very precisely [25].

In our system we could not make dimensional measurements with a sufficient precision. However the effective conductance of the orifice can also be measured "in-situ", as it will be explained in the next section.

8.5.1 Measurement of effective conductance

For "in-situ" calibration of effective conductance we need to measure generated pressure in orifice flow calibration system with a vacuum gauge which has been already calibrated with a sufficiently small uncertainty (secondary standard gauge) on another system. This means that in the case when the effective conductance is determined by calibration, the orifice flow system cannot be strictly considered as a primary, but it is a "secondary standard".

When the flow of calibration gas in our XHV system is high enough, the generated pressure in the calibration system (chamber V2) increases into 10^{-6} mbar range. This pressure can be easily measured with a high precision using the spinning rotor gauge SRG1 (Figure 67). We have previously calibrated our SRG1 for Ar gas by direct comparison with another SRG, which was calibrated at PTB in Germany. Calibration was done for argon and helium. This means that the measured conductance in our system is traceable to PTB vacuum standards.

We have made repeated measurements of generated pressure as a function of argon and helium gas flow. Effective conductance of our system was determined using this equation:

$$C_{\text{eff}} = \frac{Q}{P} \tag{57}$$

where Q is the gas flow which is produced by flow meter and P is the pressure measured in the calibration chamber with the calibrated SRG1.

Calculated values of effective conductance versus pressure for argon are given in the Figure 75 and for helium in Figure 76. From both figures it can be seen that in the range of measured pressure the effective conductance is constant and we can suppose that the effective conductance will be also the same for lower generated pressures.

Mean values and standard uncertainties of calculated effective conductance for argon and helium are given in Table 19.

Table 19: Mean Values and standard uncertainties of calculated effective conductance for argon and helium

Gas	Mean value [l/s]	SD [l/s]	No. of measurements	SD of the mean [l/s]	Relative SD of mean %
Ar	4.067	0.011619	28	0.0022	0.05
He	12.845	0.015865	21	0.0035	0.03

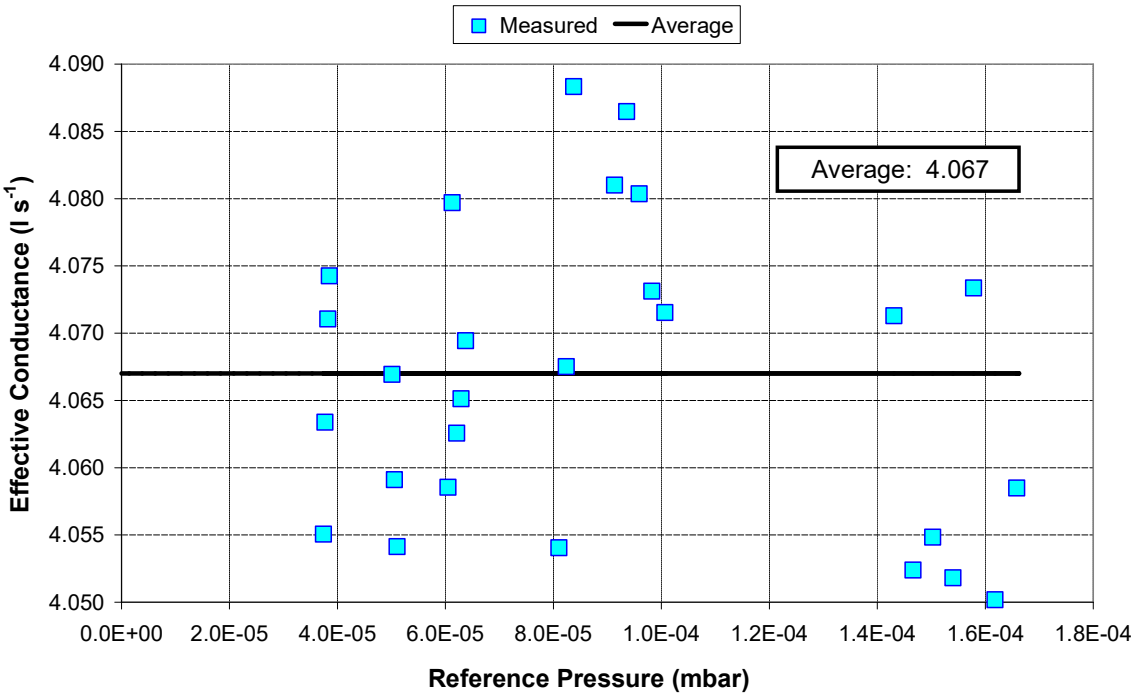

Figure 75: Effective conductance versus reference pressure for argon of XHV calibration system.

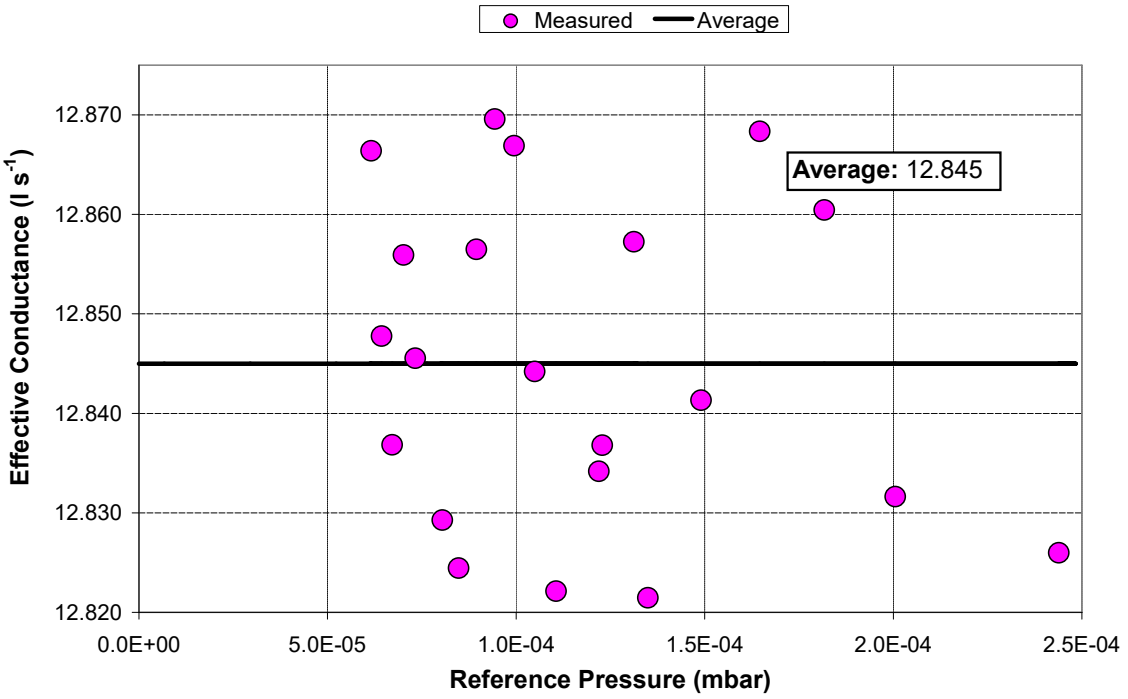

Figure 76: Effective conductance versus reference pressure for helium of XHV calibration system

8.5.2 Uncertainty analysis of effective conductance

Based on Eq. (57) the relative standard uncertainty of C_{eff} can be estimated:

$$\frac{u(C_{\text{eff}})}{C_{\text{eff}}} = \sqrt{\left(\frac{u(Q)}{Q}\right)^2 + \left(\frac{u(P)}{P}\right)^2} \tag{58}$$

Gas flow was measured by pressure rise method so the relative uncertainty of gas flow is $u(Q)/Q$ = 1.1%. Uncertainty of measured P using SRG1 above 4×10^{-5} mbar is mainly determined by the uncertainty of calibration and long term stability of momentum accommodation coefficient of the rotor. It was estimated that $u(P)/P$= 0.5%.

The resulting uncertainty is $u(C_{\text{eff}})/C_{\text{eff}}$ =1.2%.

9 Demonstration of measurement capabilities of XHV calibration system

Two extractors which were tested on our XHV calibration system are Leybold IE514 gauge heads connected to IM520 controllers. A very low calibration pressure down 10^{-12} mbar were generated, by operation of the flowmeter in constant conductance mode. Calibrations of those two extractor gauges were performed using argon and helium as the test gas. In the case of argon the calibrations were done in the range from 8×10^{-13} mbar to 2×10^{-7} mbar, whereas for helium the calibrations were performed in the range 7×10^{-12} to 1.3×10^{-7} mbar.

9.1 Uncertainty analysis of generated calibration pressure

The generated calibration pressure in the orifice flow system is calculated using Eq. (56). The associated relative uncertainty of the generated pressure which follows from Eq. (56) is given by:

$$\frac{u(P)}{P} = \sqrt{\left(\frac{u(Q)}{Q}\right)^2 + \left(\frac{u(C_{\text{eff}})}{C_{\text{eff}}}\right)^2} \tag{59}$$

Individual contributions have been already determined. In Chapter 8.5.2 we have estimated $u(C_{\text{eff}})/C_{\text{eff}}$ = 1.2%. Uncertainty of a generated gas flow depends on the measurement method of gas flow.

9.1.1 Uncertainty of generated pressure using pressure rise method of flow measurement

We have estimated in chapter 7.7.1 the uncertainty of the flowmeter operating in "pressure rise mode". It amounts to $u(Q_{\text{VdP}})/Q_{\text{VdP}}$ = 1.1%. Inserting this value in Eq. (59) we get for the uncertainty of generated pressure:

$$\frac{u(P)}{P} = 1.6\% \tag{60}$$

Minimum and maximum gas flow which can be measured with the pressure rise method in our system are: $Q_{\text{min}} = 5\times10^{-10}$ mbar l s^{-1} and $Q_{\text{max}} = 5\times10^{-5}$ mbar l s^{-1}.

In the case of argon gas the effective conductance is 4 l s^{-1}, so Eq. (60) is therefore valid for pressures between the minimum generated pressure $P_{\text{min}}=1.3\times10^{-10}$ mbar and the maximum generated pressure and $P_{\text{max}} = 1.3\times10^{-5}$ mbar.

All uncertainties were estimated as standard uncertainties at 68.3% confidence level (coverage factor k = 1). Expanded uncertainty of generated pressure at 95.5 confidence level (coverage factor k = 2) is obtained by multiplying the value in Eq. (60) with factor 2.

9.1.2 Uncertainty of generated pressure using constant conductance method of gas flow measurement

In chapter 7.7.2 we have estimated the uncertainty of the flowmeter operating in "constant conductance mode". Estimated value is $\underline{u}(Q_{cc})/Q_{cc}$ = 1.9%. Inserting this value in Eq. (59) we get for the uncertainty of generated pressure by the constant conductance method:

$$\frac{u(P)}{P} = 2.3\% \tag{61}$$

Using the constant conductance method the gas flow can be measured from $Q_{min} = 2\times10^{-12}$ mbar l s^{-1} to $Q_{max} = 5\times10^{-9}$ mbar l s^{-1}.

The corresponding minimum pressure of argon gas which can be generated in our system with this uncertainty is $P_{min} = 5\times10^{-13}$ mbar and the maximum pressure is $P_{max} = 1.3\times10^{-9}$ mbar.

There is an overlap from 1.3×10^{-10} mbar to 1.3×10^{-9} mbar where both methods of flow generation can be used.

9.2 Extractor gauge readings at ultimate pressure

After final assembly of NEGP to XHV system in "nude" configuration (see Chapter 8) and with two extractor gauges mounted, the system has been baked at 200 °C for 90 hours to remove gases that were adsorbed during exposure to atmosphere. After that the temperature was reduced to 100 °C and NEGP was re-activated at 450°C for 1 hour. Immediately after activation of NEGP the extractor gauges were switched on and degased for a period of 30 minutes.

Then the heating of the chamber was switched off and system was allowed to cool down to room temperature over night. Degassing of the extractor gauges was repeated for 10 minutes. The pressure in the system immediately after degassing was of the order of 5×10^{-10} mbar and decreased in few hours to 2×10^{-11} mbar. After that the system was left to be pumped at room temperature with XHV pumping unit and NEGP for one week. Extractor gauges were switched on continuously during this period. Time chart of extractor gauge readings is shown in Figure 77.

After one week the reading of extractor gauge EXT1 was switching between 2×10^{-12} mbar and 3×10^{-12} mbar (on this controller the resolution of display was only 1×10^{-12} mbar). For EXT2 the reading was in the range from 5.4×10^{-12} mbar to 6.1×10^{-12} mbar. Photos of the gauge controllers with a display of these pressure readings are shown in Figure 78.

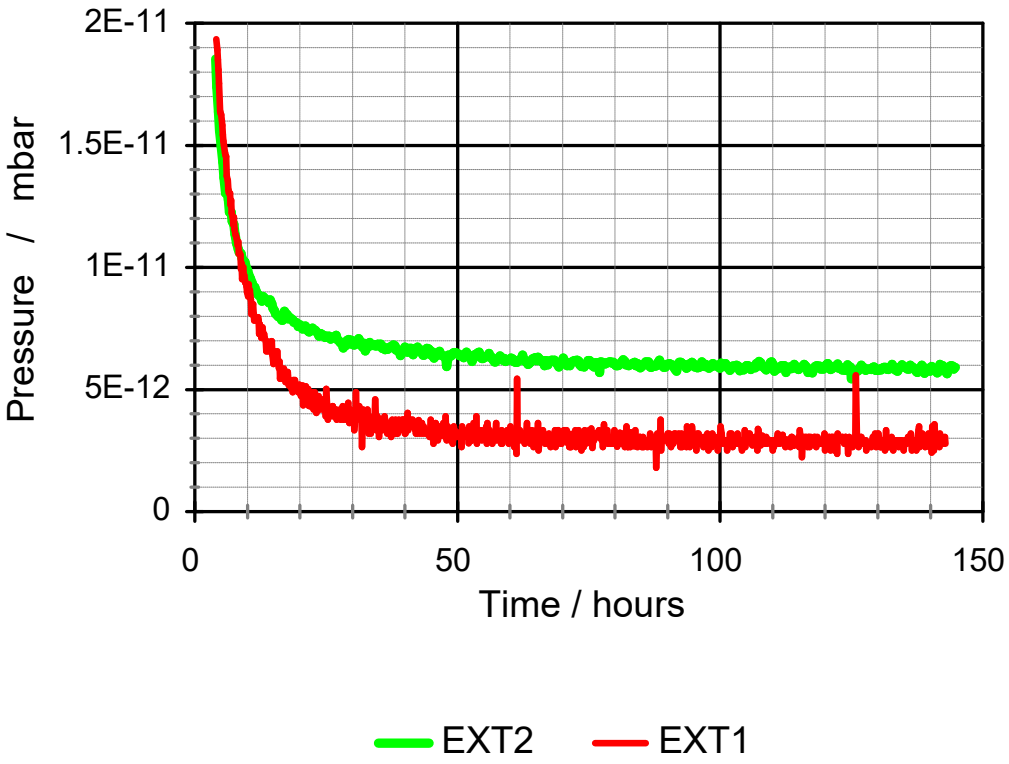

Figure 77: Time chart of extractor gauge readings approaching ultimate pressure

Figure 78: Photo of extractor gauge readings at ultimate pressure.

The difference of the readings was unexpectedly high. Final readings in Figure 77 differ by a factor of 2. The two extractor gauge heads were mounted to the calibration chamber in almost identical way. Both mounting ports had high and practically the same conductance to the chamber. The distance of the extractor gauges from the NEG pump element was the same. There were no localized sources of gas close to either of the gauge. So we can conclude that the both gauges were exposed to the same ultimate pressure of gas in the calibration chamber.

At higher pressures, in the 10^{-11} mbar range and above, the readings were nearly the same. This means that the sensitivity factors of both heads are almost identical. This was also confirmed by calibration of both gauges in Ar and He. The corrections factors did not differ by more than 15 %.

Limitations of hot cathode ionization gauges were discussed in section 3.5.3. The lowest measurable pressure of ionization gauges can be limited by X-ray effect, ESD ions and excessive outgassing of the gauge and its surrounding.

A nominal sensitivity of IE514 gauge heads for nitrogen equals 6.6 / mbar. They are operated at 1.6 mA electron emission current. This means that the ion current to the collector is only 1×10^{-14} A at pressure 1×10^{-12} mbar. So there may also be errors in measuring such low currents associated with electrometer in the controller and leakage currents in cables and insulators.

We have made several experiments to investigate possible cause for the large difference of readings in 10^{-12} mbar range.

9.2.1 Effect of exchanging the cable

Cables for measuring very low currents must be shielded and with very good insulation. The best would be to use triaxial cables. However the connector for the ion collector cable on the controller is coaxial, and also the cable supplied by the manufacturer is coaxial.

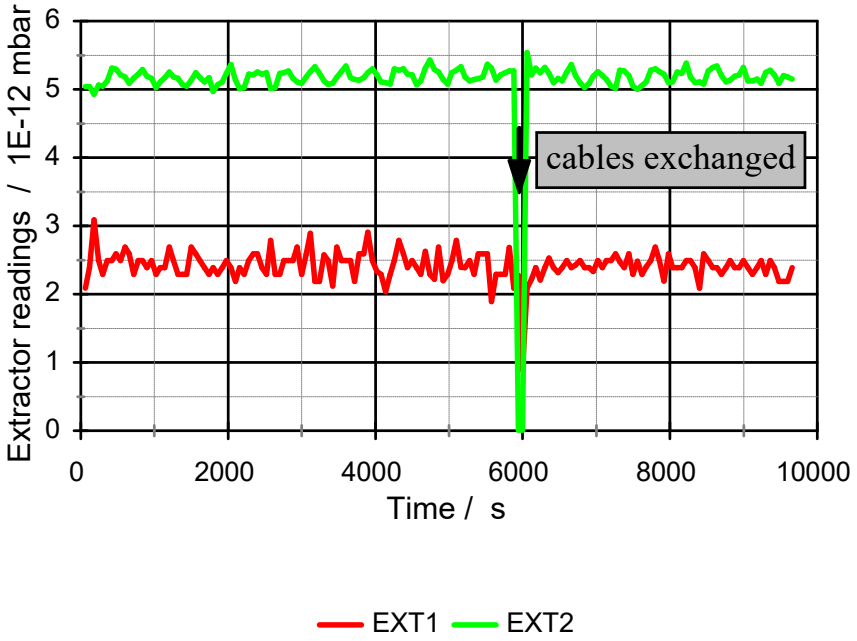

Figure 79: Exchanging of a cable has no significant effect on ultimate pressure readings

We had two different types of cables. One was coax cable with ”regular” insulation and the other was bakeable coax cable with Teflon insulation. EXT1 was first connected to controller 1 by Teflon cable and EXT2 to controller 2 with “regular” cable. The time chart of readings is shown in Figure 79. At t = 6000 s the cables were exchanged. The displayed readings on the controllers were not changed. The only difference was that can be seen in Figure 79 is slightly reduced the noise of EXT1 with regular cable (after t = 6000 s), but the mean value remained the same.

By this we have excluded that the ion collector cables can be the cause for the difference in the readings. We have also proved that both cables are of sufficiently good quality for ion current measurements down to 10^{-12} mbar, even if they are not triaxial.

9.2.2 Exchange of controller

The controller for extractor gauge must be capable of measuring very low ion currents. Controller 1 was manufactured in 1990s and controller 2 in year 2000. This means, that both were quite old, and certain drifts in electronics could happen. For sure there were some changes in the design of electronic circuits, which is evident from different display resolution. To check if there is a significant difference in the controllers we have connected first EXT1 with controller 1 and EXT2 with controller 2. Time chart of readings is shown in Figure 80. At t = 8200 s we have disconnected cables from controllers and exchanged the connection. The cable connection to the gauge heads was not touched.

Figure 80 shows a small difference of the readings after exchange of controllers. But the difference was less than 3×10^{-13} mbar. Reading of EXT1 was slightly higher with controller 2 and the same was observed with EXT2.

It is also evident from Figure 80 that newer controller 2 (with better display resolution) has also smaller noise on the analog output, which was used for recording the readings.

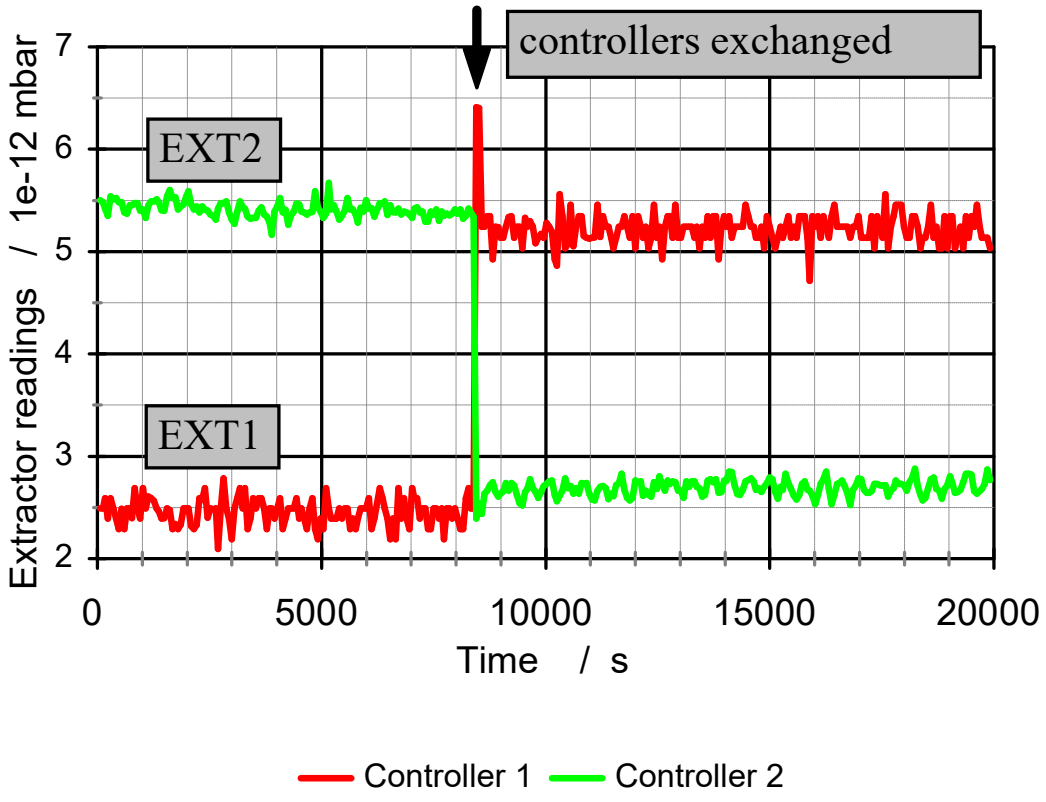

Figure 80: Exchanging of controllers has no significant effect on ultimate pressure readings

9.2.3 Outgassing of individual gauge

Hot cathode ionization gauges employ heated filaments which can outgass during operation. Also the temperature of surrounding surfaces is increased, which increases their thermal outgassing. To check the level of outgassing of our extractor gauges during operation we have made an experiment with switching on/off of individual gauge, while the other gauge used as an indicator of the change of ultimate pressure in the system. Results are shown in Figure 81.

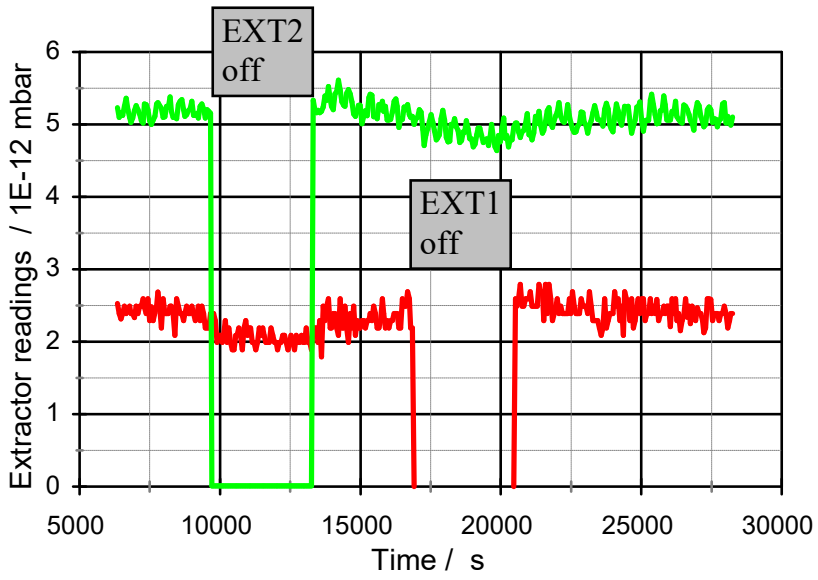

Figure 81: Switching on/off showed negligible outgassing of extractor gauges (at 400 l s^{-1} pumping speed of NEG)

During switch-off period, which lasted for 1 h, we have observed a slight decrease of displayed pressure on another gauge. The decrease was less than 3×10^{-13} mbar and it was not an instantaneous decrease, when filament was switched off, but a slow decrease with a time constant of the order of 10 minutes. We have also observed a very short pressure burst after switching on the filament, which lasted less than 5 s, so it was not recorded in the time chart in Figure 81, because data points were taken with 30 s intervals. This short pressure burst was then followed by a similar slow increase in pressure.

The long time constant of pressure decrease/increase when the filament is switched off/on can be contributed to the heating and thermal outgassing of surfaces of the calibration chamber in the vicinity of hot filament.

9.3 Generation of very low calibration pressure of 8×10^{-13} mbar of Ar gas

Ability of generation of very low calibration pressures down to below 1×10^{-12} mbar by operation of the flowmeter in constant conductance mode is demonstrated in Figure 82. First we have repeated two times the generation of argon calibration pressure of 1.6×10^{-12} mbar. Figure 82 shows good time stability over a period of 1 h and good repeatability of generated pressure. Despite a big difference in residual reading the change in reading for the generated argon pressure (1.6×10^{-12} mbar) was nearly the same ($\Delta P_{EXT} \approx 2.3\times10^{-12}$ mbar) for both gauges, indicating that the sensitivity of the gauges is very similar.

In the second part of the time chart in Figure 82 the change in reading for the generated Ar pressure of 7.8×10^{-13} mbar is shown. Also for this generated pressure the response of both extractors was nearly the same: $\Delta P_{EXT} \approx 1.2\times10^{-12}$ mbar. The results of calibration from Figure 82 are also included in Figures 83 and 84.

At the generated Ar pressure of 1.6×10^{-12} mbar the measurements were repeated 7 times. Results are given in Table 20. Mean ΔP_{EXT} were calculated from 30 readings. Standard deviations of mean ΔP_{EXT} values were less than 1×10^{-13} mbar.

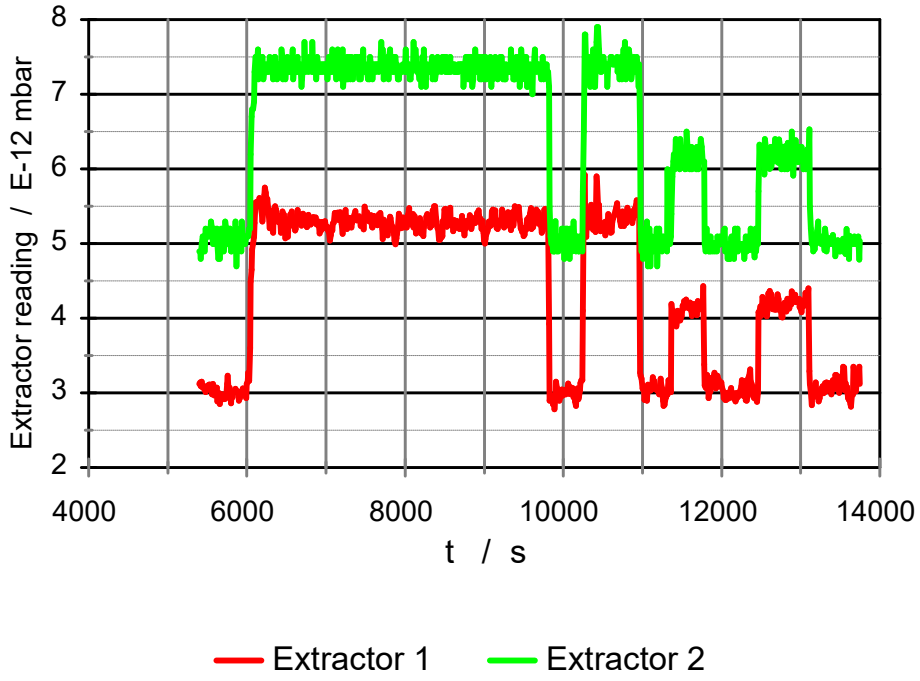

Figure 82: Repeatability of generation of very low argon calibration pressures 1.6×10^{-12} mbar and 7.8×10^{-13} mbar

Table 20: Repeatability of extractor gauges at generated Ar pressure of 1.6×10^{-12} mbar

Generated pressure (mbar) (calculated by constant conductance method)	Mean ΔP of EXT1 (mbar)	Mean ΔP of EXT2 (mbar)
1.566×10^{-12}	2.29×10^{-12}	2.31×10^{-12}
1.568×10^{-12}	2.33×10^{-12}	2.38×10^{-12}
1.569×10^{-12}	2.35×10^{-12}	2.27×10^{-12}
1.569×10^{-12}	2.43×10^{-12}	2.39×10^{-12}
1.573×10^{-12}	2.50×10^{-12}	2.43×10^{-12}
1.569×10^{-12}	2.34×10^{-12}	2.29×10^{-12}
1.573×10^{-12}	2.38×10^{-12}	2.30×10^{-12}
Standard deviations		
2.5×10^{-15}	6.44×10^{-14}	5.72×10^{-14}

9.4 Calibration results of two extractor gauges in Argon from $8x10^{-13}$ to $2x10^{-7}$ mbar

Calibrations of two extractor gauge heads were performed in Ar gas in a range from 8×10^{-13} to 2×10^{-7} mbar. Results of a large number of calibration runs are shown in Figures 83 and 84.

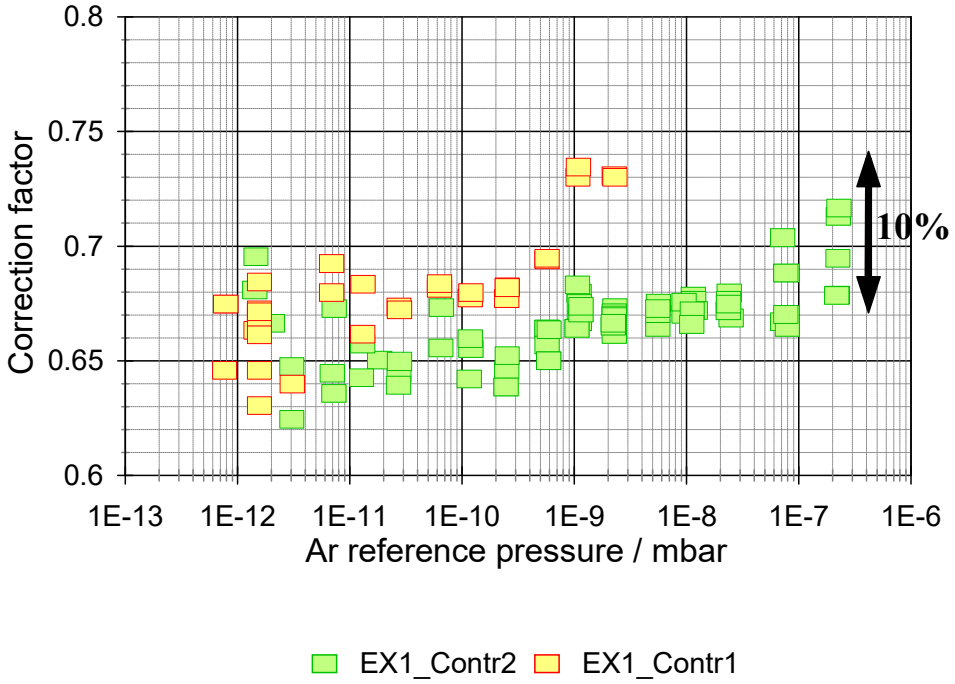

Figure 83: Results of calibration in argon gas of extractor gauge 1 connected to two different controllers

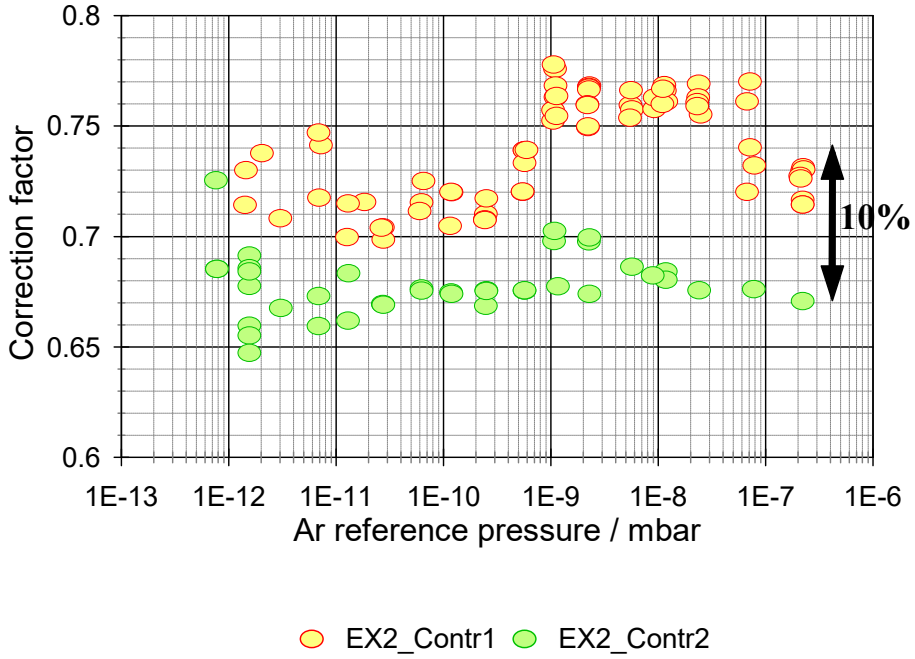

Figure 84: Results of calibration in argon gas of extractor gauge 2 connected to two different controllers

Correction factors were calculated as:

$$K = \frac{P_{\text{standard}}}{\Delta P_{\text{EXT}}} \qquad (62)$$

Argon reference pressure P_{standard} was calculated from effective conductance and generated gas flow using Eq. (56). Gas flow was measured by direct pressure rise method for pressures $P_{\text{standard}} > 5\times10^{-10}$ mbar and below this with constant conductance method. Calibrations were repeated for each gauge head with two different controllers. It can be seen from Figures 83 and 84 that the linearity of controller 2 is better than controller 1, which exhibited a step change of the order of 10% in the range from 10^{-9} mbar to 10^{-7} mbar.

9.5 Calibration results of two extractor gauges in Helium from $7x10^{-12}$ to $1.3x10^{-7}$ mbar

Calibrations of both extractors were also done with Helium gas. Results are shown in Figure 85. A step change in the sensitivity of the order of 10% for the controller 1 is evident in this case also.

The correction factor for He is significantly higher than for Ar. This was also expected based on relative sensitivities of different gauges for an ionization gauge (see table 6).

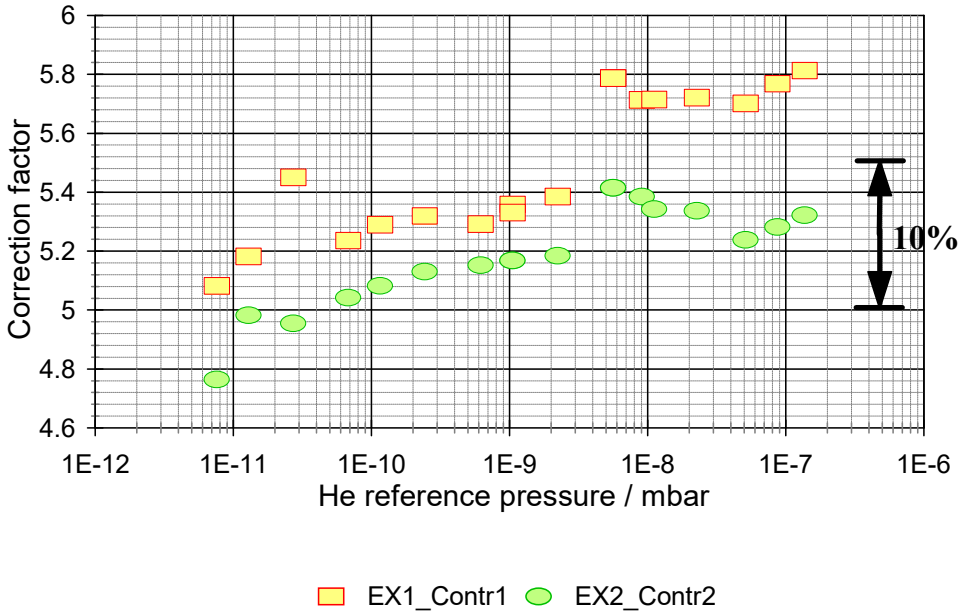

Figure 85: Results of calibration in helium gas of extractor gauge 1 and 2 in the range from 7×10^{-12} mbar to 1×10^{-7} mbar

10 Conclusions

In this thesis the possible improvements in vacuum metrology by advanced pumping techniques have been investigated. We have focused on the use of nonevaporable getters (NEG) in primary static expansion and dynamic expansion calibration systems.

NEGs have to be activated in high vacuum to achieve pumping action. Activation is performed by heating the getter material to sufficiently high temperature to enable removal of surface passivation layer. During activation a diffusion of the chemically bound atoms on the surface (mainly O, C and N) into the bulk material takes place. We have investigated oxygen diffusion in St 707 non evaporable getter material and the distribution of oxygen in different phases of the alloy using EDS, AES and XRD techniques. The XRD together with EDS and AES confirms that the as-received alloy is biphasic. The hexagonal zirconium and cubic Laves phases coexist in this material. The presence of oxygen in the oxidized specimens is more observable in the zirconium than in the Laves phase, whereas in the as-received specimen, the presence of oxygen is almost the same in both phases. XRD analysis of the sample oxidized at 450 °C showed a decrease in the intensity of the Laves phase reflections and the formation of ZrO_2 was indicated. With AES depth profiling we determined the size of the zones affected by the oxygen. The presence of the oxide layer composed of the ZrO_2 was confirmed on the Zr phase.

To build an XHV calibration system with a residual pressure below 1×10^{-12} mbar outgassing rate of the main calibration chamber shall be reduced below 10^{-13} mbar l $s^{-1}cm^{-2}$. This can be achieved by: (i) a high temperature firing, or (ii) by a degassing of a vacuum chamber in a temperature range of 250 °C to 350 °C for sufficiently long period. We have investigate reduction of hydrogen outgassing by long term bakeout at temperatures 250 °C and 350 °C. Study was done on a sample stainless steel (304 L) vacuum chamber having a wall with well defined thickness of 2.62 mm. Room temperature outgassing rate q =2.9×10^{-13} mbar l $s^{-1}cm^{-2}$ was achieved after baking the system at 250 °C for 380 h (equivalent to dimensionless Fourier number F_0=3.09). Outgassing rate was further reduced to q =5.7×10^{-14} mbar l $s^{-1}cm^{-2}$ after additional baking at T=350 °C for 140 h (F_0=8.66).

We demonstrated and proved the benefit of use of NEG in the procedure of determination of volume ratio of SE chambers. The use of NEG pump in the small and large volume of the static expansion system can diminish the influence of outgassing and offers the possibility to reliably generate lower calibration pressures. Contamination of the inert calibration gas by outgassing was found to be the main reason for the pressure dependence of the calculated volume ratio when the gas expansion was done at lower pressures. The NEG pump facilitates the condition of having the same amount of gas in the calibrating chambers before and after the expansion, which is the basis for the use of gas laws to calculate the pressure after the expansion.

We have constructed a model dynamic expansion calibration system with a built-in NEGP. Reduction of hydrogen outgassing rate from the walls of calibration chamber below 10^{-13} mbar l $s^{-1}cm^{-2}$ by extensive bake-out and inserting NEGP directly in the chamber to maximize the pumping speed for hydrogen enabled us to achieve the ultimate pressure of the order of 2×10^{-12} mbar. In the construction of XHV dynamic calibration

chamber the amount of surfaces of massive parts that can be difficult to degas (valves, flanges) has to be kept as small as possible, so that the total outgassing of H_2 in the chamber is kept below 10^{-11} mbar l s^{-1} per each cm^2 of orifice opening. This is important point in designing of the system.

System is equipped with a gas flow meter for very low flows of inert gases. Flow is measured by pressure rise method. The use of another NEG in the flowmeter practically diminishes the effect of hydrogen outgassing on measured flow. Lower limit of pressure rise method is 5×10^{-10} mbar l s^{-1} and can be extended by constant conductance method down to 3×10^{-12} mbar l s^{-1}.

With this flowmeter we demonstrated generation of calibration pressures of Ar in our XHV calibration system in the range from 8×10^{-13} mbar up to 2×10^{-7} mbar. Two extractor gauges were calibrated over this range. They were quite linear from 1×10^{-12} to 1×10^{-7} mbar.

The behavior of two extractor gauges at the ultimate pressure in the system $<2\times10^{-12}$ mbar was also investigated. We have found large difference of the readings of extractor gauges, for EXT1 the lowest reading was around 2.5×10^{-12} mbar, while EXT2 had a residual reading as large as 5×10^{-12} mbar. This means that zero reading due to X-ray effect can be a problem to use extractor gauges for reliable pressure measurements in the 10^{-12} mbar range. For calibration of extractor gauges over its full range it is necessary to evaluate in calibration procedure also the X-ray limit of individual gauge.

11 Acknowledgements

Firstly I would like to express my greatest appreciation to my family, in particular to my wife, Teuta, for all the patience and sacrifice shown during the time I was studying for my PhD, especially in taking care of our children while I was away.

I am sincerely and wholeheartedly grateful to my supervisor Janez Šetina for the support and guidance provided throughout my PhD studies and dissertation writing, and for everything he has taught me, because indeed this field was completely new for me.

I would like to express my gratitude to the Evaluation Committee for the fruitful comments and suggestions they gave during the evaluation of my PhD studies.

I am sincerely and earnestly thankful to Dr. Igor Belič for his precious advice throughout my PhD studies.

Finally I would like to acknowledge the European Social Fund. It would have not been possible to do this research work without their financial support, because the presented work was partly financed by the European Union. This program was implemented in the framework of the Operational Programme for Human Resources Development for the period 2007-2013, Priority axis 1: Promoting entrepreneurship and adaptability, Main type of activity 1.1: Experts and researchers for competitive enterprises.

12 References

1. Jousten, K.; Rohl, P.; Aranda Contreras, V. Volume ratio determination in static expansion systems by means of a spinning rotor gauge. *Vacuum* **52**, 491 (1999).
2. Redgrave, F.; Forbes, A.; Harris, P. A Discussion of Methods of the Estimation of Volumetric Ratios Determined by Multiple Expansions. *Vacuum* **53**, 159 (1999).
3. Greenwood, J. The reference Gauge technique for static expansion ratios – Applied to NPL medium vacuum standard SEA3, *Vacuum* **81**, 427 (2006).
4. Berman, A. Vacuum Gauge Calibration by the Static Method. *Vacuum* **29**, 417 **(**1979).
5. Akram, H.; Maqsood, M.; Rashid, H. Develpment and Characterization of Volume Expansion Vacuum Standard. *World Applied Sciences* **6**, 894 (2009).
6. Berman, A and Fremerey, J. Precision Calibration of a Static Pressure Divider by Means of Spinning Rotor Gauge. *Journal of Vacuum Science and Technology A* **5**, 2436 (1987).
7. Wuthrich, C, Coulibaly, M. Determination of volume ratios by gas depletion through multiple expansions. *Vacuum* **81**, 453 (2006).
8. Poulter, K, The Calibration of Vacuum Gauges, *Journal of Physics: Scientific Instruments* **10**, 112 (1977).
9. Holanda, R. Evaluation of a Volume Ratio System for a Vacuum Gauge Calibration from 10^{-8} to 10 Torr. *NASA Tech. Note NASA TN D_5406* (1969), p.1-19
10. Sharma, J.; Mohan, P. Use a successive expansion technique to determine volme ratio of ~500 for vacuum gauge calibration. *Journal of Vacuum Science and Technology A* **6**, 3148 (1988).
11. Steckelmacher, W. The calibration of vacuum gauges. *Vacuum*. **37**, 269 (1987).
12. Lafferty, M. *Foundations of Vacuum Science and Technology* (John Wiley & Sons, New York, 1998)
13. Jousten, K. *Handbook of Vacuum Technology*, (Wiley-VCH Verlag GmbH & Co.KgaA, Weinheim, 2008)
14. Jousten, K. and Rupschus, G. The uncertainties of calibration pressures at PTB,*Vacuum* **44**, 569 (1993).
15. Poulter, K. Vacuum gauge calibration by the orifice flow method in the pressure range 10^{-4}-10 Pa, *Vacuum* **28**, 135 (1978).
16. Bergoglio, M.; Calcatelli, A.; Marzola, L.; Rumiano, G. Primary pressure measuremnts down to 10^{-6} Pa. *Vacuum* **38**, (1988) p.887-891
17. Bennewitch, G. and Dohmann, H. Dynamic pressure calibration system, *Vakuumtechnik* **14,** 8 (1965).
18. Jousten, K.; Menzer, H.; Niepraschk, R. New fully automated, primary standard for generating pressures between 10^{-10}Pa and 3×10^{-2}Pa with respekt to residual pressures, *Metrologia* **36**, 493 (1999).
19. Detian, L.; Meiru, G.; Youngjun, C.; Feng, Y.; Zhang, D. Vacuum calibration apparatus with the pressure down to 10^{-10} Pa. *Journal of Vacuum. Science and.*

Technology A **28**, 1099 (2010).

20. Akram, H.; Maqsood, M.; Rashid, H. Technique used for vacuum standartization. *World Applied Sciences Journal* **7**, 76 (2009).
21. Peggs, G. N. The measurement of the gas throughput in the range 10^{-4} to 10^{-10} Pa m^3s^{-1}. *Vacuum* **26**, 321 (1976).
22. Tison, A.; Tilford, C. R. In: *Workshop on Moisture Measurement and Control for Microelectronics*. 19-29 (NIST, 1993).
23. Jousten, K. Temperature corrections for the calibration of vacuum gauges. *Vacuum* **49**, 81 (1998).
24. McCulloh, K.E.; Tilford, C.R.; Ehrlich, C.D.; Long, F.G. Low range flowmeters for use with vacuum and leak standards. *Journal of Vacuum Science and Technology A* **5**, 376 (1987).
25. Dittmann, S. High Vacuum Standards and Its Use. *National Institute of Standards and Technology (NIST)*, Special publication 250-34. (1989), p.1-45
26. Tilford, C.; Dittmann, S.; McCulloh K. The National Bureau of Standards primary high-vacuum standard. *Journal of Vacuum Science and Technology A* **6**, 2853 (1988).
27. Mohan, P. Vacuum gauge calibration at the NPL (India) using orifice flow method. *Vacuum* **51**, 69 (1998).
28. Peksa, L.; Pražak, D.; Gronych, T.; Repa, P.; Vičar, M.; Tesar, J.; Krajiček, Z.; Stanek, F. Primary Vacuum Standard for UHV Range – Standing Experiences and Present Problems. *Journal of Metrology Society of India – MAPAN* **24**, 77 (2009).
29. Jousten, K.; Filippelli, A.; Tilford, C.; Redgrave, F. Comparison of the standards for high and ultrahigh vacuum at three national standards laboratories. *Journal of Vacuum Science and Technology A* **15**, 2395 (1997).
30. Kuz'min, V. Precise measurements of small gas flows – Metrological basis for the calibration of leak detectors. *Measurement Techniques* **40**, 130 (1997).
31. Wright, J.D.; Mattingly, G.E. NIST Calibration Services for Gas Flow Meters. *National Institute of Standards and Technology (NIST)*, Special publication 250-49. (1998), p.1-41
32. Avdiaj, S.; Šetina Batič, B.; Šetina, J.; Erjavec, B. Oxygen diffusion in The nonevaporable getter St 707 during heat treatment. *Materials and Technology* **45**, 33 (2011).
33. Rajeshuni, R. Getters for Reliable Hermetic Packages, JPL Publication D-17920, National Aeronautics and Space Administration. Washington (1999), p.5-40
34. Marquardt, N. Introduction to the Principles of Vacuum Physics. In: Turner, S (ed). *Proceedings of the CERN Accelerator School*. 1-24 (CERN report, Snekersten, 1999).
35. Benvenuti, C., Molecular Surface Pumping: the Getter Pump, in Vacuum Technology. In: Turner, S (ed). *Proceedings of the CERN Accelerator School*. 43-50 (CERN report, Snekersten, 1999).
36. Prodromides A. Non-Evaporable Getter Thin Film Coatings for Vacuum Applications, *These No. 2652*. (2002).
37. Redhead, P. The Ultimate Vacuum. *Vacuum* **53**, 137 (1999).
38. Ferrario, B. Chemical Pumping in vacuum technology. *Vacuum* **47**, 363 (1996).
39. Redhead, P.A.; Hobson, J.P.; Kornelsen, E.V. *The physical Basis of Ultrahigh Vacuum*, (American Institute of Physics, New York, 1993).
40. SAES Getters * http://www.saesgetters.com/default.aspx?idPage=125

41. Hoffman, D.; Singh,B.; Thomas, J. *Handbook of Vacuum Science and Technology*. (American press, Chestnut Hill MA, 1998).
42. Benvenuti, C.,J.; Cazeneuve, J.; Chiggiato, P.; Cicoira, F.; Escudeiro Santana, A.; Johanek, V.; Ruzinov, V.;Fraxedas, J. A Novel Route to Extreme Vacua: the Non Evaporable Getter Thin Film Coatings. *Vacuum* **53**, 219 (1999).
43. Benvenuti, C. Chiggiato, P. Cicoira, F. L'Aminot, Y. Nonevaporable Getter Films For Ultrahigh Vacuum Applications. *Journal of Vacuum Science & Technology A* **16**, 148 (1998).
44. Jousten K, Thermal outgassing. In: Turner, S (ed). *Proceedings of the CERN Accelerator School*. 111-125 (CERN report, Snekersten, 1999).
45. Setina J. 45 IUVSTA workshop on NEG coating for particle accelerators and vacuum system; 2006. Italy. http://www.aiv.it/aivevento3/index.html
46. Detian, L.; Guangping, Z.; Meiru, G.; Jie, X.; Yongjun, C. Static expansion vacuum standard with extended low pressure range. *Journal of Metrology Society of India – MAPAN* **24**, 95 (2009).
47. Chambers, A. *Modern Vacuum Physics*. (CRC Press LLC, Florida, 2005).
48. Detian, L.; Yongjun, C. Applications of nonevaporable getter pump in vacuum metrology. *Vacuum* **85**, 739 (2011).
49. Leisch, M. Hydrogen Outgassing of stainless steel http://www.ss.dsl.pipex.com/rgaug/pdfs/vs1/Leisch.pdf
50. Weston, G.F. *Ultrahigh Vacuum Practice*. (Butterworth & Co, Cambridge, 1985).
51. Redhead, P. Extreme high vacuum. In: Turner, S (ed). *Procedings of the CERN Accelerator School.* 213-226 (CERN report, Snekersten, 1999).
52. Redhead P, Recommended practices for measuring and reporting outgassing data. *Journal of Vacuum Science & Technology A* **20**, 1667 (2002).
53. Ishikava, Y.; Nemanic, V. An overview of methods to suppress hydrogen outgassing rate from austentic stainless steel with reference to UHV and XHV. *Vacuum* **69**, 501 (2003).
54. Bernardini, M.; Braccini, S.; De Salvo, R.; Di Virgilio, A.; Gaddi, A.; Gennai, A.; Genuini, G.; Giazotto, A.; Losurdo, G.; Pan, H.B.; Pasqualetti, A.; Passuello, D.; Popolizio, P.; Raffaelli, F.; Torelli, G.; Zhang, Z.; Bradaschia, C.; Del Fabbro, R.; Ferrante, I.; Fidecaro, F.; La Penna, P.; Mancini, S.; Poggiani, R.; Narducci, P.; Solina, A.; Valentini, R. Air bake-out to reduce hydrogen outgassing from stainless steel. *Journal of Vacuum Science & Technology A* **16**, 188 (1998).
55. Reid R, Outgassing Surface Conditioning, 2009, www.stfc.ac.uk/resources/pdf/ronreid25209.pdf
56. Benvenuti, C.; Chiggiato, P.; Cicoira, F.; Ruzinov, V. Decreasing surface outgassing by thin film getter coatings. *Vacuum* **50**, 57 (1998).
57. Outlaw, R.; Tompkins, H. *Ultrahigh Vacuum Design and Practice: AVS Educational Committee* (AVS, New York, 2009).
58. Tompkins, H. *Vacuum Technology: A Beginning* (AVS, New York, 2000).
59. https://us.trinos.com/cgi-bin/trinos/iboshop.cgi?show1220,0
60. Welch, M. *Capture Pumping Technology* (Elsevier science, Amsterdam, 2001).
61. O'Hanlon, J. A user's guide to vacuum technology (John Wiley and Sons, New Jersey, 2003).
62. Hucknall, D.; Morris, A. *Vacuum Technology: Calculations in chemistry* (Royal Society of Chemsitry, Cambridge, 2003).
63. Dylla, H. Challenges for Extreme High Vacuum (XHV)

http://cas.web.cern.ch/cas/Spain-2006/PDFs/Dylla-4.pdf

64. Calcatelli, A. A develoment of vacuum measurements down to extremely high vacuum (XHV). http://www.imeko.org/publications/tc16-2007/IMEKO-TC16-2007-KL-034u.pdf
65. Jousten K, Ultrahigh Vacuum Gauges. In: Brand, D. (ed.) *Proceedings of the CERN Accelerator School: Vacuum in Accelerators*. 145-168 (CERN, Geneva, 2007)
66. Watanabe, F. My never-ending story towards XHV pressure measurements. *Vacuum*, **53**, 151 (1999).
67. Redhead P. A, Hydrogen in vacuum systems; an Overview. In: *First International Workshop on Hydrogen in Materials and Vacuum Systems*. 243-254 (AIP Conference Proceedings, Volume 671, 2003).
http://adsabs.harvard.edu/abs/2003AIPC..671..243R
68. St 707 Non Evaporable Getters activatable at low temperatures, SAES Getters http://psec.uchicago.edu/getters/St%20707%20Brochure.pdf ,
69. Gunter M.; Herein, R.; Schumacher, R.; Weinberg, G.; Schlogl, R. Microstructure and bulk reactivity of the nonevaporable getter $Zr_{57}V_{36}Fe_7$. *Journal of Vacuum Science & Technology A* **16**, 3526 (1998).
70. Sharma, R.K.; Mithal, N.; Jagannath, Bhushan, K.G.; Srivastava, D.; Prabhakara, H.R.; Gadkari, S.C.; Yakhmi, J.V.; Sahni, V.C. Ti_Zr-V Thin Films as Non-Evaporable Getters (NEG) to Produce Extreme High Vacuum. *Journal of Physics: Conference Series* **114**, 012050 (2008).
71. Erjavec, B.; Šetina, J. Investigation of a method for determinating pumping speed and sorption capacity of nonevaporable getters based on *in situ* calibrated throughput. *Journal of Vacuum Science and Technology A* **29**, 051602 (2011).
72. Brundle, R; Evans, C; Wilson, S. *Encyclopedia of MaterialsCharacterization*: *Surface, Interface, Thin films* (Manning Publications Co, Butterworth-Heinemann, 1992).
73. Settle, F. *Handbook of Instrumental Techniques for Analytical Chemistry*: *Auger Electron Spectroscopy* (Prentice Hall PTR, New Jersey, 1997).
74. Settle, F. *Handbook of Instrumental Techniques for Analytical Chemistry*: *X-ray diffraction* (Prentice Hall PTR, New Jersey, 1997).
75. Prodromides, A.; Scheuerlein, C.; Taborelli M. The characterization of non-evaporable getters by Auger electron spectroscopy: analytical potential and artifacts. *Applied Surface Science* **191**, 300 (2002).
76. Prodromides A.; Scheuerlein, C.; Taborelli M. Lowering the activation temperature of TiZrV non-evaporable getter films. *Vacuum* **60**, 35 (2001).
77. Boffito C.; Ferrario B.; Della Porta P.; Rosai L. A nonevaporbale low temperature activatable getter material. *Journal of Vacuum Science and Technology* **18**, 1117 (1981).
78. Fast, J. *Gases in Metals* (N.V. Philips Gloeilampenfabrieken, Eindhoven, 1976).
79. Moore B. Recombination limited outgassing of stainless steel, *Jouranl of vacuum Science and Technology A* **13**, 545 (1995).
80. Nemanic, V.; Šetina, J. Outgassing in thin wall stainless steel cells. *Journal of Vacuum Science and Technology A* **17**, 1040 (1999).
81. Nemaic, V.; Bogataj, T. Outgassing of thin wall stainless steel chamber. *Vacuum* **50**, 431 (1998).
82. Nemanic, V.; Zajec, B.; Setina, J. Anomalies in kinetics of hydrogen evolution

from austenitic stainless steel from 300 to 1000 ºC. *Journals of Vacuum Science and Technology A* **19**, 215 (2001).

83. www.mksinst.com
84. Grant, D.M.; Cummings, D.L.; Blackburn, D.A. Hydrogen in 304: Diffusion, permeation and surface reaction. *Journal of Nuclear Materials* **149**, 180 (1987).
85. Park, C.; Chung, S.; Liu, X.; Li, Y.; Reduction in hydrogen outgassing from stainless steels by a medium-temperature heat treatment. *Journal of Vacuum Science and Technology A* **26**, 1166 (2008).
86. Redgrave, F. Downes S. Some comments on the stability of spinning rotor gauges. *Vacuum* **38**, 839 (1988).
87. Setina, J.; Looney, J. Behavior of commercial spinning rotor gauges in the transition regime. *Vacuum* **44**, 577 (1993).
88. Setina, J. Effect of ambient temperature on the offset correction of a spinning rotor gauge. *Vacuum* **40**, **51** (1990).
89. Setina, J. Measurements of spining rotor gauge response to step change of suspension head temperature. *Vacuum* **71**, 341 (2003).
90. Bock, T.; Jousten, K. Experimetal verification of Monte-Carlo simulation of the gas density in a vacuum chamber. *Vacuum* **81**, 234 (2006).
91. Malyshev, O.; Middleman, K.; Colligon, J.; Valizadeh, R. The activation and measurement of non-evaporable getter films. Journal of Vacuum Science and Technology A **27**, 3081969 (2009).
92. Jousten, K.; Messer, G.; Wandrey, D. A precision gas flowmeter for vacuum metrology. *Vacuum* **44**, 135 (1993).
93. Umrath, W. *Fundamentals of Vacuum Technology* (Oerlikon leybold vacuum, Cologne, 2007).
94. Ferris M. NEG pumps: Magic in the Vacuum Chamber. *Vacuum Technology and Coating*. **August** (2002). http://www.saesgetters.com/default.aspx?idPage=158
95. Watanabe, F. Total pressure measurement down to 10^{-12} Pa without electron stimulated desorption. *Journal of Vacuum Science and Technology A* **11**, 1620 (1993).
96. Redhead, P. A. History of ultrahigh vacuum pressure measurements. *Journal of Vacuum Science and Technology A* **12**, 904 (1994).
97. Jousten, K. Problems in vacuum metrology for industrial applications that call for solutions by rarefied gas dynamics. 64th IUVSTA Workshop on Practical Applications and Methods of Gas Dynamics for Vacuum Science and Technology, 2011. www.itep.kit.edu/downloads/2_Jousten.pps
98. http://www.saesgetters.com/documents/CapaciTorr%20MK5%20Series_general_1814.pdf
99. http://www.pfeiffer-vacuum.com/know-how/vacuum-measuring-equipment/fundamentals-of-total-pressure-measurement/indirect-gas-dependent-pressure-measurement/technology.action?chapter=tec3.1.2
100. ChilBrigs, D.; Seah, M. P. *Practical Surface Analyse, Volume 1s: Auger and X-ray Photoelectron Spectroscopy* (John Wiley, Chichester, 1994).
101. Brigs, D.; Grant, J. T. *Surface Analyses by Auger and X-ray Photoelectron Spectroscopy.* (Cromwell, Trowbridge, 2003).
102. Childs, K. D et al (Ed),. *Handbook of Auger Electron Spectroscopy*. (Physical Electronics Inc, Eden Prairie, 1995).

Index of Figures

Index of Tables

Appendix

List of publications related to this PhD

Original scientific article

1. Avdiaj, S.; Šetina Batič, B.; Šetina, J.; Erjavec, B. Oxygen diffusion in the nonevaporable getter St 707 during heat treatment. *Materials and Technology* **45**, 33 (2011).

2. Avdiaj, S.; Erjavec, B. Outgassing of hydrogen from stainless steel vacuum chamber (Accepted for publication to *Materials and Technology* **46**, 2012).

3. Šetina, J.; Avdiaj, S.; Erjavec, B. Volume ratio measurements of vacuum vessels containing non-evaporable getter (submitted for publication to *Vacuum*).

Published scientific conference contribution abstract (From COBISS)

4. AVDIAJ, Sefer, ŠETINA, Janez, ŠETINA, Barbara. Investigation of oxygen diffusion in St 707 non-evapoable getter material. V: JENKO, Monika (ur.). 17. konferenca o materialih in tehnologijah, 16.-18. november 2009, Portorož, Slovenija = 17. conference on materials and technology, 16.-18. november 2009, Portorož, Slovenija. *Program in knjiga povzetkov*. Ljubljana: Inštitut za kovinske materiale in tehnologije, 2009, str. 47. [COBISS.SI-ID 776618]

5. AVDIAJ, Sefer, ŠETINA, Barbara, ŠETINA, Janez. Investigation of oxygen diffusion in St 707 non evaporbale[!] getter material. V: 14th European Conference on Composite Materials, ECCM 14, 7-10 June, 2010, Budapest, Hungary. *14th European conference on Composite materials : [book of abstract]*. Budapest: University of Technology and Economics, 2010, str. 78. [COBISS.SI-ID 819114]

6. ŠETINA, Janez, DRNOVŠEK, Janko, SEFA, Makfir, AVDIAJ, Sefer, ERJAVEC, Bojan, HUDOKLIN, Domen. Modeling of water vapor diffusion in elastomers with impact in humidity and vacuum measurements. V: BOJKOVSKI, Jovan (ur.), GERŠAK, Gregor (ur.), ŽUŽEK, Vincencij (ur.), PUŠNIK, Igor (ur.), HUDOKLIN, Domen (ur.), BEGEŠ, Gaber (ur.), BATAGELJ, Valentin (ur.), DRNOVŠEK, Janko (ur.). *Book of abstracts*. Ljubljana: Faculty of Electrical Engineering, Laboratory of Metorology and Quality, 2010, vol. B, str. 372. [COBISS.SI-ID 819370]

7. AVDIAJ, Sefer, ŠETINA, Janez. Extension of the range of primary vacuum-calibration methods using non-evaporable getters. V: JENKO, Monika (ur.). 18. konferenca o

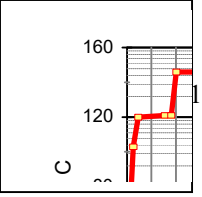

materialih in tehnologijah, 15.-17. november 2010, Portorož, Slovenija = 18th Conference on Materials and Technology, 15-17 November 2010, Portorož, Slovenia. *Program in knjiga povzetkov*. Ljubljana: Inštitut za kovinske materiale in tehnologije, 2010, str. 52. [COBISS.SI-ID 842154]

8. AVDIAJ, Sefer, ŠETINA, Janez, ERJAVEC, Bojan. Volume ratio measurements of vacuum vessels containing nonevaporable getters. V: VESELÝ, Marian (ur.), VINCZE, Andrej (ur.), VÁVRA, Ivo (ur.). 13th Joint Vacuum Conference, June 20-24, 2010, Hotel Patria, Štrbské Pleso High Tatras, Slovak Republic. *Programme and book of abstracts*. Brno: Tribun EU s.r.o., 2010, str. 134. [COBISS.SI-ID 814506]

9. AVDIAJ, Sefer, ŠETINA, Janez. Outgassing [i.e. Outgassing] of hydrogen from stainless steel vacuum chamber. V: MOZETIČ, Miran (ur.), VESEL, Alenka (ur.). 18. mednarodno znanstveno srečanje Vakuumska znanost in tehnika, Bohinjsko Jezero, 2.-3. junij 2011 = 18th International Scientific Meeting on Vacuum Science and Techniques, Bohinjsko Jezero, 2-3 June 2011. *Program in knjiga povzetkov*. Ljubljana: Društvo za vakuumsko tehniko Slovenije: = Slovenian Society for Vacuum Technique, 2011, str. 43. [COBISS.SI-ID 867498]